Dissertation
submitted to the
Combined Faculties for the Natural Sciences and for Mathematics
of the Ruperto–Carola University of Heidelberg, Germany
for the degree of
Doctor of Natural Sciences

presented by

Diplom–Physikerin Monika Maintz
born in Sinsheim

Oral examination: December 17th, 2003

Be binary stars with hot, compact companions

Referees: **Prof. Dr. Immo Appenzeller**
Prof. Dr. Wolfgang Duschl

ZUSAMMENFASSUNG

Be-Doppelsterne mit heißen, kompakten Begleitern

In dieser Arbeit wurde untersucht, welche Bedeutung die Entwicklung enger Doppelsternsysteme für die Entstehung der Be-Sterne hat. Es wurde nachgewiesen, daß der Be-Stern 59 Cyg ein entwickelter Doppelstern ist, der einen sdO-Begleiter hat. Der Begleiter wurde durch eine schwache He II -Absorption nachgewiesen. Die Bahnelemente und die Sternmassen wurden bestimmt. Im Spektrum von 59 Cyg wurden charakteristische Strukturen identifiziert. Dies sind eine Emissionskomponente mit nur einem Emissionspeak, eine phasengekoppelte V/R-Variation und eine "knotige" Struktur der Absorptionslinien. Laut Štefl et al. (2000) werden diese Strukturen von einem heißen, kompakten Begleiter verursacht (sdO oder WD), der einen Sektor der Scheibe des Be-Sterns photoionisiert. Aufgrund dieses Modells und mit einem Programm von Hummel & Štefl (2001) wurde die Emissionsvariabilität von 59 Cyg erfolgreich reproduziert. Die Strukturen, die im Spektrum von 59 Cyg beobachtet wurden, wurden auch für den Be + sdO -Doppelstern ϕ Per und für HR 2142 nachgewiesen. Diese Strukturen wuden daher als Indikatoren für Be-Doppelsterne mit heißen, kompakten Begleitern betrachtet. Es wurde nachgewiesen, daß HR 2142 ein Be + sdO -Doppelstern ist. Die spektrale Variabilität weiterer Kandidaten wurde untersucht. Es wurde vorgeschlagen, daß FY CMa ein Be + sdO -Doppelstern und daß κ Dra ein Be + WD-Doppelstern ist. Die Annahme, daß ein bestimmter Anteil der Be-Sterne durch Massen- und Drehimpulsübertrag in einem engen Doppelsternsystem entstanden ist, wurde bestätigt.

SUMMARY

Be binary stars with hot, compact companions

In this study the importance of close binary evolution for Be star formation was investigated. The Be star 59 Cyg was confirmed to be an evolved binary with a sdO companion. The companion was confirmed by a weak He II absorption. Orbital elements and stellar masses were determined. In the spectrum of 59 Cyg, characteristic features were identified. These are a single-peaked emission component, a phase-locked V/R variability, and a "knotty" structure of the absorption lines. According to Štefl et al. (2000), these features are caused by a hot, compact companion (sdO or WD) that photoionizes a sector of the disc of the Be star. Assuming this model and a code of Hummel & Štefl (2001), the emission variability of 59 Cyg was successfully reproduced. The features, observed in the spectrum of 59 Cyg, were confirmed for the Be + sdO binary ϕ Per and for HR 2142, too. Hence, these features were taken as indicators for Be binaries with hot, compact companions. HR 2142 was confirmed to be a Be + sdO binary. The spectral variability of further candidates was examined. It was suggested that FY CMa is a Be + sdO binary and that κ Dra is a Be + WD binary. The assumption that a fraction of the Be stars formed by mass and angular momentum transfer in close binary systems was confirmed.

Contents

List of Figures

List of Tables

Chapter 1

Introduction

About 10 to 20% of all B-type stars in the Milky Way are Be stars, short for B emission line stars (Maeder et al. 1999). By definition these stars are B-type stars of luminosity class III, IV or V having one or more Balmer lines in emission at some time (Jaschek et al. 1981). They are known since the second half of the 19th century when Secchi (1867) discovered the first star showing line emission in its spectrum (γ Cas). The emission arises from a geometrically thin, gaseous, circumstellar disc which is excited by the UV radiation of the Be star.

Be stars are variable on different time scales ranging from seconds, minutes and hours (Harmanec 1984) to several years and decades (Porter & Rivinius 2003). Variability on intermediate time scales of $P \simeq 3$ to 500 days is usually explained with binarity (Carrier et al. 2002). Although they have been known for quite a long time, due to their numerous spectral pecularities, Be stars are still not yet fully explained and a matter of debate (Slettebak 1976; Jaschek & Groth 1982; Slettebak & Snow 1987; Balona et al. 1994; Smith et al. 2000; Maeder & Eenens 2003).

1.1 Astrophysical context

Apart from mass and metallicity, stellar evolution is affected by angular velocity (Maeder & Meynet 2000). This holds especially for stars on the upper main sequence. However, the effect of rotation and, hence, the evolution of massive stars is still not fully understood. Langer & Heger (1998); Heger & Langer (2000) found that the outer layers of rotating massive stars may spin up due to the evolution of the angular momentum distribution. In this context the Ω limit (Maeder 1999) is of specific interest where the effective gravity becomes zero due to critical rotation.

Be stars are a group of stars that belongs to the most rapid rotators. With rota-

tional velocities of roughly 70% (Slettebak 1982), 75% (Van Bever & Vanbeveren 1997) of their break-up velocity, they rotate closest to the critical limit. Recently, Owocki (2003) demonstrated that it is very likely that Be stars rotate even about 100% critical. Due to their rapid rotation, Be stars are important for studies of the evolution of massive stars.

1.2 Formation scenarios of Be stars

Three scenarios have been proposed to explain the rapid rotation of the Be stars: Firstly, Be stars are born as rapid rotators and are able to avoid spin-down during their further evolution. Secondly, they get spun up due to core contraction occuring when the hydrogen inside the core is exhausted. And thirdly, they form due to close binary evolution.

Initially, Kříž & Harmanec (1975) suggested that all Be stars may be interacting, close binaries. In that case, the disc would be an accretion disc. However, this was ruled out, since most Be stars do not belong to active mass transfer binaries with Roche lobe filling giants (Baade 1992; Waters et al. 1991; Floquet et al. 1989; Gies 2000). Hence, current binary scenarios discuss the Be stars not as components of close binaries where mass and angular momentum transfer occurs, but as remnants of close binaries after the mass and angular momentum transfer was completed (Rappaport & van den Heuvel 1982; Pols et al. 1991; Van Bever & Vanbeveren 1997; Berger & Gies 2001). The Roche lobe overflow of the original primary component can result in a rejuvenated, spun-up new primary that appears as a rapidly rotating Be star.

The fraction of Be stars within visual binary systems corresponds to that of normal B-type stars (Jaschek & Jaschek 1987). The fraction of Be stars in spectroscopic binaries is more difficult to estimate. Due to the large rotation velocities, the spectral lines of Be stars are very broad. Accurate measurements of radial velocities (Verschueren & David 1999) and thus studies on radial velocity variations are difficult. Therefore, the detection of spectroscopic Be binaries is seriously inhibited (Jaschek & Jaschek 1987). According to observational results, there is a lack of eclipsing Be binaries (Plavec 1976) and interacting Be binaries with cool companions (Baade 1992).

A hypothesis on the formation of single B stars is that they are ejected from binary systems after catastrophic events like supernova explosions. In this case the distribution of tangential velocities, resulting from a velocity kick when the binary is disrupted, would be expected to be wider than that of normal B-type stars. However, Rinehart (2000) showed that the velocity distributions for both kinds of stars are in agreement. Therefore, the large deficit of proven Be binaries remains.

Due to the lack of confirmed Be binaries, close binary evolution as a general mechanism for Be star formation has been largely dismissed. But even if close binary evolution does not hold for the formation of Be stars in general, it can explain the formation of at least a fraction of that population. To understand the role of close binary evolution for the physics of Be stars, it is necessary to know the true fraction of Be binary systems among them.

1.3 Model predictions for evolved Be binaries

Calculations for case B[1] close binary evolution for intermediate-mass main sequence stars lead to the result that between 5% and 20% (Van Bever & Vanbeveren 1997) and up to 50% (Pols et al. 1991) of all Be stars could have formed this way representing post mass exchange binaries. Therefore, many Be binary systems with evolved companions should exist which have not yet been discovered. Due to the expected low masses for the companions it is difficult to detect them by currently established methods of radial velocities.

Pols et al. (1991) and Vanbeveren et al. (1998) show evolution scenarios for intermediate-mass case B close binary evolution for several initial masses and rates of mass and angular momentum transfer. At the end of the case B mass transfer a binary system with a Be star and a helium star is formed.Typically, the mass of the helium star lies between 0.3 and 2.5 $\mathrm{M}_{\odot}$. This mass and the remaining lifeftimes of the rejuvenated Be star and the He-burning secondary are crucial for the further evolution of the system.

If the lifetime of the helium star exceeds that of the Be star, it will remain a helium star as long as the Be component will stay on the main sequence. Upon leaving the main sequence a final stage as Be + sdO binary is reached. If the lifetime of the helium star is shorter than that of the Be star and the mass of the helium star lies within 0.85 and 2.5–3.0 $\mathrm{M}_{\odot}$, a second period of mass transfer can occur (case BB[2]). If the mass of the helium star at this stage of evolution is smaller than 2.2 $\mathrm{M}_{\odot}$, it will lose enough mass by mass transfer or a stellar wind to form a Be + WD binary. Otherwise, it cannot lose enough mass and will develop into a neutron star forming a Be/X-ray binary as its final stage.

According to Van Bever & Vanbeveren (1997) and Raguzova (2001), 70% of the evolved Be binary systems should have a white dwarf companion (WD), 20%

[1]The primary component of the binary system fills its Roche lobe during its hydrogen shell burning phase. This occurs in most massive close binaries with orbital periods between $4 < \mathcal{P} \leq \sim$1000 d and initial primary masses smaller than $40-50\ \mathrm{M}_{\odot}$ (Vanbeveren et al. 1998).

[2]The primary component of the massive close binary expands significantly during its helium shell buring phase and can fill its Roche lobe for a second time. Therefore, a second period of mass transfer can occur (Vanbeveren et al. 1998).

a helium star (sdO), and 10% a neutron star (NS). Following Pols et al. (1991), even more than 80% of the evolved companions should be helium stars, and the white dwarfs should outnumber the neutron star companions by a factor of 10.

About 30 Be/X-ray binaries with a neutron star companion have been detected (van den Heuvel & Rappaport 1987). These optically faint systems are well observable as high-luminosity X-ray sources with typical X-ray luminosities of 10^{34}–10^{38} $\mathrm{erg/s}$. The X-rays are formed due to accretion of the dense stellar wind of the Be star by the neutron star.

Despite their large predicted number Be + WD binaries are yet to be observed. These systems should be detectable as low-luminosity X-ray sources with typical X-ray luminosities of 10^{29}–10^{33} $\mathrm{erg/s}$ (Waters et al. 1989). The X-rays are generated as in Be/X-ray binaries by wind accretion by the WD.

The best way to discover helium star companions is to study the XUV flux of Be stars at wavelengths below 900 Å (Pols et al. 1991). In this spectral region the flux is increasingly dominated by the helium star. However, due to the strong interstellar extinction in this wavelength range, only nearby objects will be detectable by this method. Contradictory to the large number predicted, only one Be + sdO binary, ϕ Per, has so far been found.

1.4 The Be + sdO binary ϕ Per

The Be + sdO nature of ϕ Per was discovered by Poeckert (1979, 1981). He found a double-peaked He II emission at 4686 Å that does not appear in B-type stars. It has a large velocity amplitude and moves out of phase with the He I lines, attributed to the Be primary. He suggested that this feature should arise in a disc around a small hot secondary.

Thaller et al. (1995) and Gies et al. (1998) found the spectral signature of the secondary component of ϕ Per by Doppler tomographic reconstruction of high resolution UV spectra, observed with the IUE satellite (International Ultraviolet Explorer) and the Hubble Space Telescope respectively. The secondary spectrum is dominated by Fe IV and Fe V lines which are similar to those observed in hot sdO stars. Moreover, ϕ Per has not been identified as an X-ray source. With an orbital period of roughly 127 d and masses of 21 $\mathrm{M}_\odot$ and $3-4$ $\mathrm{M}_\odot$ according to Poeckert (1981) and 9.3 $\mathrm{M}_\odot$ and 1.14 $\mathrm{M}_\odot$ according to Gies et al. (1998), respectively, ϕ Per matches the Be + sdO scenario.

Besides the He II emission, ϕ Per shows additional features that are inherent in a Be + sdO nature. These are single-peaked He I emission, moving in anti-phase to the Be star analogous to the He II emission, phase-linked V/R variations of the line profiles, and the formation of deep shell lines, reappearing periodically at specific orbital phases.

Hummel & Štefl (2001) showed that these features are explicable, if it is assumed that a sector of the Be disc is illuminated by the UV continuum radiation of the hot secondary. This area becomes hotter and more ionized and gives rise to extra emission. This emission is single-peaked and is the cause of the V/R variability of the line profiles. The shell lines occur when the heated sector passes the line of sight between the observer and the Be star.

1.5 Candidates for Be binaries with sdO/ WD companions

Similar features like those observed in the spectrum of ϕ Per were also found in the spectrum of 59 Cyg. Tarasov & Tuominen (1987) reported a V/R variability and variations of the radial velocities of Hα. They suggested that 59 Cyg is a binary with an orbital period of roughly 29 d. Rivinius & Štefl (2000) found a periodicity of the radial velocities of He I 4471 and C IV 1548 and derived an orbital period of 28.1702 d. They discovered that the He I emission at 6678 Å moves in anti-phase to the Be star and found a possible He II emission at 4686 Å. Harmanec et al. (2002) analyzed photometric data of 59 Cyg and determined an orbital period of 28.1971 d. They reported a cyclic V/R variability of He I at 6678 Å. These findings suggest that 59 Cyg is also a Be + sdO binary.

HR 2142 is a known Be binary with an orbital period of roughly 86 d (Peters 1983). It shows two short-lived shell phases which are connected to the orbital phase. They appear shortly before and after superior conjunction when the secondary is in front of the primary. Peters (1983) argues that the observed shell phases occur due to mass transfer in a close binary system. The secondary should, therefore, be a Roche lobe filling giant. Waters et al. (1991) studied the energy distribution of HR 2142. They were unable to establish the signature of a giant star and hence suggest that the secondary is a hot helium star.

Further candidates for Be binaries with evolved companions were selected. One criterion was the occurance of satellite absorptions. These small absorption cores appear in the blue or red wing of specific emission lines at certain orbital phases. Since they cannot be explained by a disc around a single star and are found in the spectra of many known Be binaries like ϕ Per, 59 Cyg, HR 2142, 4 Her, and 48 Per, they are taken as indicators for binarity (Maintz et al. 2003).

Promising candidates for Be + WD binaries are κ Dra and 48 Per. They are suspected to be X-ray sources with X-ray luminosities of a few 10^{31} $\mathrm{erg/s}$ (Peters 1982). Further candidates for Be binaries with hot, compact companions are 4 Her, 88 Her, 17 Tau, η Tau, and ζ Tau (Pols et al. 1991). Like κ Dra and 48 Per, these are known or suspected spectroscopic Be binary stars showing satel-

lite absorptions. Strange variations in the spectrum of FY CMa in early 1987 were reported by Peters (1988). As they resemble the features observed in ϕ Per this star is also a candidate for an evolved Be binary.

1.6 Scientific aim of this work

The scientific aim of the present study is to confirm 59 Cyg as a Be + sdO binary and to establish spectral features that characterize Be binaries with hot, compact companions. These characteristic features are to be identified by comparing the short-periodic features visible in the spectra of the three stars in question, namely 59 Cyg, the suspected Be + sdO binary HR 2142, and the confirmed Be + sdO binary ϕ Per. Finally, by searching these features in the spectra of candidate stars, it is expected to reveal further evolved Be binaries with sdO or hot WD companions from a sample of promising candidates.

For that purpose, archived spectroscopic data of 59 Cyg, ϕ Per, HR 2142, and some of the above mentioned further programme stars were available, observed with the echelle spectrographs HEROS, described in section 2.1, and FEROS during several observing runs from 1990 till 1999 (section 2.2). Further spectra were obtained within the scope of joint projects between the Landessternwarte Heidelberg (LSW), the Universitätssternwarte München (USM) and the Czech Academy of Sciences between 2000 and 2003 (section 2.3 and 2.4). Additional spectra for 59 Cyg were observed during the NEON summer school at the Observatoire de Haute Provence (OHP), France, in 2001 (section 2.5.1). Spectra of 59 Cyg and HR 2142, covering the spectral range around Hα and He I 6678, were provided by the Stellar Department of the Czech Academy of Sciences (section 2.5.2). Furthermore, spectra of 59 Cyg, observed during the MUSICOS-campaign in 1998, covering Hα and He I 6678, (section 2.5.3) as well as IUE data were also available (section 2.5.4).

In chapter 3 the individual characteristics of 59 Cyg are analysed. Based on the description of the stellar spectrum (section 3.1), the measurement of radial velocities and the problems occuring due to rapid rotation are discussed (section 3.2). By applying the frequency analysis to the radial velocities the orbital period is derived (section 3.3). The direct evidence for the secondary, the He II 4686 absorption line, is described in section 3.4, where also possible implications for the determination of the orbital parameters due to this result are discussed. The orbital elements are estimated in section 3.5. Masses for both binary components are derived for likely values of binary inclinations. Stellar parameters derived in this study are compared to those found in the literature (section 3.6). In section 3.7 the phase-locked variability is analysed.

The He I 6678 emission of 59 Cyg was modelled using the sector model of Hum-

mel & Štefl (2001). In this model it is assumed that a sector of the circumstellar disc of the Be star is photoionized by the continuum radiation of the hot companion. This causes extra emission which is responsible for the short-term variability observed in the line profiles of 59 Cyg. The modelling results are presented in chapter 4.

In chapter 5 it is demonstrated that ϕ Per and HR 2142 show the same phase-locked variability features as 59 Cyg. They are taken to identify further Be binaries with sdO or hot WD companions within a preselected sample of candidate stars.

Chapter 6 marks the discussion of this work's results and chapter 7 its summary.

Chapter 2

Observations and data reduction

2.1 The HEROS spectrograph

This study is based upon long-term observations. Most of the data were obtained with the high-resolution spectrograph HEROS (Fig. 2.1 and 2.2). HEROS, short for **H**eidelberg **E**xtended **R**ange **O**ptical **S**pectrograph (Kaufer 1996, 1998), is an upgrade of the fibre-linked echelle spectrograph FLASH (**F**iber-**L**inked **A**stronomical **S**pectrograph of **H**eidelberg), developed at the Landessternwarte (LSW) Heidelberg in 1988 (Mandel 1988, 1994).

HEROS has two separate optical channels with a resolving power of $\lambda/\Delta\lambda \approx 20\,000$. After the light is dispersed at the echelle grating of the spectrograph, the beam is divided by a dichroic beam splitter into a blue and a red channel at roughly 5700 Å. The blue channel covers a spectral range of about 3450 – 5600 Å, the red channel of roughly 5800 – 8650 Å. Both channels are controlled by independent computer systems. Due to the two optical channels a large wavelength range of more than 5200 Å can be observed simultaneously. The former FLASH spectrograph consisted of the red HEROS channel only with a spectral coverage of about 4000 – 6700 Å. The technical data of the spectrograph are summarized in Tables 2.1 and 2.2.

The spectrograph is linked to a guiding unit at the telescope by means of a 10 m optical fibre connection. The guiding unit includes a flatfield and a thorium-argon lamp for the calibrations through the fibre. This makes possible to install the spectrograph detached from the telescope at a mechanically and thermally stable place. Since only the guiding unit with a weight of 30 kg needs to be installed at the telescope itself, the spectrograph can also be used in combination with small telescopes.

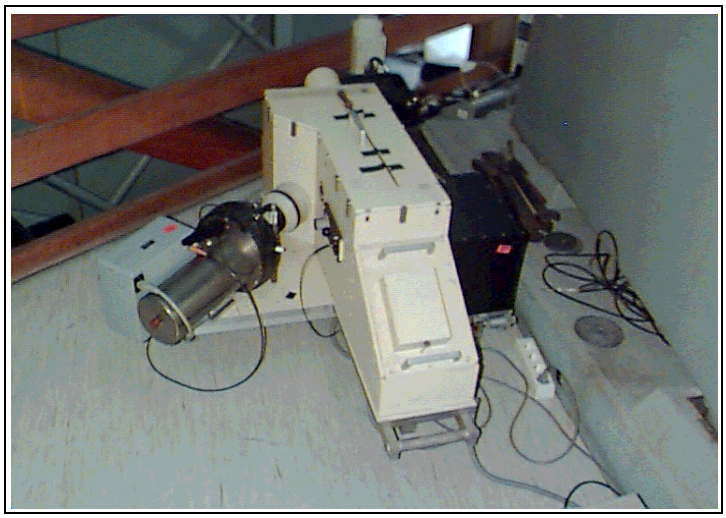

Figure 2.1: Echelle spectrograph HEROS. The former FLASH spectrograph consisting of the white box and the CCD system (small metal cylinder, attached to the left side of the box) constitutes the "red channel" of HEROS. HEROS is an upgrade of FLASH where a second optical system (the "blue channel", the long black tube at the right side of the box) was added. The white box contains the optical fibre mounting, the collimator, the echelle grating, and the beam splitter.

2.2 Archived HEROS and FEROS data

Spectra of 59 Cyg, ϕ Per, HR 2142, and further candidates for Be binaries with hot, compact companions were taken with HEROS and FLASH respectively during five observing runs between 1990 and 1999. These campaigns are listed in Table 2.3. The individual stars and the number of spectra obtained are shown in Table 2.4. These data, stored in the HEROS / FLASH archives, were available for the present study.

With the high-resolution spectrograph FEROS (**F**iberfed **E**xtended **R**ange **O**ptical **S**pectrograph) and the ESO 1.52 m telescope at La Silla spectra of HR 2142 and another Be binary candidate, HR 6819, were observed in 1999. FEROS is a fibre-linked echelle spectrograph with a resolving power of $\lambda/\Delta\lambda \approx 48\,000$. It covers a spectral range of about 3600 to 9200 Å. The spectrograph was mainly developed and built at the Landessternwarte Heidelberg (Kaufer et al. 1997, 1999). Two optical fibres are installed. This allows simultaneous exposure of object and sky, or simultaneous observation and calibration. It has an EEV 2048 $\times$ 4096 15 μm pixel CCD detector with a maximum quantum efficiency of 98% at 4500 Å. Including telescope and detector, FEROS reaches a peak efficiency of 27%. At 3700 Å, in the extreme blue, the efficiency is 7%, and at 9000 Å, in the extreme red, it is 8%. The spectrograph is mounted in the thermally stabilized and humid-

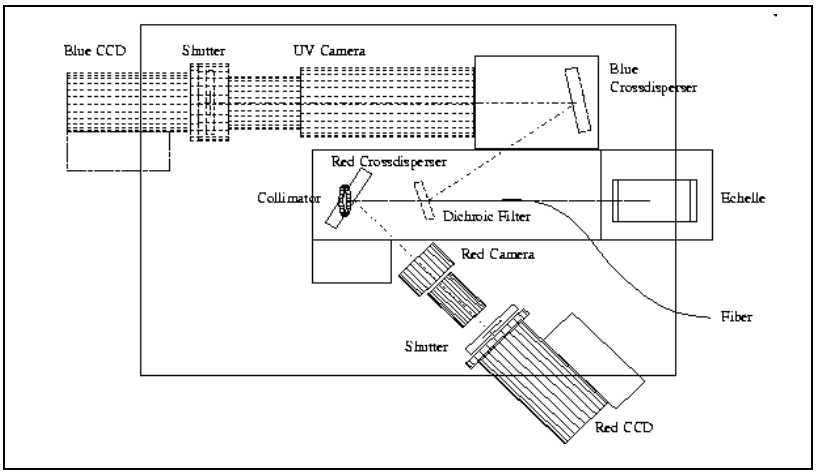

Figure 2.2: Schematic layout of FLASH (solid lines) respectively HEROS (with additional optical system, dashed lines). The light beam (long single dashes) enters the spectrograph by the optical fibre. After deflection at the echelle grating the beam is divided by a dichroic filter. The red light ($\lambda > 5700$ Å) passes into the red channel (short dashes), the blue light is reflected into the blue channel (dashed dotted line).

ity controlled Coudé room of the ESO 1.52 m telescope.

During an observing run from 1998 December till 1999 January one spectrum of HR 2142 was taken. During a further campaign in July and August 1999 nine more spectra of HR 2142 and twelve spectra of HR 6819 were observed. These data were also available for this study.

2.3 Joint projects

Within the scope of joint projects with the Universitätssternwarte München (USM) and the Czech Academy of Sciences (AV ČR) a new monitoring campaign of active Be and Bn stars with the HEROS spectrograph started in May 2000. The co-operation with the Czech Academy of Sciences was planned to last for the following two to three years. For that purpose a new (longer) electronic cable had to be prepared for the connection of the CCD camera to the computer of the blue HEROS channel. It had to be extended by several meters which turned out to be quite critical.

HEROS was installed at the 60 cm telescope of the USM at the Wendelstein Observatory from mid-May till the end of July 2000 (Tab. 2.5). Due to technical problems with the new cable for the blue channel, HEROS was used in "FLASH configuration". This means that only the red channel with the spectral range shifted to 4000 – 6700 Å was used. 50% of the observing nights were available to the

Table 2.1: Technical data of the echelle spectrograph HEROS.

General technical data	
Optical fibre (core diameter)	100 μm
Collimator	f/4.5, f = 360 mm
Echelle grating	31.6 lines/mm
Blaze angle	63.4°
Spectral resolving power, $\lambda/\Delta\lambda$	$\approx$ 20 000 [1]
Signal-to-noise ratio, S/N	$\approx$ 100 per Pixel [2]
Stability	$<$ 1 km/s

[1] : Over the whole wavelength range of the spectrograph
[2] : For a 6 mag star and a 1 hour exposure at 5500 Å with a 50 cm telescope, measured as the inverse of the rms in units of the continuum

Table 2.2: Technical data of the blue and the red channel of the HEROS spectograph.

	Red channel	Blue channel
Wavelength range	5800 – 8650 Å	3450 – 5600 Å
Cross-disperser	300 lines/mm	400 lines/mm
Blaze wavelength	5000 Å	3900 Å
Camera	f/2.8, f = 300 mm	f/2.8, f = 300 mm
CCD	EEV, LN_2-cooled, 1152×770 22μm pixel	SiTE, LN_2-cooled, 2000×800 15μm pixel

Be-star project.

At the end of July 2000 HEROS was dismounted at Wendelstein and transported to the Observatory of the Czech Academy of Sciences in Ondřejov where it was installed at the 2-m telescope of the Stellar Department. The telescope unit was attached to the Cassegrain focus. The telescope is in operation since 1967 and is used for high dispersion spectroscopy. A Coudé slit spectrograph with a new CCD system is also available. The CCD has replaced an earlier Reticon detector.

A long-term cooperation between the Ondřejov Observatory and the Landessternwarte Heidelberg granted 50% of the observing time to the Be star project. The problems with the extended cable could be fixed in early August 2000. Integrated circuits of the control card, responsible for the data transfer, had to be replaced. Then, the observations could be carried out with both HEROS channels as planned. At the end of September 2001 problems with the blue channel oc-

Table 2.3: Observing campaigns with HEROS / FLASH between 1990 and 1999. During these campaigns spectra were obtained of 59 Cyg, ϕ Per, HR 2142, and further candidates for Be binaries with evolved hot companions. (LSW: Landessternwarte; DSAZ: German-Spanish Astronomical Center; ESO: European Southern Observatory)

Observing campaign	Observatory	Telescope	Instrument
1990	LSW Heidelberg, Germany	Waltz – 72 cm	FLASH
1991	LSW Tautenburg, Germany	2 m	FLASH
1997 Aug. – 1998 Feb.	LSW Heidelberg, Germany	Waltz – 72 cm	HEROS
1998 July – Oct.	Calar Alto, DSAZ, Spain	1.23 m	HEROS
1999 May – July	La Silla, ESO, Chile	ESO 50 cm	HEROS

Table 2.4: Spectra of 59 Cyg, ϕ Per, HR 2142, and other Be binary candidates with hot, compact companions. They were obtained with the HEROS / FLASH spectrograph at different observatories during 1990 and 1999 (cf. Tab. 2.3). Spectra observed with FLASH are indicated with "f". Spectra observed with the blue / red channel of HEROS are marked with "b" / "r".

Year	59 Cyg	ϕ Per	HR 2142	κ Dra	4 Her	48 Per	ζ Tau
1990	10 f	—	—	—	—	—	—
1991	—	—	—	195 f	—	—	1 f
1997	1 b / 1 r	4 b / 7 r	—	—	—	1 b / 1 r	—
1998	38 b / 38 r	8 b / 8 r	—	—	2 b / 2 r	—	3 b / 3 r
1999	—	—	11 b / 11 r	—	—	—	—

cured again. As it was planned to dismount HEROS during the winter months, it was decided to continue the observations only with the red channel in the spectral range of 5800 – 8650 Å.

Due to the bad weather in Ondřejov, HEROS was dismounted in October 2001 and observations were interrupted for the winter season. The HEROS observations were restarted at beginning of March 2002. During the winter break the problems with the blue channel were fixed. Due to these problems more spectra in the red wavelength range of 5800 – 8650 Å than in the blue one were recorded (cf. Tab. 2.6).

During the winter of 2002/2003 the HEROS observations were again discontinued. In 2003 the observations were restarted already in February. HEROS was dismounted again at the end of May 2003. In June 2003 the mirror of the 2 m telescope was removed and newly coated.

Table 2.5: Observing campaigns with HEROS / FLASH between 2000 and 2003. One major aim of these campaigns was to obtain further series of spectra for 59 Cyg, ϕ Per, HR 2142, and a number of suspected Be binaries with evolved hot companions. (USM: Universitätssternwarte München)

Observing campaign	Observatory	Telescope	Instrument
2000 May – July	Wendelstein, USM	60 cm	FLASH
2000 August – 2001 October	Ondřejov Observatory	2 m	HEROS
2002 March – October	Ondřejov Observatory	2 m	HEROS
2003 February – May	Ondřejov Observatory	2 m	HEROS

The number of spectra obtained of 59 Cyg and the other stars scheduled for observation during May 2000 and May 2003 are listed in Table 2.6. Due to this monitoring campaign the number of available spectra has increased considerably. Except for 48 Per, at least ten spectra were obtained for those stars, for which no spectra were available before. 67 spectra covering the red spectral range and 58 covering the blue one could be secured for 59 Cyg. The time basis for the observations could thereby be extended for three more years. The long-term HEROS / FLASH observations allowed for collection of very homogeneous data sets.

2.4 HEROS data reduction

Good observing conditions and the large number of available nights, allowed for a large number of spectra to be obtained during the seasons 2000 and 2001. Therefore, data reduction required a lot of time in the early phase of the project. It was carried out with the help of a MIDAS package for the reduction of echelle spectra that was specially modified and adapted to HEROS data (Stahl et al. 1995). Since both HEROS channels are controlled by independent computer systems, the "red" and the "blue" data had to be reduced separately.

First the calibration exposures were checked. If the echelle orders had shifted less than 0.3 pixel on exposures taken every two hours, all flatfields could be averaged to create a master flat. This was necessary to increase the S/N ratio of the flatfield in blue spectral region. The master flat was taken for the flatfield correction. In this way an increase of noise in the spectra due to reduction could be avoided, in particular in the blue wavelength range, where the CCD is less sensitive.

Then the amount of scattered light between the echelle orders was determined.

Table 2.6: Number of spectra obtained for the programme stars of this study between May 2000 and May 2003. (f/W: FLASH observations at Wendelstein; f/O: FLASH observations in Ondřejov; blue: Observations with the blue HEROS channel; red: Observations with the red HEROS channel)

Programme	2000				2001		2002		2003	
Stars	f/W	f/O	blue	red	blue	red	blue	red	blue	red
59 Cyg	13	4	21	21	10	18	10	11	—	—
ϕ Per	21	4	24	25	4	12	1	1	—	—
HR 2142	—	—	10	10	1	5	3	3	3	3
κ Dra	20	1	1	1	14	22	23	23	—	—
4 Her	15	—	1	1	1	4	19	19	—	—
88 Her	—	—	1	1	—	—	—	—	—	—
48 Per	—	—	6	7	—	3	—	—	—	—
η Tau	—	—	9	9	—	2	1	1	—	—
ζ Tau	—	—	6	6	2	4	—	—	—	—
17 Tau	—	—	8	9	—	3	—	—	—	—

The stray-light was modelled by a two-dimensional spline function and subtracted from the object and flatfield spectrum.

The order definition was done by a fit to the echelle orders visible in the master flat. This procedure was not applicable to very blue objects. For these objects more echelle orders were visible in the blue part of the spectrum than for the master flat. To avoid the loss of these orders, object spectra were used for the order definition instead, where the echelle orders were clearly defined. After definition and extraction of the echelle orders, the object spectra were corrected for the background.

For the wavelength calibration thorium-argon spectra, taken before and after the object spectrum, were averaged. About 300 thorium and argon lines, identified in the averaged thorium-argon spectrum, were used for deriving the dispersion coefficients of the echelle orders of the object spectrum. They were used to rebin the object spectrum to a wavelength scale. Simultaneously the heliocentric correction was applied.

Finally, the calibrated orders were merged. Due to imperfections of the flatfielding procedure, low frequency waves, the so-called ripples, remained. In the overlapping parts these ripples were of the order of 1% of the continuum flux. Thus, they could be neglected.

In earlier reductions of HEROS data the normalisation was done by fitting a spline function to the merged and calibrated spectra. The continuum was de-

fined by a number of fixed points. It turned out that this procedure fails in the case of the spectra observed since 2000. The positions of optical components of the HEROS spectrograph seem to have changed slightly compared to the previous years. Therefore, the orders are more bent than in the years before. To overcome this problem a two-dimensional polynomial fit was performed for every spectrum, before extracting the individual orders. This fit was used for the final normalisation of the data.

2.5 Additional spectra

2.5.1 NEON summer school 2001

Eleven additional spectra for 59 Cyg were obtained during the NEON summer school for observing. It was held at the Observatoire de Haute Provence (OHP), France, from July 9 – 21, 2001. Two of these spectra were kindly provided by Yulia Goranova, Arjan Bik, Martin Stuhlinger, and Thomas Rivinius. Seven spectra cover the wavelength range of 4600 – 5100 Å. This range includes the He II line at 4686 Å which is the most prominent line in sdO stars. Four spectra ranging from 4400 to 4600 Å.

The spectra were observed with the slit spectrograph AURELIE and the 1.52 m telescope at a spectral resolution of $\lambda/\Delta\lambda$ = 25 000. The telescope is a twin of the ESO 1.52 m telescope at La Silla and is in operation since 1969. The spectrograph's resolving power reaches up to $\lambda/\Delta\lambda$ = 110 000. The CCD detector has 1024×2048 13.5 $\mu\mathrm{m}$ pixel and was manufactured by EEV.

The data were reduced using the standard MIDAS tools for long-slit data reduction. The normalisation was done with a spline fit to the calibrated spectra. The continuum was defined by a number of fixed wavelength points. The S/N ratio was measured in the wavelength range of 4760 – 4800 Å as the inverse of the rms in units of the continuum and turned out to be roughly 160.

The four spectra covering the region of roughly 4400 – 4600 Å could not be normalized. In this spectral range a lot of line emission is present, and many blended lines are visible (cf. Fig. 3.1, section 3). Therefore, it is not possible to find reliable wavelength points for the continuum definition. These spectra were not taken into account for quantitative analyses.

2.5.2 Reticon spectra

Additionally, 27 spectra for 59 Cyg and two spectra for HR 2142 were kindly provided by the Stellar Department of the Czech Academy of Sciences in Ondřejov. They cover the spectral region of about 6300 – 6740 Å, including Hα and

Table 2.7: Numbers of optical spectra available for 59 Cyg obtaind from 1990 till 2002 (f: Observations with the FLASH spectrograph; b: Observations with the blue HEROS channel; r: Observations with the red HEROS channel; Ret: Reticon spectra from Ondřejov, covering Hα / He I 6678; MUS: Data taken during the MUSICOS campaign, covering Hα / He I 6678; NEON: Data obtained during the NEON summer school at OHP, covering the He II line at 4686 Å). The total numbers of spectra covering the blue and red spectral range, the spectral region of Hα and He I 6678, and the spectral region of He II 4686 are given in the last for colums.

59 Cyg	FLASH / HEROS			Ret	MUS	NEON	Total			
Year	f	b	r				blue	red	Hα	He II
1990	10	—	—	—	—	—	10	10	10	10
1994	—	—	—	7	—	—	—	—	7	—
1995	—	—	—	4	—	—	—	—	4	—
1996	—	—	—	4	—	—	—	—	4	—
1997	—	1	1	2	—	—	1	1	3	1
1998	—	38	38	—	7	—	38	38	45	38
1999	—	—	—	11	—	—	—	—	11	—
2000	17	21	21	—	—	—	38	38	38	38
2001	—	10	18	—	—	7	10	18	18	10
2002	—	10	11	—	—	—	10	11	11	10

He I 6678. The S/N ratio, measured in the wavelength range of 6620 – 6650 Å as the inverse of the rms in units of the continuum, is roughly 400.

The spectra were taken with a Reticon 1872 RF detector on loan from the Lick Observatory and the 2 m telescope of the Stellar Department in Ondřejov in Coudé focus. The Reticon system was installed in 1992. It has one row of 1872 pixels (photodiodes) with a width of 15 μm. The spectral resolution $\lambda/\Delta\lambda$ is roughly 8500.

The spectra were of high interest to the present study, since they were obtained in the years 1994 till 1997 and 1999, when FLASH and later HEROS provided no or only one single spectrum. Thereby, the large six-year gap between 1991 and 1996 in the data set of 59 Cyg, could at least be filled with respect to Hα and He I 6678.

2.5.3 MUSICOS campaign 1998

During the MUSICOS (**M**ulti-**S**ite **Co**ntinuous **S**pectroscopy) campaign from 1998 November 20 till December 13 (Schäfer 2000) seven spectra of 59 Cyg were

obtained. They cover the spectral range of 6530 – 6720 Å, including Hα and He I 6678. The S/N ratio is roughly 200. It was measured in the wavelength range of 6620 – 6650 Å as the inverse of the rms in units of the continuum.

The spectra were observed with the slit spectrograph AURELIE and the 1.52 m telescope at OHP, France (cf. section 2.5.1). The spectral resolution was $\lambda/\Delta\lambda$ = 25 000. These spectra were kindly made available for this study.

An overview of all optical data available for 59 Cyg is given in Table 2.7.

2.5.4 IUE data

The IUE (**I**nternational **U**ltraviolet **E**xplorer) satellite was launched in 1978 and was in operation till 1996. It collected more than 110 000 spectra in the ultraviolet range of more than 9000 objects with -1.5 to 21 mag. The satellite carried a 45 cm Cassegrain telescope and two spectrographs, covering the spectral ranges of about 1150 – 2000 Å and 1900 – 3300 Å. Both spectrographs could be operated in high and low resolution with spectral resolving powers of $\lambda/\Delta\lambda$ = 12 000 and $\lambda/\Delta\lambda \approx$ a few 100.

IUE high resolution spectra of 59 Cyg, ϕ Per, HR 2142, and FY CMa in the spectral range of about 1150 – 2000 Å were investigated. They were downloaded from the IUE Final Archive. The data in this archive are already reduced. For 59 Cyg 193 spectra were available. For ϕ Per only 16 spectra could be obtained. For HR 2142 and for FY CMa as many as 88 and 96 spectra, respectively, were available.

Chapter 3

59 Cyg, a second Be + sdO binary

The Be star 59 Cyg (HD 200 120, HR 8047; B1Ve, Slettebak 1982; B1.5Vne, Chauville et al. 2001) is the brightest component of a multiple system of stars which belongs to the Cyg OB7 association. Emission lines were discovered by Edward S. King in 1904 (reported by Pickering 1905). A variability on a timescale of 28 to 29 days was reported by several authors (Barker 1983; Doazan et al. 1985). Tarasov & Tuominen (1987) found a V/R variability and a variation of the radial velocities of Hα. They suggested that 59 Cyg is a spectroscopic binary with an orbital period of roughly 29 d. Rivinius & Štefl (2000) analysed the radial velocities of He I 4471 and C IV 1548. They found a periodicity and derived an orbital period of 28.1702 d. They discovered that the He I emission at 6678 Å moves in anti-phase to the Be star. Furthermore, they found a possible emission of He II 4686. Harmanec et al. (2002) analyzed photometric data of 59 Cyg, spanning 43 years, and determined an orbital period of 28.1971 d. They found a cyclic V/R variability of He I 6678. These findings suggest that 59 Cyg is also a Be + sdO binary like ϕ Per.

3.1 The optical spectrum of 59 Cyg

The optical spectrum of 59 Cyg is characterized by very broad lines, revealing the star to be a rapid rotator. Literature values for $v \sin i$ range from a low estimate of 260 $\mathrm{km/s}$ (Slettebak 1982), up to 450 $\mathrm{km/s}$ (Hutchings & Stoeckley 1977; Harmanec et al. 2002). As a consequence, most of the weaker lines in the observed wavelength range from 3800 to 8600 Å, which are formed by typically single ionized metals and He I, are smeared out or blended into broad absorption bands. Such bands are visible in the wings of the stronger photospheric absorption lines, namely the Balmer series and some of the stronger He I lines.

Furthermore, during the entire interval, observed from 1990 to 2002, the spec-

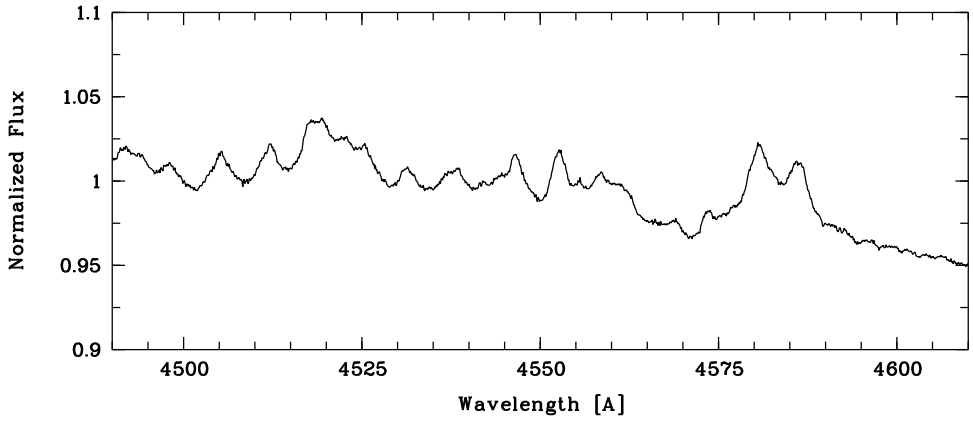

Figure 3.1: A typical region of the spectrum of 59 Cyg, where it is difficult to distinguish between emission and absorption lines.

trum of 59 Cyg was characterized by very strong emission. Broad double-peaked emission lines, including many blends, is visible throughout the observed wavelength range. The broad absorption bands and the strong emission lines make it quite difficult to identify single lines unambiguously, or to determine the photospheric continuum. In some parts of the spectrum, for instance between 4500 and 4600 Å, it is almost impossible to distinguish between absorption or double-peaked emission lines and, thus, to identify the continuum (Fig. 3.1).

The common procedure to handle this kind of problem, namely by subtracting the spectrum of a similar star of the same spectral type, but without emission lines fails for 59 Cyg, as it does for most Be stars. The photosphere of such rapid rotators cannot be described by a single set of parameters. Since effective temperature, $T_{\rm eff}$, and gravity, $g_{\rm eff}$, are not constant throughout the stellar surface of rapidly rotating stars, their spectra are composite spectra arising from local atmospheres with different values for $T_{\rm eff}$ and $g_{\rm eff}$ (Maeder & Meynet 2000). Therefore, it is normally not possible to find a suitable star for a correction.

Modelling the photospheric flux of a rapid rotator with local atmospheres would be an alternative. A model, however, is only as good as the parameters used. This holds for the knowledge of the true rotation velocity and inclination as well as for the assumed stellar input parameters like polar temperature or polar gravity, which are used to calculate the local values on the stellar surface.

Only few spectral lines are strong or conspicuous enough to be clearly identifiable. The useful lines are the Balmer lines from Hα to H_{10}, the Paschen lines P_{14} to P_{20}, the helium singlet lines He I 5016 ($S - P^0$), He I 6678, 4922, 4388, 4144, 4009 ($P^0 - D$), He I 5048 ($P^0 - S$), the helium triplet lines He I 7065, 4713, 4121 ($P^0 - S$),

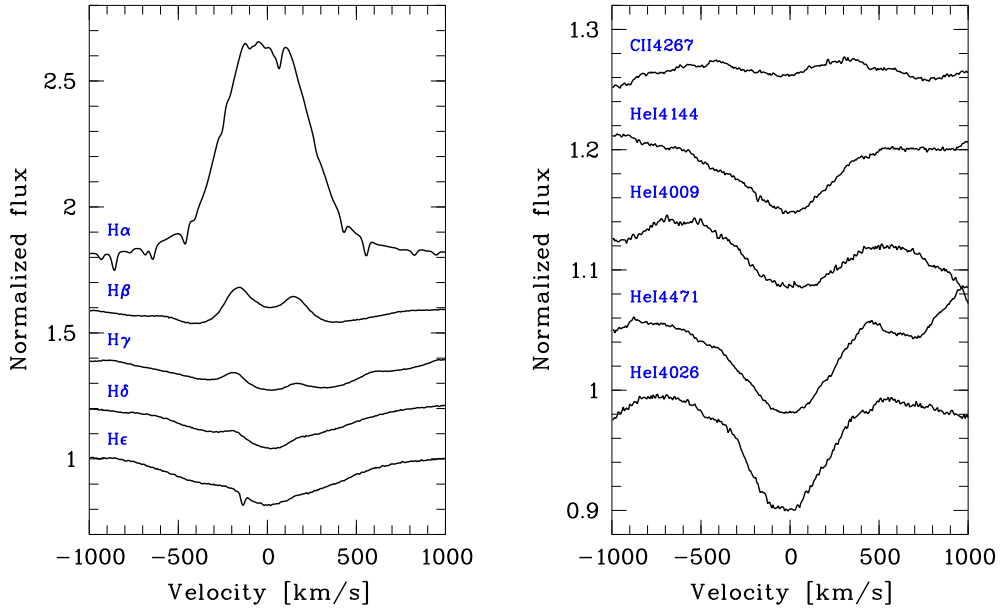

Figure 3.2: Balmer lines (left) and absorption lines (right) of 59 Cyg. The line profiles are the average of all suitable individual spectra. The sharp absorption feature in Hϵ at about -150 km/s is caused by interstellar Ca II absorption at 3968 Å. He I 4471 is blended with Mg II 4481, which is centred at roughly $+650$ km/s.

He I 5876, 4471, 4026, 3820 ($P^0 - D$), and the metal lines C II 4267, Mg II 4481, Fe II 5018, 5169, Si II 6347, O I 7772–5, and 8446. Most of these lines show emission components and/or blends.

Due to very strong line emission, E/C ≈ 1.9 on average, Hα is very broad and no photospheric absorption wings are visible (Fig. 3.2, left). The other Balmer lines are visible in absorption with a central emission component (Fig. 3.2, left). This emission is still strong in Hβ, but weakens from Hγ to H_{10} very quickly. The Paschen lines as well as He I 7065, Si II 6347, and Fe II 5169 are visible in pure emission (Fig. 3.3, left). P_{18} is blended with O I 8446, which is also in emission. He I 6678, 4388, 5876, and O I 7772 show absorption wings and, in part, strong central emission (Fig. 3.3, right).

The blended He I 4471 and Mg II 4481 lines, as well as the He I 4026, 4144, 4009, and 3820 lines are visible in absorption (Fig. 3.2, right). He I 5048, 4713, and C II 4267 (Fig. 3.2, right) are very weak absorption lines and seem to be filled in by emission and/or almost completely smeared out by rotation. The He I 5016 line is blended with Fe II 5018 and the He I 4922 line with Fe II4925 (Fig. 3.3, right). These helium lines show absorption wings. The iron lines are in emission. He I 4121 is in absorption and blended with Hδ.

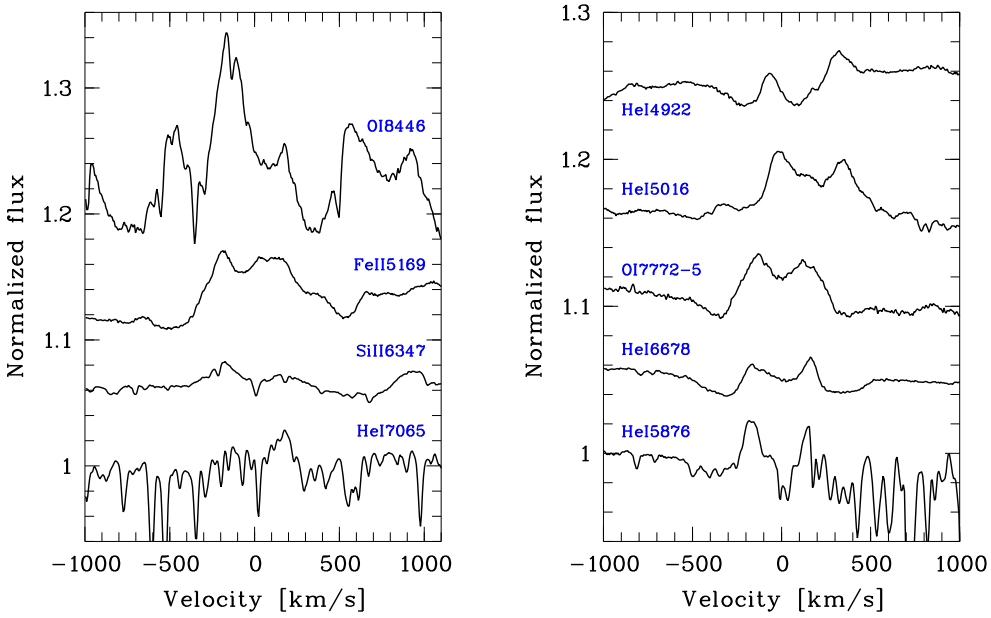

Figure 3.3: Pure emission lines (left), emission lines with photospheric absorption wings, and blended lines (right) of 59 Cyg. The line profiles are the average of all suitable individual spectra. The blue emission wing of O I 8446 is blended with the Paschen line P18. Next to that blend the double-peaked emission line P17 is visible, centred at roughly $+750$ km/s. The red emission wing of Fe II 5169 is broadened by blending with other lines. He I 7065 and the red emission wing of He I 5876 are pervaded by atmospheric absorption bands. The interstellar Na I absorption line at 5890 Å is visible at about $+700$ km/s next to He I 5876.

3.2 Radial velocities

Since most of the identified absorption lines show emission features or blends, only four strong photospheric lines can be considered for reliable radial velocity measurements in order to determine the orbital parameters of the binary system. These are the helium triplet lines He I 4471 and 4026 and the helium singlet lines He I 4144 and 4009 (Figs. 3.2, right, and 3.4). These lines are clearly defined, i.e. they have sufficient contrast between line depth and continuum flux, and show almost no emission contribution from the circumstellar disc of the Be star (cf. section 3.7).

The number of spectra suited for accurate radial velocity measurements compared to the number of available spectra differs considerably for the individual lines (Tab. 3.1). This is most obvious for He I 4026 and 4009, for which no spectra taken earlier than 1997 can be used. The main reason is that these spectra were

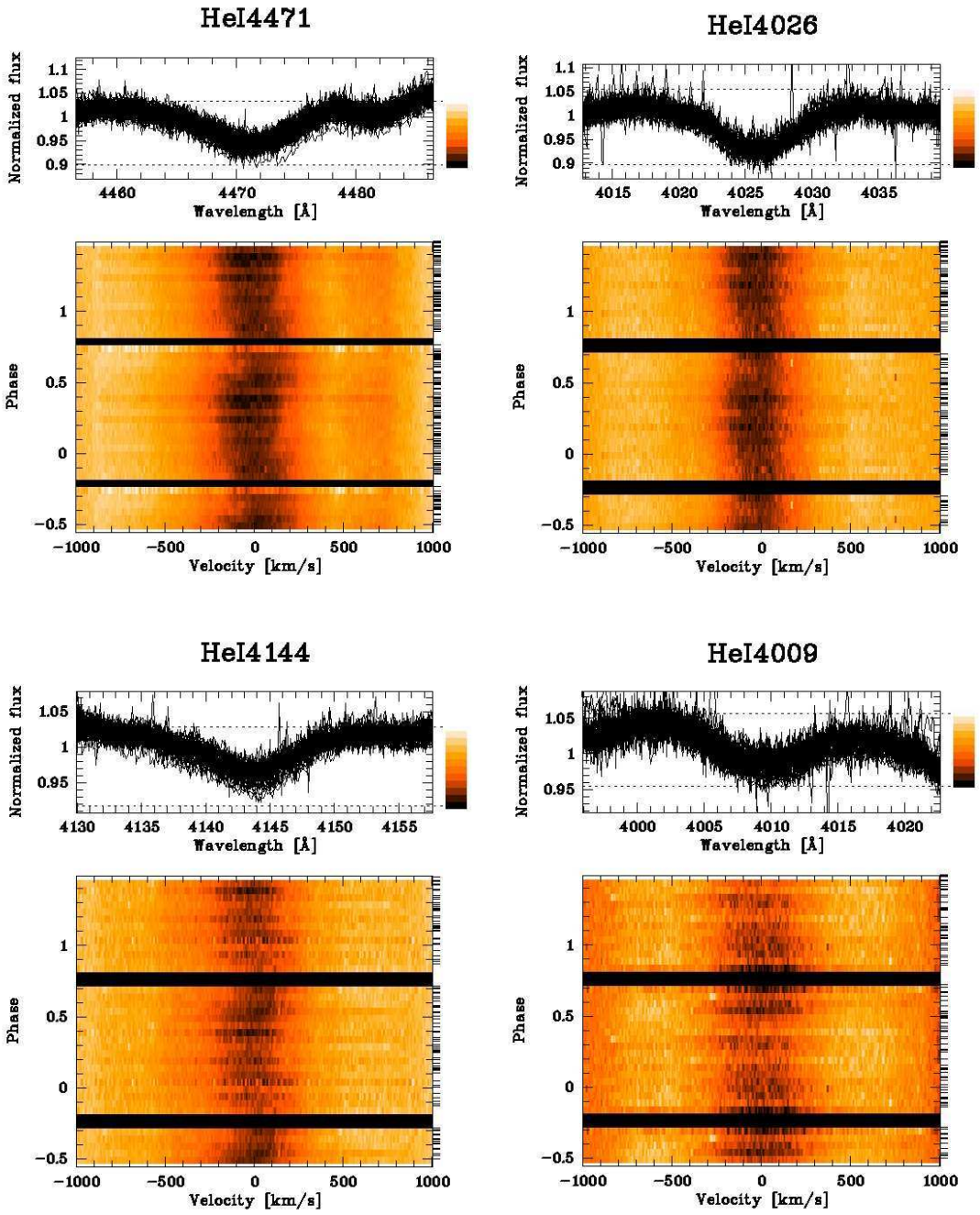

Figure 3.4: Dynamical spectra (cf. section 3.4) of the absorption lines used for radial velocity measurements.

Table 3.1: Number of spectra for the absorption lines of 59 Cyg, suitable for radial velocity measurements, per year and in total. The resulting time basis for the period analysis for each of those lines is also given.

Line	He I 4009	He I 4026	He I 4144	He I 4471
1990	–	–	8	9
1997	1	1	1	1
1998	24	34	22	34
2000	21	21	19	35
2001	5	9	5	10
2002	1	2	–	2
Total number	52	67	55	91
Time basis	6 years	6 years	12 years	13 years

taken with the spectrograph FLASH with a spectral range of about 4000 to 6700 Å. In this case He I 4026 and 4009 were too close to the beginning of the finally reduced spectra, where errors due to CCD artefacts and bad normalization can play a major role. In some cases this was even true for He I 4144. Furthermore, those spectra with a very low signal to noise ratio were not considered.

For measuring radial velocities, three methods were tested for best accuracy: Firstly, determination of the position of spectral lines by fitting a Gaussian to the line centres interactively; secondly, decomposition of observed spectra by minimizing the Fourier transform of the composite spectra with KOREL (Hadrava 1995, 1997); and thirdly, standard cross-correlation (Simkin 1973; Hill 1993).

3.2.1 Fitting the line position with a Gaussian

In the case of rapidly rotating stars visible at high inclination, measuring the position of the line centres by fitting a Gaussian to the profile does not typically yield good results. Due to the high stellar rotation neighbouring lines may blend into one profile, resulting in an asymmetric line shape. Fitting a symmetric Gaussian to such an asymmetric profile leads to ambiguous results. In the case of 59 Cyg the same is true for fitting a Gaussian to the line cores only, even if the fit is performed interactively. This is visible when the starting and ending points for the fits are varied, even if the Gaussian is fitted only to a small region around the deepest point of the profile. The uncertainties of such measurements were much larger than any real Doppler-shift.

3.2.2 Fourier disentangling of composite spectra

The program KOREL from Hadrava (1995, 1997) simultaneously decomposes spectral lines of multiple stellar systems into individual components and determines the orbital solution of the system. This is done by optimizing the coefficients of the Fourier transforms of the composite spectra by a least square method.

An observed spectrum is treated mathematically as a composite spectrum of several stellar components in terms of convolution with shifted delta functions which correspond to the Doppler-shift. The Fourier transform separates the unknown modes of each component spectrum into an independent set of equations for multipliers of known functions of the radial velocities of the individual components. These are solved by direct calculation of the coefficients and optimized by a simplex method as a least square fit with regard to the orbital elements. In contrast to standard cross-correlation, KOREL correlates a number of observed spectra taken at different orbital phases at once. The decomposed individual spectra are used instead of a chosen template. KOREL enables a simultaneous spectral disentangling and derivation of radial velocities and orbital elements of a multiple stellar system with up to five components. As a by-product the contribution of the individual stellar components to the observed line profiles are determined.

This method can be successfully applied if the shape of the observed line profiles do not vary. The strength of the individual lines can vary during the orbital motion due to effects of binarity like eclipses of binary components or due to airmass and humidity influencing the telluric spectrum. It fails if the line profiles show additional intrinsic variability leading to a variable shape of the profiles. This could be misinterpreted as variability according to the above mentioned variations.

As demonstrated in section 3.7, even the four strong helium absorption lines show variable emission, which is caused by the hot companion. This emission turned out to be too strong for the program to work properly. Therefore, it could not be used for radial velocity measurements and the determination of the orbital elements of 59 Cyg.

3.2.3 Cross-correlation

Due to the problems sketched above, standard cross-correlation (Simkin 1973; Hill 1993) remained the only method applicable for reliable radial velocity measurements of the photospheric absorption lines. The average spectrum of all suitable individual spectra was used as a template for the correlation. Since the width of the individual line profiles (roughly 1000 $\mathrm{km/s}$) is much larger than the maximum shift between the single spectra relative to the template (less than roughly 70 $\mathrm{km/s}$), a correction of the template spectrum for the individual Doppler-shifts

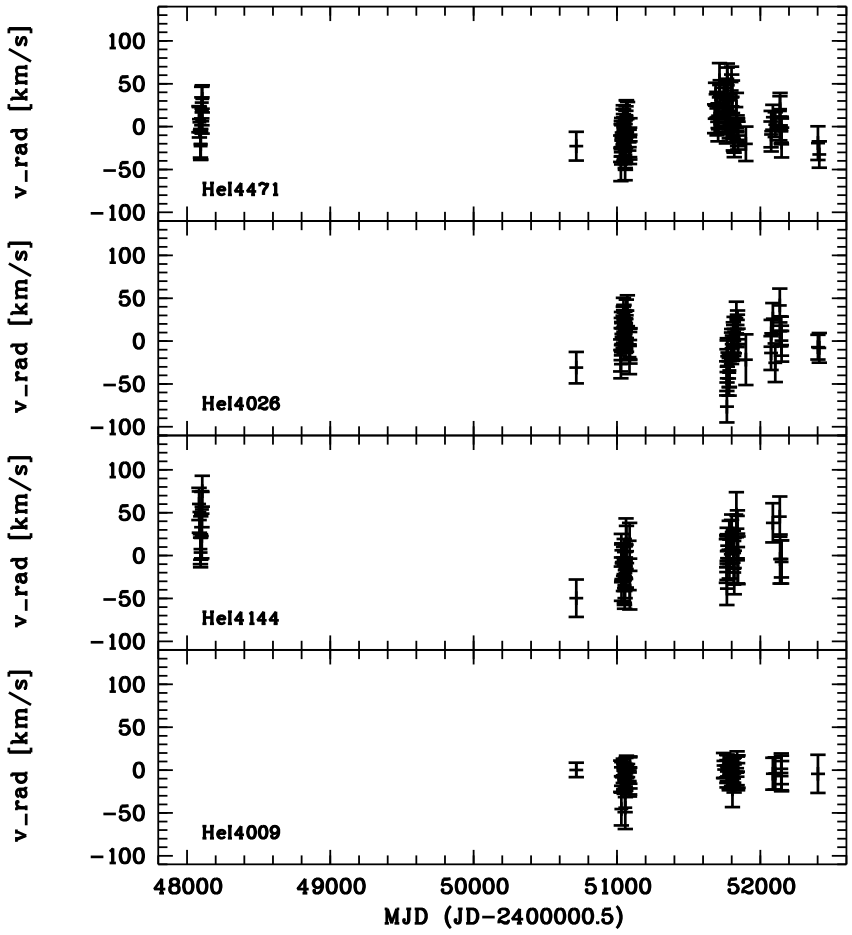

Figure 3.5: Radial velocities and errors for He I 4471, 4026, 4144, and 4009, measured by cross-correlation.

does not improve the final results. Therefore, the template was not corrected.

The broad absorption lines with their asymmetrical shape were also problematic for the cross-correlation method. Since the resulting correlation peaks were broad and asymmetric, the exact position of the peaks, corresponding to the radial velocity of the spectral line, was difficult to determine (Verschueren & David 1999). Owing to very strong line emission throughout the stellar spectrum, only individual lines were suitable for the correlation. Spectral regions including several lines, enabling minimisation of individual uncertainties, could not be used. Spectra with comparatively high noise caused a substructure in the correlation peaks.

As mentioned before, the four absorption lines suitable for radial velocity mea-

Table 3.2: Number of Hα spectra of 59 Cyg, given per year. The total number of spectra is 150. The resulting time basis is 13 years.

Year	1990	1994	1995	1996	1997	1998	1999	2000	2001	2002
Spectra	10	7	4	4	3	45	10	38	18	11

surements are not absolutely free of emission. In these lines emission appears at specific orbital phases and is confined to the line centres. Since the shape of the individual lines is compared to the shape of the template, the position of the correlation peak is affected mainly by the position of the line as a whole, especially the position of the line wings. Emission components in the line centre are less critical and only enhance a possible substructure of the correlation peak. It turned out that noise is a much bigger problem. For each spectral line the profiles which are too noisy are not taken into account for the measurements. Therefore, the number of spectra for which radial velocities were measured varies for the different spectral lines.

The most objective method would appear to be an automated measuring procedure. This does, howerver, not render the most consistent results because of the broad, asymmetric, and more or less finely structured correlation peaks. Instead, the peak position was measured interactively by centreing a Gaussian to the uppermost part of the correlation peak (Verschueren & David 1999). The central position of this Gaussian was then taken as the Doppler-shift of the spectrum.

The uncertainty was estimated by measuring the width of the uppermost part of the correlation peak, where the peak is clearly defined. In that region the broadening resulting from the broad correlated spectra does not play an important role. This allows for consideration of possible mistakes concerning the definition of the peak centres due to the fine structure. These rather large uncertainties (about 10 to 25 $\mathrm{km/s}$), should also provide a good estimate for the systematic errors and, therefore, include uncertainties due to errors of calibration or normalization. In Figure 3.5 the measured data for He I 4471, 4026, 4144, and 4009 are shown.

In addition, radial velocities were measured for Hα, for which 150 suitable spectra were available taken within a period of 13 years (Tab. 3.2). This was done by cross-correlation analogous to the absorption lines. That means the whole of the line profiles were used for the correlation. The average spectrum of all suitable spectra was taken as the template. Unlike the absorption lines, Hα is dominated by strong disc emission varying in strength and shape on a timescale of about a year between 1990 and 2002 (Fig. 3.6). Only emission wings are visible. The absorption is filled in completely. The shape of the upper part of the line profiles

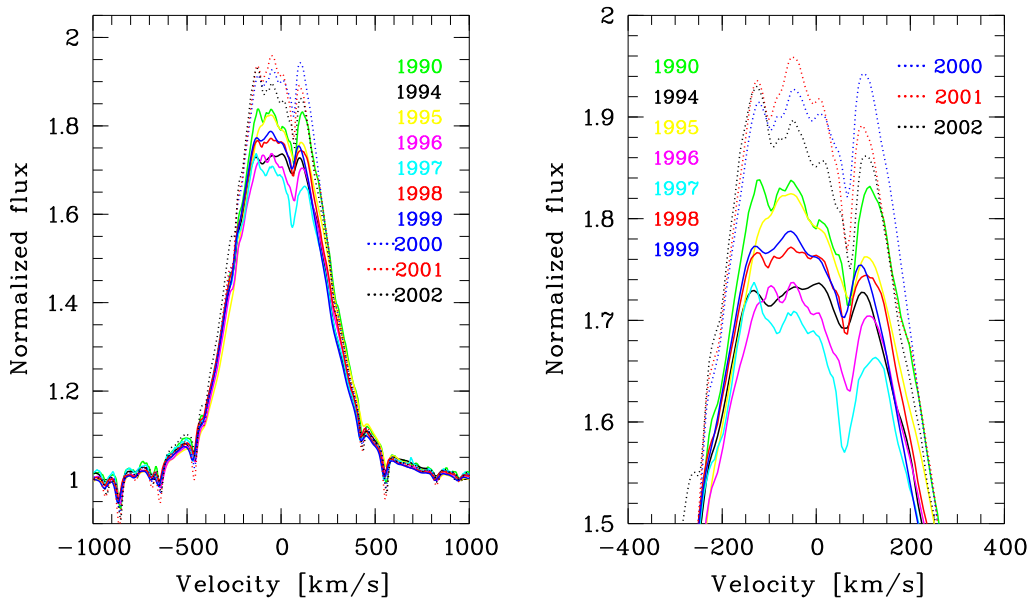

Figure 3.6: Longterm variability of the emission intensity of Hα between 1990 and 2002. The profiles are averaged for the individual years (Tab. 3.2). Since the number of available spectra and the orbital phases represented differ for every year, substructures may occur in the uppermost part of the averaged profiles.

is strongly influenced by the phase-locked short-term emission variability. During specific orbital phases the profiles differ strongly from the averaged line profile (Fig. 3.7).

It is not clear whether the phase-locked emission variability affects the bottom parts of the Hα emission, as well, or if there are additional processes, possibly altering the emission wings arbitrarily. Therefore, the radial velocities measured in the emission have to be used with care. In contrast, Harmanec et al. (2002) favour radial velocities determined for the bottom parts of the Hα and He I 6678 emission lines. They argue that these parts of the emission wings form close to the Be star in a symmetrically stable part of the disc. Therefore, they should be less influenced by variable emission components and represent the motion of the Be star better than absorption lines which are partly filled with emission.

In this study only the radial velocities derived for the strong helium absorption lines were used for the further investigations of the Be primary. They are preferred, since they form directly in the photosphere of the Be star and should represent the orbital motion of the Be star best. In section 3.5 it will be demonstrated that the emission contribution observed during special orbital phases indeed slightly alters the radial velocities measured during these phases. The effects

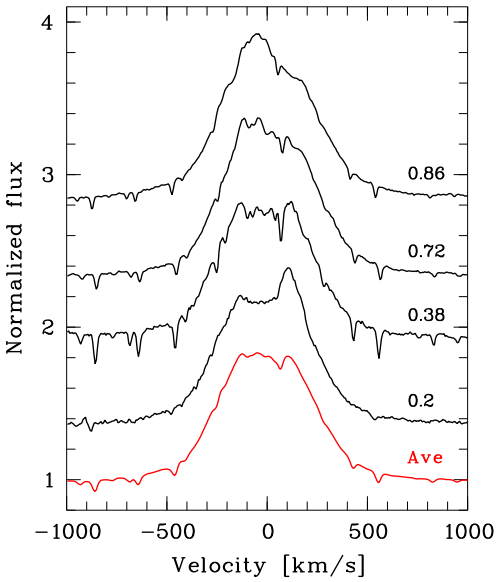

Figure 3.7: Individual profiles (black) and averaged profile (red) of Hα. The average spectrum was taken as template for the cross-correlation. The numbers denote the orbital phases during which to the individual spectra were taken.

on the radial velocity curve of the Be star and the determination of the orbital elements are discussed.

3.3 Orbital period

The study of Rivinius & Štefl (2000) used HEROS spectra obtained between 1990 and 1998 in combination with IUE data for their analysis. The present study determines the orbital parameters of 59 Cyg on the basis of radial velocities of the HEROS data alone. This was made possible by the monitoring campaign carried out at Wendelstein and Ondřejov observatories from 2000 to 2002. About 50 additional spectra of 59 Cyg were taken, extending the time basis by three more years (Tab. 3.1) totalling 13 years.

For each of the four helium lines discussed above, He I 4471, 4144, 4026, and 4009, a separate time series analysis was carried out. In a first step the phase dispersion minimization method, PDM, as described by Stellingwerf (1978), was applied to the radial velocities of the absorption lines. The method works in the following way: Assuming a range of possible periods, for each of the observed line profiles the corresponding phases are determined. Then the radial velocities derived for those spectral lines are sorted into a number of phase bins, according

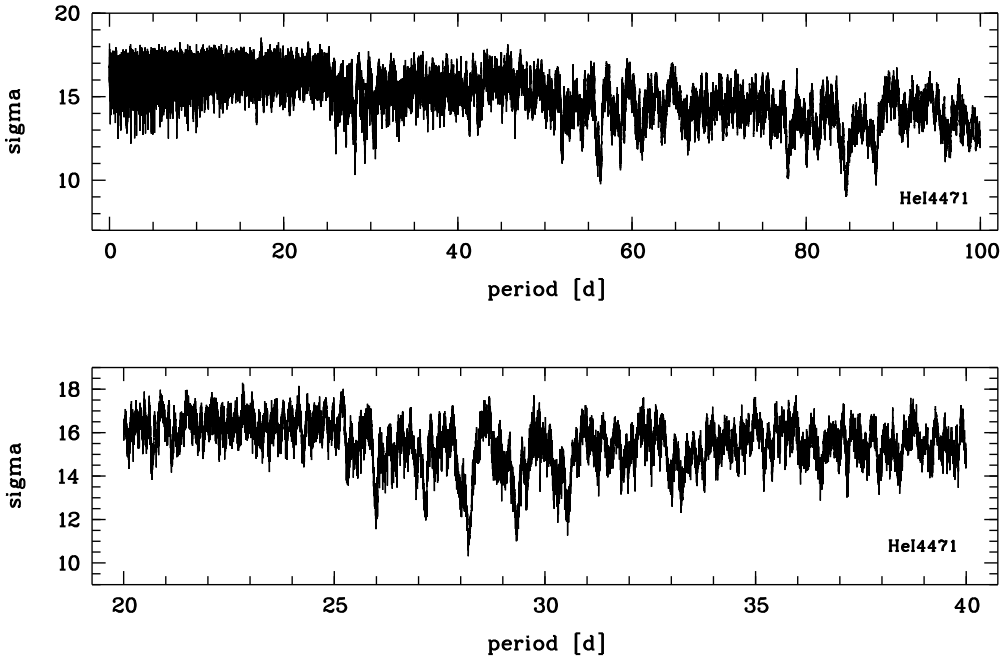

Figure 3.8: Results obtained with the PDM method for He I 4471 radial velocities, using a step size of 0.001 d and 20 phase bins. In the upper panel the entire explored period range from 0 up to 100 days is displayed. The lower panel shows the range around the earlier reported 28/29-days periodicity.

to the computed phases. The mean of the standard deviations is calculated for each individual bin. The better the data are sorted into those bins of the given period the lower the respective standard deviations will be. Since this method is independent of the signal shape and can handle less homogeneous data sets, it is well suited to give an overview of possible periods and problems arising from aliasing.

The period search was carried out for a period interval from 0 up to 100 days, using step sizes between 0.001 and 0.0001 d. The number of phase bins was varied from 5 up to 30. Only for He I 4471 and 4026 more than 20 bins were used, where more than 60 suitable spectra were available. For the other lines this many bins would have caused problems because of empty bins (Tab. 3.1). Varying the step sizes for the period-search and the number of phase bins did not lead to significantly different results.

Together with some aliases, the earlier reported periodicity of 28 to 29 days is present unambiguously in the He I 4471 radial velocities (Fig. 3.8), but cannot be detected reliably in the other lines. In He I 4471 additional stronger minima appear at about twice and three times the 28 to 29 day period, but significant

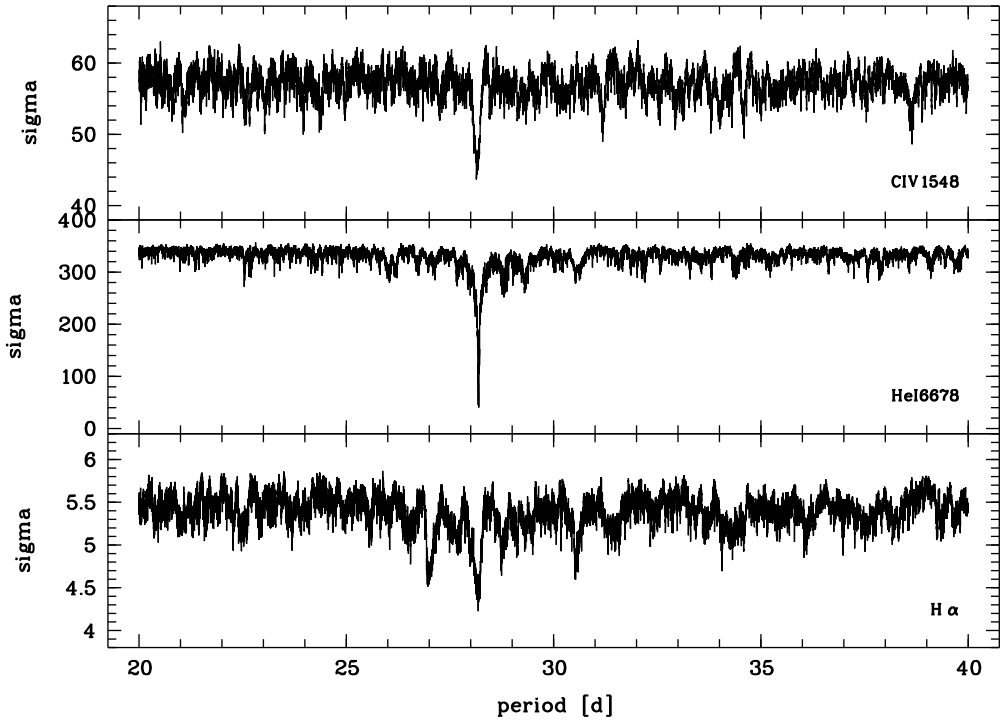

Figure 3.9: Results of the period search obtained with the PDM method for C IV 1548, He I 6678, and Hα. Since there are no other relevant minima, only the time interval around the 28-day period is shown. The method was applied with 20 phase bins and a step size in time of 0.001 d.

minima corresponding to alternative orbital periods are not to be be found.

It is not too surprising that He I 4144, 4026, and 4009 do not show any significant minima. As demonstrated in Table 3.1, the time basis of He I 4026 and 4009 spans only over 6 years, and only 67 and 52 measured radial velocities respectively are trustworthy. This is about half the amount of time compared to He I 4471 for which a time basis of 13 years and 91 spectra are available. The time basis of 12 years for He I 4144 is about the same as for He I 4471. But there are only 55 suitable spectra available for He I 4144. This is only roughly half the amount of data compared to He I 4471.

To confirm that the 28-day period is the only relevant one, the PDM method was also applied to the radial velocities of the ultraviolet C IV doublet line at 1548 Å. For this line 181 IUE spectra obtained between 1978 and 1994 are available, i.e. a time basis of 17 years. The radial velocities were determined by measuring the position of the blue line wing relative to the central wavelength using the graphical cursor. This is preferable to other methods, since the blue part of the line profile

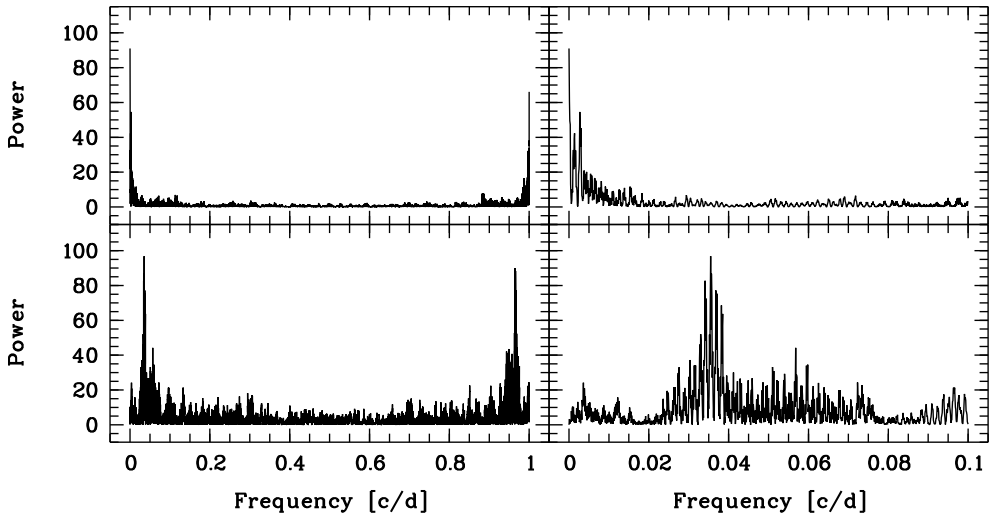

Figure 3.10: Results of the frequency analysis with AOV for He I 4471: Window function (upper panel) and power spectrum (lower panel) are shown for the entire investigated frequency space (left) and in the range of the orbital period (right).

is less variable compared to the rest of the profile, which is blended with the other line of the doublet at 1551 Å.

Furthermore, the radial velocities of the short-term variable emission component were measured in He I 6678, where this emission is visible best. This characteristic feature occurs in most lines with emission and is assumed to arise due to the secondary component of the binary. It is discussed in section 3.7. The PDM method was also applied to these data. 137 spectra were available for He I 6678, spanning a time interval of 13 years. The radial velocities were measure by fitting a Gaussian to the peak of the emission feature.

For C IV 1548 and He I 6678 the period search was carried out within an interval from 0 up to 100 days, too, using a step size of 0.001 d and 20 phase bins. Strong minima appear only for a period around 28 days with additional strong minima at about twice and three times that value. These results confirm the findings for He I 4471. The minima found for C IV 1548 and He I 6678 are more pronounced and better defined (i.e. narrower) than for He I 4471, in particular for He I 6678 (Fig. 3.9, top and central panel).

The PDM method was also applied to Hα and led to the same results as for He I 4471, C IV 1548, and He I 6678 (Fig. 3.9, lower panel). The periodicity around 28 days is confirmed. In all data available for this work, there is only one period found with the PDM method, representing the orbital motion of the binary.

Two more time series analysis techniques were applied to the radial velocity

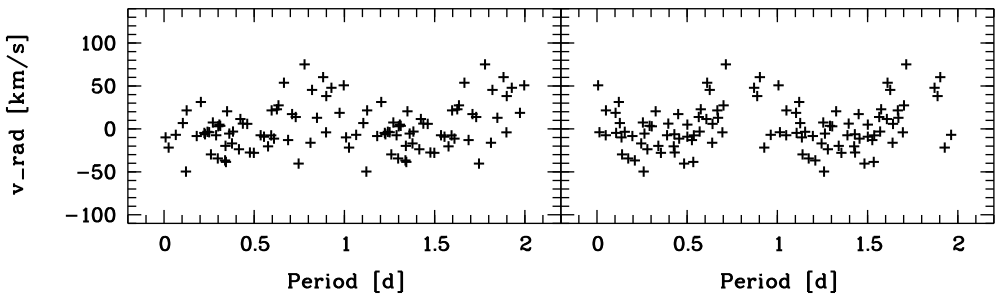

Figure 3.11: Radial velocities of He I 4144 sorted with periods of 25.49 d (left) and 28.192 d (right).

data of the four photospheric lines. These methods are the analysis-of-variance method, AOV, from Schwarzenberg-Czerny (1989) and the method from Scargle (1982) to compute periodogrammes for unevenly distributed data. Other than the PDM method, they also provide information about amplitude and phase of the variability, and will also identify non-sinusoidal variations through the power of the harmonic frequencies, to allow for an initial guess of the eccentricity. Both methods are implemented in the MIDAS TSA package for time series analyses (Schwarzenberg-Czerny 1993; ESO-MIDAS 1995). In order to be able to search for more than one period, i.e. including the harmonics, a procedure as described by Kaufer et al. (1996) was used, where previously found periods are removed iteratively by fitting sinusoids to the original data. This is equivalent to a CLEAN procedure with unity gain. The explored frequency space ranged from 0 up to 1 c/d, using a step size of 10^{-4} and 10^{-5} c/d. Both methods were applied to all data from all four photospheric absorption lines.

For He I 4471 one significant period was found, as expected, between 28 and 29 days. Both methods, AOV and Scargle, yielded the same value of P = 28.192 $\pm$0.004 d. In Figure 3.10 window function and power spectrum are shown, computed with AOV. The window function has no features in the frequency range of the detected period and should, therefore, have no influence. Figure 3.12 shows the radial velocities for He I 4471, sorted with the 28.192 d period.

When a step size of 10^{-5} c/d was applied, a period above the significance level of 3σ was also found for He I 4144 with both methods. With a value of 25.49 $\pm$0.02 d it is outside the expected range. Its power is less than half the power of the 28.192 d period detected for He I 4471. As shown in Figure 3.11, the data are sorted well by the 28.192 d period, with even less scatter than with the 25.49 d period (see also Figure 3.12). The velocity amplitude is roughly the same as the one of He I 4471 sorted with the 28.192 d period (Fig. 3.12).

For He I 4026 and 4009 no reliable period was found. But as shown in Fig-

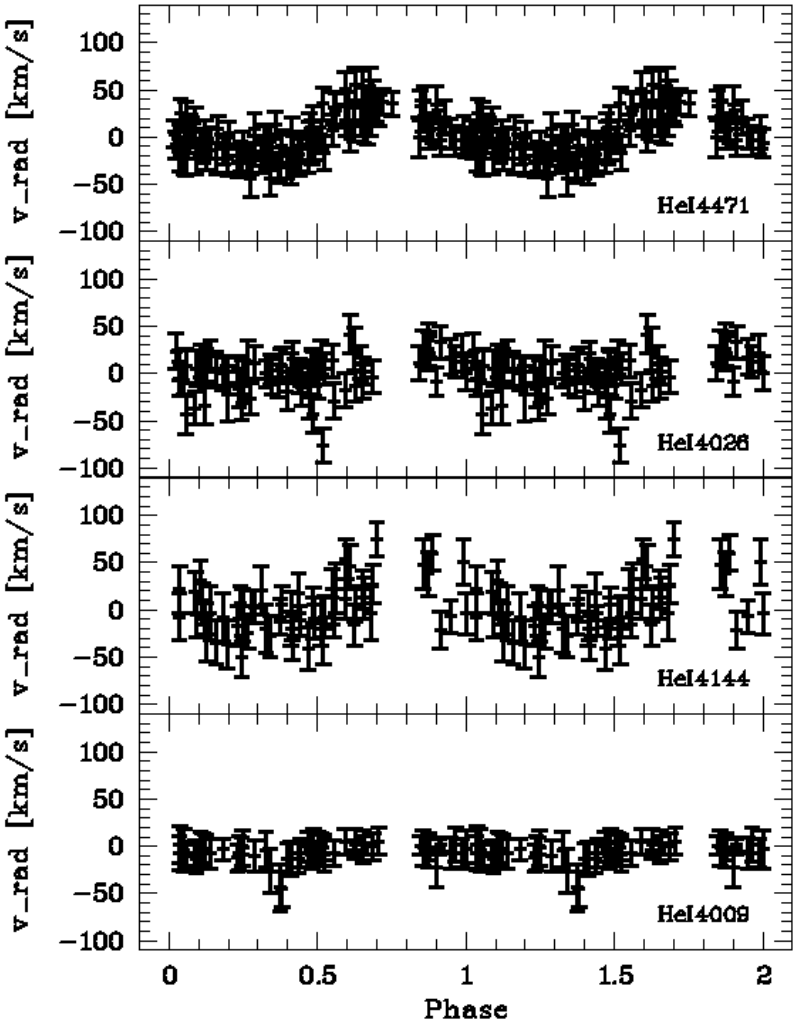

Figure 3.12: Radial velocities of the absorption lines He I 4471, 4026, 4144, and 4009, sorted with the orbital period of 28.192 d.

ure 3.12, also He I 4026 is sorted well by the 28.192 d period, again with roughly the same velocity amplitude. He I 4009 may vary with that period, too (Fig. 3.12), but the radial velocity variations are small. It is not clear why it does not behave like the other three lines. Therefore, it is not possible to make a reliable statement about this line.

Again it is not surprising that no period above the 3σ threshold was found for He I 4026, since the time basis for He I 4026 is only about half that for He I 4471 and 4144 (Tab. 3.1). The 25.49 d period, detected for He I 4144, is very likely not real. It only turns up if the very small step size of 10^{-5} c/d is applied, but

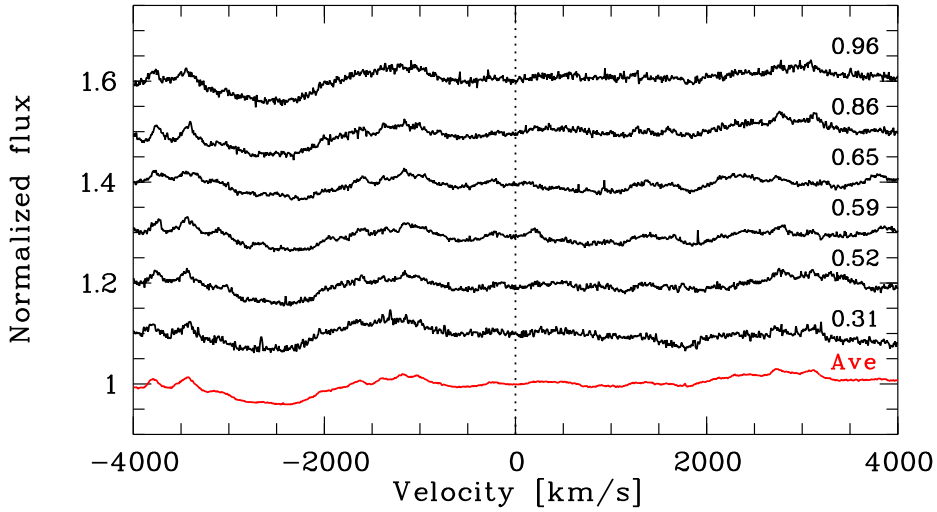

Figure 3.13: Averaged spectrum and individual line profiles showing the spectral region of He II 4686. A reliable He II emission is hardly detectable. The numbers on the right indicate the orbital phases during which the single sectra were obseved.

not if 10^{-4} c/d is used. In contrast, the 28.192 d period in He I 4471 is found with both step sizes and has about twice the power than the 25.49 d period. Since there are about twice as many spectra available for He I 4471 than for He I 4144 (Tab. 3.1), the detection of a true periodicity for He I 4471 is much more likely than for He I 4144. Considering also the results of the PDM method, in particular for C IV 1548 and He I 6678, the 28.192 d period is the only trustworthy one, considered to be the orbital period of the Be binary system. All following investigations in this work will use this period.

Orbital parameters were calculated using the radial velocities of He I 4471 and will be discussed in section 3.5.

Based on a study of *V* magnitude observations spanning over 43 years Harmanec et al. (2002) found a period for 59 Cyg of 28.1971 ±0.0038 d. Within the errors that period agrees with the period obtained in the present study.

3.4 He II 4686

Due to the strong line broadening, the resulting blends, and the strong line emission in large parts of the spectrum of 59 Cyg (see section 3.1), it was not possible to find a clear signature of a hot, compact companion in the individual spectra or the averaged one (Fig. 3.13). Therefore, dynamical spectra had to be computed

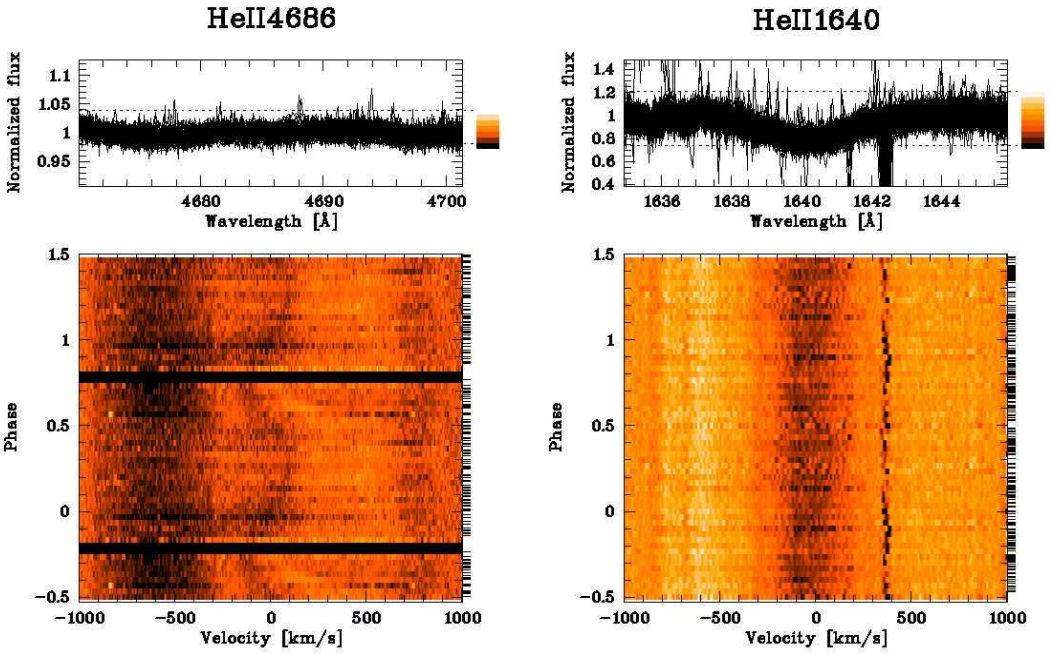

Figure 3.14: Line profiles and dynamical spectra of the He II 4686 and He II 1640 lines. The individual spectra were sorted into 30 phase bins and averaged in each bin seperatly. Weak absorption features are visible, moving in anti-phase to the Be primary (cf. Figs. 3.15 and 3.24). These features are interpreted as absorption lines, formed in the photosphere of the secondary star.

which are more sensitive to weak features.

For that purpose the full cycle was divided evenly by sorting the single line profiles into 30 phase bins. All spectra within one bin were averaged. The averaged spectra were plotted bin by bin into a two-dimensional frame using velocity as abscissa and phase as ordinate. The local intensities are represented by different colours. Phase 0.0 corresponds with the superior conjunction of the primary, i.e. when the secondary is in front of the Be star.

Several He II lines, in particular He II 4686 which should be very prominent in an sdO-star, and several multiple ionized metal lines characteristic for O-type stars were searched for.

A weak absorption feature was found in the dynamical spectra of He II 4686 and He II 1640 (Fig.3.14). As it moves in anti-phase to the Be primary with a velocity amplitude of roughly ± 100 km/s in both lines (Fig. 3.15, cf. Fig. 3.14 for He II 1640). This a distinctive feature of the secondary star only. Since even early B-type stars do not show He II 4686, the absorption must originate in the photosphere of the secondary and, hence, contitutes a direct evidence for a hot,

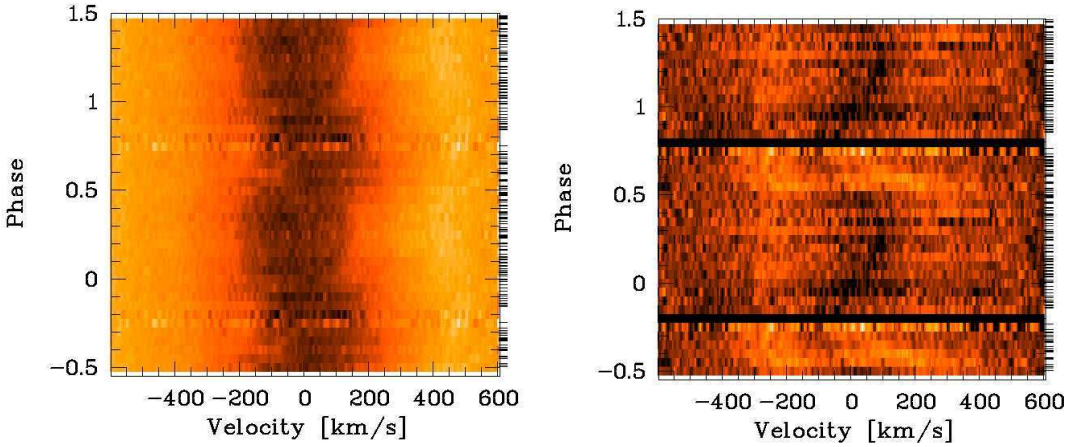

Figure 3.15: Comparison between He I 4471 (left) and He II 4686 (right). He I 4471 forms in the photoshpere of the Be star. He II 4686 moves in anti-phase to He I 4471 and has a larger velocity curve. Therefore, it must originate in the photosphere of the hot secondary.

compact companion.

Other than He II 1640, which also has some photospheric contribution from the Be star, the much clearer He II 4686 feature can easily be traced in the dynamical spectrum. The radial velocity in each phase bin was measured three times interactively with the graphical cursor and averaged. The resulting radial velocities were used for an independent study of the orbital parameters (section 3.5).

In the averaged spectrum of the 99 usable spectra the He II 4686 absorption feature is already visible, but cannot be identified unambiguously (Fig. 3.16, left column, upper panel). Since it is not yet corrected with regard to the orbital motion, the whole profile is much broader and less pronounced. For analysis, the spectra had to be corrected with respect to the orbital motion.

The radial velocities measured for He II 4686 were also used for correcting the 30 phase-binned spectra, extracted from the dynamical spectrum, for their Doppler-shift due to the orbital motion. These shift-corrected spectra were averaged and clearly show the He II 4686 absorption line, which is quite sharp compared to the broad lines of the Be star (Fig. 3.16, left column, middle panel). The equivalent width of He II 4686 in the combined spectrum is 14 mÅ.

For comparison, the same procedure was applied to the He II 1640 data (see Fig. 3.16, right column, middle panel). The core of the resulting line profile is also narrower compared to the one visible in the averaged spectrum of the original data (Fig. 3.16, right column, upper panel), but the line wings seem to be slightly broader. This suggests mean that the profile of He II 1640 is a composite of a large contribution by the Be primary and a smaller one from the secondary, which

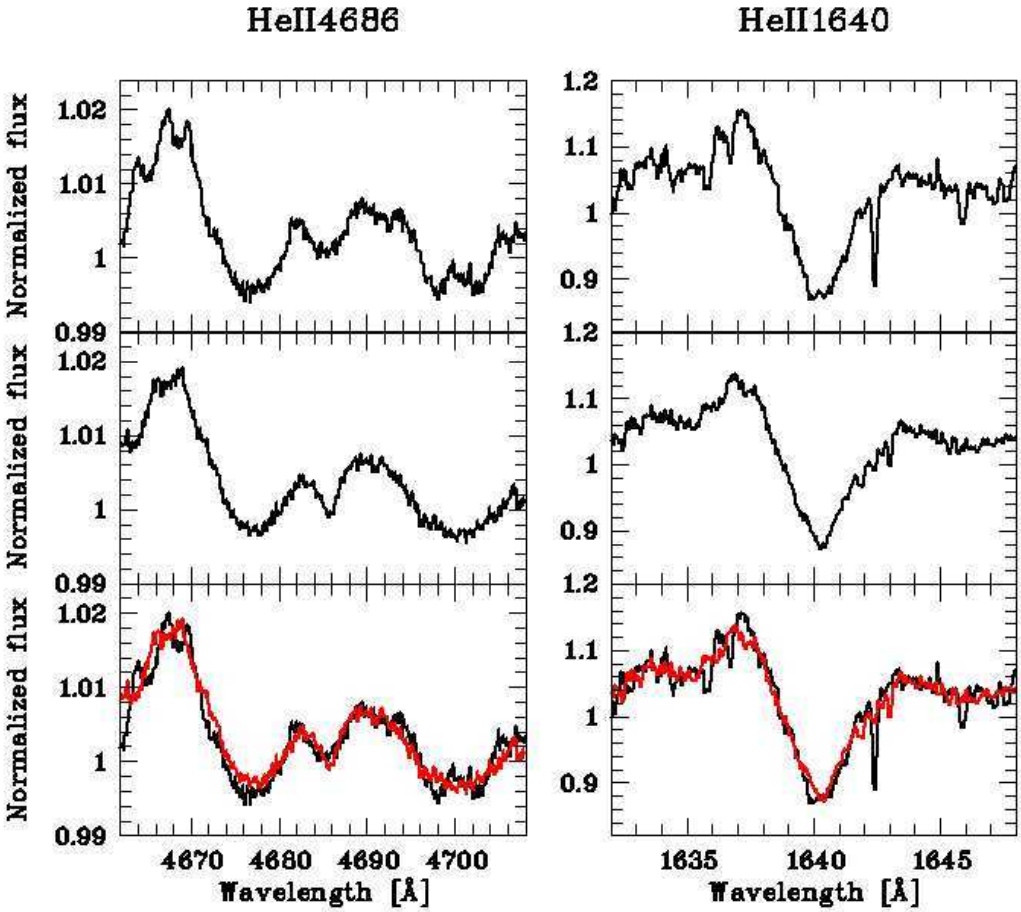

Figure 3.16: Averaged spectra of He II 4686 and He II 1640: Average of all original spectra (upper panels), average of Doppler-shift corrected profiles (middle panels), comparison between the means of the original (black) and the shift-corrected (red) spectra (bottom panels).

is focused around the line centre with a lower rotational broadening.

The same procedure, namely extracting, shift-correcting, and averaging the phase-binned profiles of a dynamical spectrum was also applied to several other lines characteristic for O-type stars. Their examination, however, rendered no further features.

The detection of the He II 4686 absorption line i.e the direct proof of the secondary component of 59 Cyg enables an independent check of the orbital elements. This discovery gave room to narrow down the characteristic parameters of the binary system.

Table 3.3: Orbital elements of 59 Cyg computed for He I 4471 (photospheric absorption of the primary) with VELOC and FOTEL.

Orbital parameter	VELOC 1. Solution	VELOC 2. Solution	FOTEL
Orbital period, $\mathcal{P}$	28.192 d fixed	28.192 d fixed	28.192 d fixed
Superior conj., $T_{\rm SC}$ (MJD)	51018.85	51019.25 fixed	51018.78 $\pm$1.4
Periastron, T_0 (MJD)	51034.62	51035.37 fixed	51034.55 $\pm$1.4
Eccentricity, e	0.27	0.11 fixed	0.266 $\pm$0.076
Periastron length, Φ	287.5°	294.9°	288.3 $\pm$19.8°
Velocity amplitude, K_1	24.77 km/s	24.73 km/s	26.4 $\pm$3.9 km/s
System velocity, v_0	3.46 km/s	4.56 km/s	4.25 $\pm$1.51 km/s

Table 3.4: Orbital elements of 59 Cyg computed for He II 4686 (photospheric absorption of the secondary) with VELOC and FOTEL.

Orbital parameter	VELOC	FOTEL
Orbital period, $\mathcal{P}$	28.192 d fixed	28.192 d fixed
Superior conj., $T_{\rm SC}$ (MJD)	51019.25	51019.2 $\pm$0.22
Periastron, T_0 (MJD)	51035.37	51035.32 $\pm$0.22
Eccentricity, e	0.11	0.113 $\pm$0.005
Periastron length, Φ	113.5°	112.8 $\pm$2.8°
Velocity amplitude, K_2	120.13 km/s	120.12 $\pm$0.76 km/s
System velocity, v_0	$-$0.92 km/s	$-$0.99 $\pm$0.45 km/s

3.5 Orbital parameters

The orbital elements of 59 Cyg were computed with the programs VELOC from Schmutz et al. (1997) and FOTEL from Hadrava (1990) using the radial velocities derived for the He I 4471 and He II 4686 lines. The orbital period of 28.192 d established earlier was assumed as a fixed parameter. The results are given in Tables 3.3 and 3.4.

VELOC fits a radial velocity curve to a set of measured radial velocities. The parameters of the velocity curve are the orbital elements. They are varied within seperately defined limits for each of the parameters. The optimum set of orbital elements is found if the rms error, determined by a χ^2-test, is minimal.

FOTEL allows for simultaneous fitting of radial velocity and light curves. The orbital elements are derived by fitting a radial velocity curve to measured radial

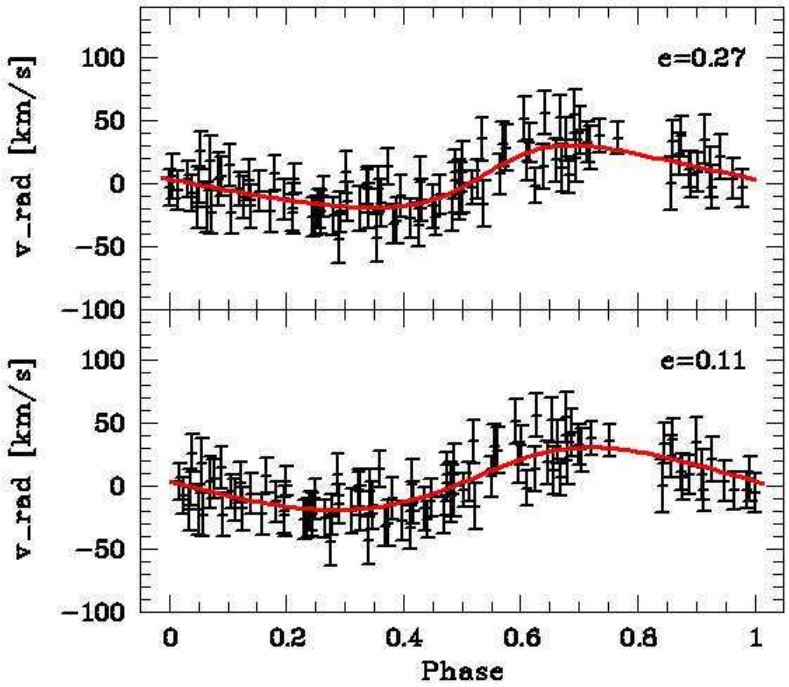

Figure 3.17: Measured radial velocities and orbital solutions for He I 4471 calculated with VELOC. In the upper panel the first solution with $e = 0.27$ is shown. Phase 0.0 corresponds to the time of superior conjuction T_{SC} = MJD 51018.85. The lower panel shows the solution for fixed eccentricity $e = 0.11$. The data are sorted using the corresponding T_{SC} = MJD 51019.25.

velocities. For each orbital parameter a start value and a step size is given for the parameter search. The quality of the fit is checked by a last square method.

The computed eccentricities of the binary orbits for the two lines differ considerably. The computation rendered an eccentricity of $e = 0.27$ for He I 4471 and of $e = 0.11$ for He II 4686 respectively. The other orbital elements (except for the velocity amplitude of course) agree quite well. In order to decide which of the derived eccentricities is the more accurate one, a further orbital solution operating He I 4471 was computed. Eccentricity and point of time of the periastron passage, T_0, were fixed to the values found for He II 4686. This was done to enable a fit of the radial velocities within the scope of the orbital solution as previously established for the secondary component. The measured radial velocities of the secondary component are less prone to dirt effects than those of the primary, and, hence, more reliable. The solution thus established differs only slightly from the first one, except for the eccentricity. The velocity amplitudes of 24.77 $\mathrm{km/s}$ found

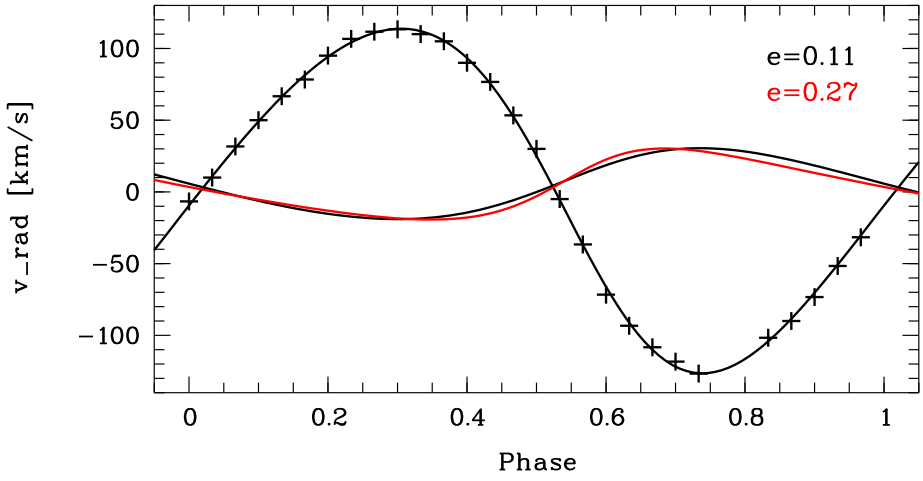

Figure 3.18: Orbital solutions for the primary and secondary component calculated with VELOC: Measured radial velocities and orbital solution for He II 4686 (black), orbital solution for He I 4471 with $e = 0.11$ (black) and $e = 0.27$ (red).

in the first solution and 24.73 $\mathrm{km/s}$ found with the fixed eccentricity of $e = 0.11$ (second solution) are almost identical. The results are given in Table 3.3.

Both solutions are plotted in Figure 3.17 including the measured radial velocities to test the fits against the data. The phases were calculated using the time of superior conjunction, T_{SC}, as epoch for phase zero. For each solution, T_{SC} was derived from the corresponding value of the periastron passage, T_0. The slightly different values of T_0 and, therefore, of T_{SC} result in a small phase shift between the solutions. Both solutions fit the measured date quite reasonable, even if the solution for $e = 0.27$ seems to be slightly better.

In Figure 3.18 the orbital solutions for the primary and secondary component are plotted. Additionally, the derived radial velocities for He II 4686 are shown, which are very well approximated by the fit. The two radial velocity curves computed for the Be primary differ due to the different eccentricities. For $e = 0.11$ the primary is maximally blueshifted and the secondary is maximally redshifted at phase 0.29. The maximal redshift of the primary or the maximal blueshift of the secondary, respectively, is reached at phase 0.72. For an eccentricity of $e = 0.27$ the primary is maximally blueshifted at phase 0.35 and maximally redshifted at phase 0.68.

The phase of the maximal redshift for $e = 0.27$ lies within a range of orbital phases in which very strong emission is visible at the inner part of the blue wing of almost all emission lines (Figs. 3.19 and 3.20, see also section 3.7, Fig. 3.25). The corresponding phase of maximal blueshift belongs to a phase interval where strong emission is visible at the inner part of the red wing of the helium emission

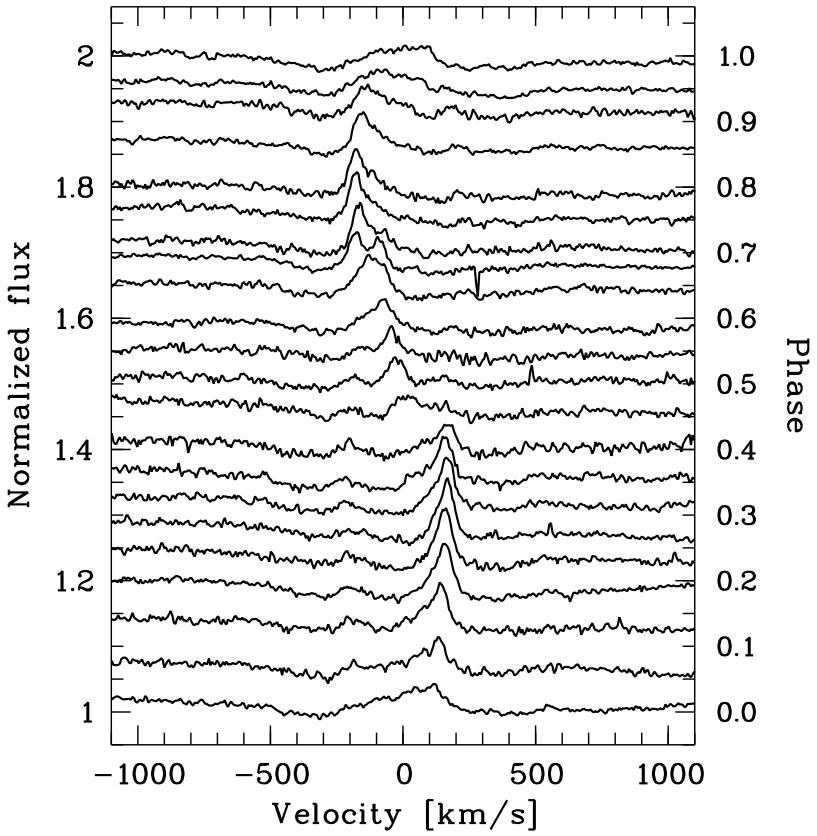

Figure 3.19: Observed line profiles of He I 6678, shown for an entire orbital cycle. The variable emission is visible in the red part of the profiles in the range of phase 0.25 at roughly $+200$ km/s. In the blue it appears around phase 0.75 at roughly -200 km/s. The invariant disc emission is only weakly pronounced, but clearly visible in the blue between phase 0.05 and 0.5 around -200 km/s. In the red it is difficult to detect, but should be found between phases 0.5 and 1.0 at roughly $+200$ km/s.

lines (Figs. 3.19 and 3.20 (right), see also section 3.7, Fig. 3.25, upper panel).

In section 3.7 it is demonstrated that almost all analysed absorption lines are contaminated at least to some extent by an emission component that varies in anti-phase to the Be primary. Asymmetric filling of the absorption wings of the line profiles during the above mentioned orbital phases can cause a shift of the apparent line cores, resulting in too high radial velocities. Hence, the phases of maximal velocities are shifted, giving a too high eccentricity. This can explain why the eccentricity derived from the radial velocities of He I 4471 is higher than the one found for He II 4686.

In Figure 3.21 the radial velocities of all components measured in the spectrum

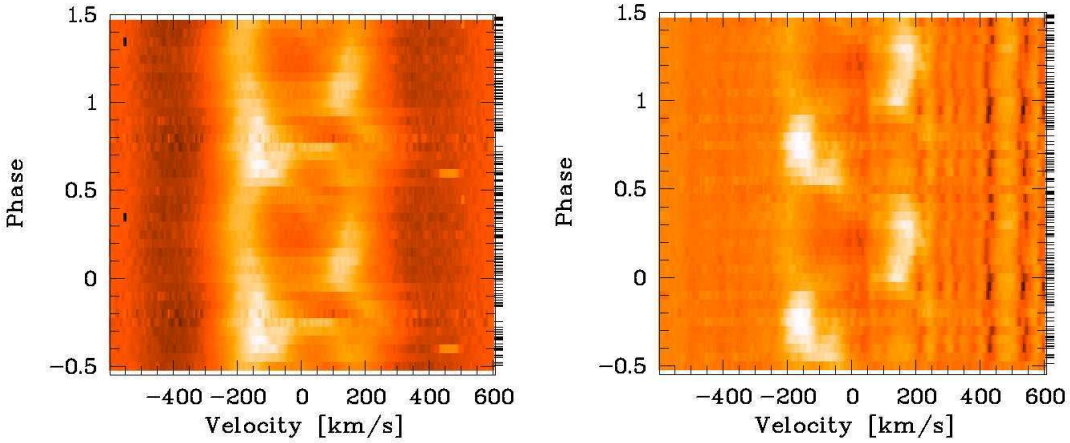

Figure 3.20: Dynamical spectra of Hβ (left) and He I 5876 (right). According to the orbital solution with eccentricity $e = 0.27$, the phase of maximal blueshift of the Be primary is 0.35 and of maximal redshift it is 0.68. Phase 0.0 corresponds to superior conjunction of the primary. Hβ and He I 5876 show the enhanced emission occuring in the blue around phase 0.68 very well. The enhanced emission in the red, visible around phase 0.35, is well ponounced in He I 5876.

of 59 Cyg are shown: He I 4471 and He II 4686, representing the photospheric absorptions of the primary and the secondary, the above mentioned variable emission, being in phase with the motion of the secondary, and the invariant emission[1] of the Be disc, very well visible in the blue wing of He I 6678 (Figs. 3.19 and 3.22, left). Additionally, the orbital solutions for the primary, calculated with the eccentricity of $e = 0.11$, and for the secondary are shown. The solution for the primary is also plotted over the radial velocities of the invariant disc emission to account for the superimposed rotational velocity of the disc.

The radial velocities of the variable emission component were measured by fitting a Gaussian to the position of the component in the individual line profiles of He I 6678. The invariant emission from the Be disc was determined analogous to the one of He II 4686 by measuring the radial velocities of the emission feature in each bin of the dynamical spectra of He I 6678 and 5876, Hγ, and Fe II 5169 using the graphical cursor. These lines were chosen because of their prominent emission feature. To finally get the radial velocities, the individual measurements are averaged. Since the invariant disc emission is clearly visible only in the blue wings of the line profiles in a phase interval from 0.0 up to 0.5 (Fig. 3.22, cf.

[1]The term "invariant emission" denotes that part of the disc emission which is not affected by the secondary component in a binary system. It corresponds to the double-peaked emission which is also visible in the spectra of single Be stars.

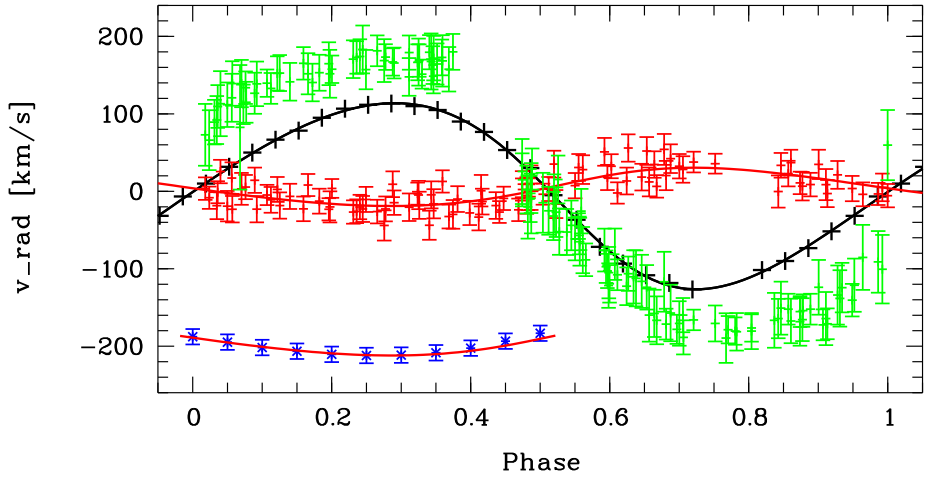

Figure 3.21: Emission and absorption components found in the spectrum of 59 Cyg. The measured radial velocities are plotted against the orbital phase. Red: Radial velocities of He I 4471, representing the photosphere of the primary, and orbital solution for $e = 0.11$; black: Radial velocities and orbital solution for He II 4686, representing the photosphere of the secondary; green: Radial velocities of the variable emission; blue: Radial velocities of the invariant disc emission, the orbital solution for the primary for $e = 0.11$ is overplotted, shifted by roughly -200 km/s (red).

Fig. 3.25, section 3.7), the radial velocities were measured in the respective phase bins only.

The radial velocities of the invariant disc emission peaks are approximated quite well by the orbital solution for the primary calculated with the values for eccentricity and time of the periastron passage of the second solution with $e = 0.11$ (see Tab. 3.3). Since they were measured during orbital phases when the significant parts of the line profiles are not disturbed by the variable emission, this is a strong hint that the eccentricity of 0.27 found for He I 4471 with freely converging parameters is too high. Additionally, He II 4686 does not seem to be contaminated by any kind of emission and is not formed by B-type stars. Therefore, the orbital solution found with the radial velocities of the secondary is favoured for the entire system. In the following, the orbital elements derived from that computation will be adopted for the orbital parameters of the system.

Harmanec et al. (2002) published orbital elements calculated with FOTEL for radial velocities of 30 Hα and 29 He I 6678 line profiles. The radial velocities were measured for the symmetric bottom parts of the Hα emission wings, for the emission wings, and for the absorption wings of He I 6678. They used a fixed orbital period of 28.1971 d, determined by photometry, and a fixed eccentricity

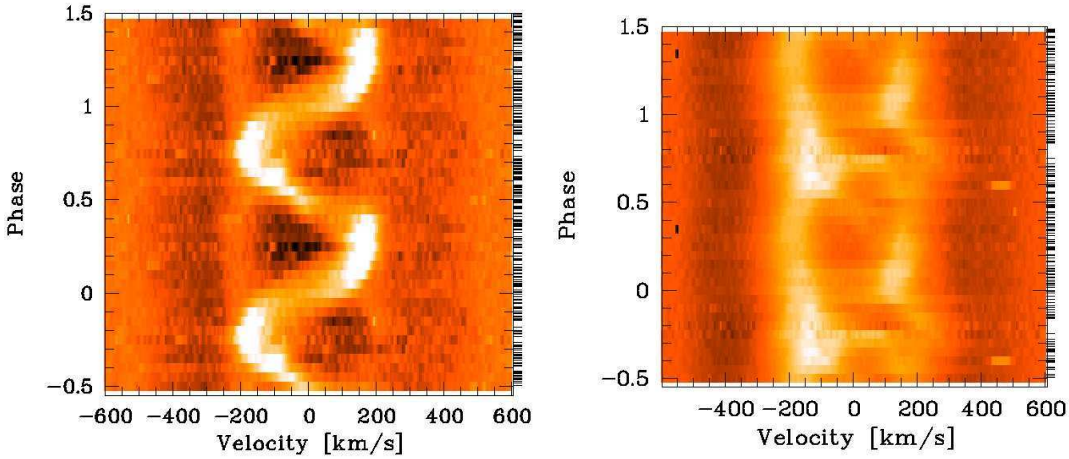

Figure 3.22: Dynamical spectra of He I 6678 (left) and Hβ (right). The invariant disc emission is clearly visible in the blue part of the line wings between orbital phases 0.0 and 0.5 at velocities of roughly -200 km/s.

of $e = 0$. For Hα they found a velocity amplitude of 13.0 $\pm$1.0 km/s, for the He I 6678 emission wings 31.3 $\pm$1.6 km/s, and for the He I 6678 absorption wings 25.4 $\pm$3.0 km/s.

Furthermore, Harmanec et al. computed sinusoidal fits to the V/R variations of 44 Hα and 36 He I 6678 profiles in order to find the point of time when the V/R variability becomes minimal and to derive the amplitude of this variation. Except for one solution for Hα, again, a circular orbit and a fixed period were assumed. The solution, where period and eccenticity were allowed to converge, gave an eccentric orbit with $e = 0.524 \pm 0.096$ and a period of 28.965 $\pm$0.0049 d. Within the errors, this period agrees well with the orbital period obtained in this work.

3.6 Parameters of the binary components

The detection of a photospheric component of the secondary, the He II 4686 absorption, allowed for the derivation of the radial velocity curves for both components of the binary system thereby enabling to determine the masses, $M_1 \sin^3 i$ and $M_2 \sin^3 i$, semi-major axes, $a_1 \sin i$ and $a_2 \sin i$, and the separation, $a \sin i$, of the primary and secondary star except for a factor of $\sin^3 i$ and $\sin i$, respectively. To assess this problem, masses and dimensions were calculated for a wide range of inclination angles. Since 59 Cyg has a very high $v \sin i$ of roughly 450 km/s and more (Fig. 3.23), and due to the shape of the emission pointing to a medium to high inclination (Hanuschik et al. 1996), inclinations lower than 40° are very unlikely and were not taken into account.

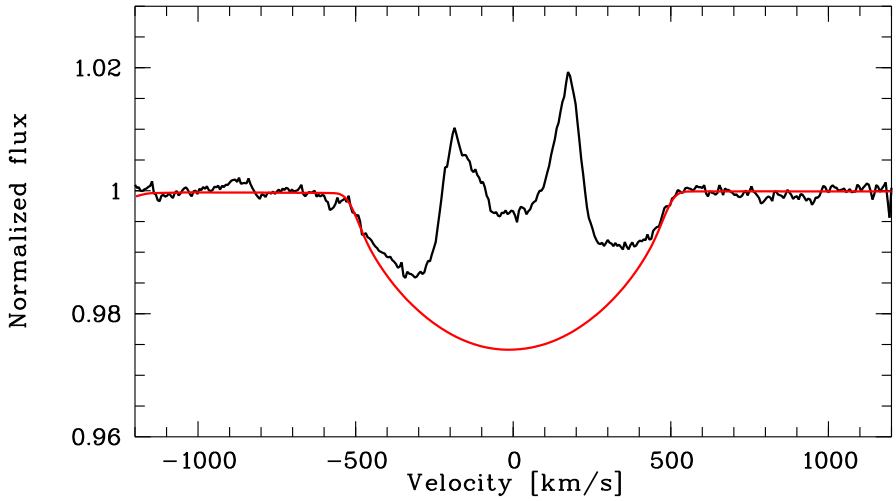

Figure 3.23: Averaged spectrum of He I 6678 (black) and rotational broadened synthetical spectrum for a B star with $T_{\rm eff}$ = 25 000 K (red). The He I 6678 line is the average of 147 Doppler-shift corrected line profiles. The synthetical spectrum was broadened with 505 $\mathrm{km/s}$.

To take the whole range of likely values into consideration, computations were performed for four possible velocity amplitudes for the primary component, K_1. Besides K_1 = 24.77 $\mathrm{km/s}$, resulting from this study, velocity amplitudes of 20 $\mathrm{km/s}$ and 30 $\mathrm{km/s}$ were investigated. These values enclose the range of radial velocities, established for the velocity amplitude of the invariant disc emission which follows the Be primary. A velocity amplitude of 13 $\mathrm{km/s}$ and an eccentricity of e = 0.5 published by Harmanec et al. (2002) were also included. For the velocity amplitude of the secondary the value of K_2 = 120.13 $\mathrm{km/s}$, as derived in the present study, was used. Both eccentricities, e = 0.11 and the presumably overestimated e = 0.27, were considered. The results for the masses are shown in Tables 3.5 and 3.6, for the semi-major axes in Tables 3.7 and 3.8, and for the binary separation in Table 3.9. In Table 3.10 values of the stellar parameters are listed as published by different authors.

According to Popper's calibration (Popper 1980), Harmanec et al. (2002) gave an effective temperature of $\log T_{\rm eff}$ = 4.413 for 59 Cyg (cf. Table 3.10). This corresponds to a slightly later spectral type than B1. Taking the mass of 11.03 $\mathrm{M}_\odot$, established for B1-type stars by Harmanec (1988), as an upper limit for the Be primary, only inclinations higher than 55 $^{\rm o}$ are possible for the system. For K_1 = 13 $\mathrm{km/s}$ and e = 0.27 or 0.5, respectively also inclinations as low as 50 $^{\rm o}$ would be in agreement with such an upper limit for the masses. But as demonstrated

Table 3.5: Masses for the Be primary, M_1, for different sets of orbital parameters and different inclination angles, given in $\mathrm{M}_\odot$.

K_1	13 km/s			20 km/s		24.77 km/s		30 km/s	
e	0.11	0.27	0.5	0.11	0.27	0.11	0.27	0.11	0.27
i									
40°	22.99	20.90	15.21	25.47	23.16	27.24	24.76	29.24	26.58
45°	17.27	15.70	11.43	19.14	17.40	20.46	18.60	21.96	19.97
50°	13.58	12.35	8.99	15.05	13.68	16.09	14.63	17.28	15.71
55°	11.11	10.10	7.35	12.31	11.19	13.16	11.97	14.13	12.84
60°	9.40	8.55	6.22	10.42	9.47	11.14	10.13	11.96	10.87
65°	8.20	7.46	5.43	9.09	8.26	9.72	8.83	10.43	9.48
70°	7.36	6.69	4.87	8.15	7.41	8.72	7.93	9.36	8.51
75°	6.78	6.16	4.48	7.51	6.83	8.03	7.30	8.62	7.83
80°	6.39	5.81	4.23	7.08	6.44	7.57	6.89	8.13	7.39
85°	6.18	5.62	4.09	6.84	6.22	7.32	6.65	7.86	7.14
90°	6.11	5.55	4.04	6.77	6.15	7.23	6.58	7.77	7.06

Table 3.6: Masses for the secondary component, M_2, for different sets of orbital parameters and different inclination angles, given in $\mathrm{M}_\odot$.

K_1	13 km/s			20 km/s		24.77 km/s		30 km/s	
e	0.11	0.27	0.5	0.11	0.27	0.11	0.27	0.11	0.27
i									
40°	2.49	2.26	1.65	4.24	3.86	5.62	5.11	7.30	6.64
45°	1.87	1.70	1.24	3.19	2.90	4.22	3.84	5.49	4.99
50°	1.47	1.34	0.97	2.51	2.28	3.32	3.02	4.31	3.92
55°	1.20	1.09	0.80	2.05	1.86	2.71	2.47	3.53	3.21
60°	1.02	0.92	0.67	1.73	1.58	2.30	2.09	2.99	2.71
65°	0.89	0.81	0.59	1.51	1.38	2.00	1.82	2.61	2.37
70°	0.80	0.72	0.53	1.36	1.23	1.80	1.63	2.34	2.12
75°	0.73	0.67	0.49	1.25	1.14	1.66	1.50	2.15	1.96
80°	0.69	0.63	0.46	1.18	1.07	1.56	1.42	2.03	1.85
85°	0.67	0.61	0.44	1.14	1.04	1.51	1.37	1.96	1.78
90°	0.66	0.60	0.44	1.13	1.02	1.49	1.36	1.94	1.76

Table 3.7: Semi-major axes for the Be primary, a_1, for different sets of orbital parameters and different inclination angles, given in $R_\odot$.

K_1	13 km/s			20 km/s		24.77 km/s		30 km/s	
e	0.11	0.27	0.5	0.11	0.27	0.11	0.27	0.11	0.27
i									
40°	11.20	10.85	9.76	17.23	16.69	21.33	20.67	25.84	25.03
45°	10.18	9.86	8.87	15.66	15.17	19.39	18.79	23.49	22.75
50°	9.40	9.10	8.19	14.45	14.00	17.90	17.34	21.68	21.00
55°	8.79	8.51	7.66	13.52	13.09	16.74	16.22	20.28	19.64
60°	8.31	8.05	7.24	12.79	12.39	15.83	15.34	19.18	18.58
65°	7.94	7.69	6.92	12.22	11.84	15.13	14.66	18.33	17.75
70°	7.66	7.42	6.67	11.78	11.41	14.59	14.14	17.67	17.12
75°	7.45	7.22	6.49	11.46	11.10	14.20	13.75	17.19	16.66
80°	7.31	7.08	6.37	11.24	10.89	13.92	13.49	16.86	16.34
85°	7.22	7.00	6.29	11.11	10.77	13.77	13.34	16.67	16.15
90°	7.20	6.97	6.27	11.07	10.73	13.71	13.28	16.61	16.09

Table 3.8: Semi-major axes for the secondary component, a_2, for different sets of orbital parameters and different inclination angles, given in $R_\odot$.

K_1	13 km/s			20 km/s		24.77 km/s		30 km/s	
e	0.11	0.27	0.5	0.11	0.27	0.11	0.27	0.11	0.27
i									
40°	103.47	100.23	90.15	103.47	100.23	103.47	100.23	103.47	100.23
45°	94.05	91.11	81.95	94.05	91.11	94.05	91.11	94.05	91.11
50°	86.82	84.10	75.64	86.82	84.10	86.82	84.10	86.82	84.10
55°	81.19	78.65	70.74	81.19	78.65	81.19	78.65	81.19	78.65
60°	76.79	74.39	66.91	76.79	74.39	76.79	74.39	76.79	74.39
65°	73.38	71.09	63.94	73.38	71.09	73.38	71.09	73.38	71.09
70°	70.77	68.56	61.67	70.77	68.56	70.77	68.56	70.77	68.56
75°	68.85	66.70	59.99	68.85	66.70	68.85	66.70	68.85	66.70
80°	67.53	65.42	58.84	67.53	65.42	67.53	65.42	67.53	65.42
85°	66.76	64.67	58.17	66.76	64.67	66.76	64.67	66.76	64.67
90°	66.51	64.43	57.95	66.51	64.43	66.51	64.43	66.51	64.43

Table 3.9: Separation of the binary components, $a = a_1 + a_2$, for different sets of orbital parameters and different inclination angles, given in $R_\odot$.

K_1	13 km/s			20 km/s		24.77 km/s		30 km/s	
e	0.11	0.27	0.5	0.11	0.27	0.11	0.27	0.11	0.27
i									
40°	114.66	111.08	99.91	120.69	116.92	124.80	120.90	129.30	125.26
45°	104.23	100.97	90.82	109.71	106.28	113.45	109.90	117.54	113.87
50°	96.21	93.20	83.83	101.27	98.11	104.72	101.44	108.50	105.11
55°	89.97	87.16	78.40	94.71	91.74	97.93	94.87	101.46	98.29
60°	85.10	82.44	74.15	89.58	86.78	92.63	89.73	95.97	92.97
65°	81.32	78.78	70.86	85.60	82.92	88.51	85.74	91.71	88.84
70°	78.43	75.98	68.34	82.56	79.98	85.37	82.70	88.45	85.68
75°	76.30	73.92	66.48	80.31	77.80	83.05	80.45	86.05	83.36
80°	74.84	72.50	65.21	78.77	76.31	81.46	78.91	84.40	81.76
85°	73.98	71.67	64.46	77.87	75.44	80.53	78.01	83.43	80.82
90°	73.70	71.40	64.22	77.58	75.15	80.22	77.71	83.11	80.52

Table 3.10: Published stellar parameters of 59 Cyg.

Parameter	Slettebak (1982)	Chauville et al. (2001)	Harmanec et al. (2002)
Spectral type	B1Ve	B1.5Vne	B1Ve
$\log T_{\rm eff}$		4.388	4.413
$\log g$		3.97	
V		4.74 mag	4.797mag
$v \sin i$	260 km/s	382 km/s	450 km/s

in section 3.5, these eccentricities are overestimated and the velocity amplitude is underestimated wherefore the resulting masses were disregarded.

59 Cyg shows no regular shell events like ϕ Per and HR 2142. Only one shell episode was reported in the 1970s (e.g. Barker 1982). Apart from that, no further shell events were observed. Therefore, the inclination of the binary is probably less than 80°.

In the present study a velocity amplitude of 24.77 km/s for the Be primary and an eccentricity of e = 0.11 for the binary system were found. Therefore, the results for the stellar masses M_1 and M_2 calculated with these parameters are the most likely ones strongly suggesting the inclination of the binary orbit to be more than 60° and less than 80°.

Table 3.11: Orbital and stellar parameters of 59 Cyg. All epochs are given in MJD (JD −2 400 000.5). All of the orbital solutions were calculated with FOTEL.

Published by	**Rivinius & Štefl (2000)**	**Harmanec et al. (2002)**	**This study**
Orbital:			
Period, $\mathcal{P}$	28.1702 ±0.0014 d	28.1971 ±0.0038 d	28.192 ±0.004 d
$T_{\rm SC}$			51019.25
$T_{\rm min.\,RV}$	50013.1 [1]	50013.31 ±0.62	
T_0	50018.9 ±2.5		51035.37
e	0.20 ±0.08	0 fixed	0.11 ±0.005
Φ	271 ±35 °	—	293±3 °
K_1	26.1 km/s	13.0 ±1.0 km/s	24.77 km/s
K_2		$60 \leq K_2 \leq 150$ km/s	120.13 km/s
v_0		-16.49 ±0.76 km/s	−0.92 km/s
Stellar:			
$M_1 \sin^3 i$			7.23 $M_\odot$
$M_2 \sin^3 i$			1.49 $M_\odot$
$a_1 \sin i$			13.71 $R_\odot$
$a_2 \sin i$			66.51 $R_\odot$
$a \sin i$			80.22 $R_\odot$
i		$45° < i < 90°$	$60° < i < 80°$
M_1		10.78 ± $M_\odot$	$7.57 < M_1 < 11.14$ $M_\odot$
M_2		$1 < M_2 < 2$ $M_\odot$	$1.56 < M_2 < 2.3$ $M_\odot$
a_1			$13.92 < a_1 < 15.83$ $R_\odot$
a_2			$67.53 < a_2 < 76.79$ $R_\odot$
a		≈ 90 $R_\odot$	$81.46 < a < 92.63$ $R_\odot$
R_1		5.31 +1.5/−0.96 $M_\odot$	

[1]: Derived by Harmanec et al. (2002) from T_0
$\mathcal{P}$: Orbital period of the binary
$T_{\rm SC}$: Time of superior conjunction of the primary, corresponds to orbital phase 0.0
$T_{\rm min.\,RV}$: Time of minimal radial velocity, corresponds to orbital phase 0.0
T_0: Time of periastron passage
e: Eccentricity
Φ: Periastron length
K_1, K_2: Velocity amplitude of primary, secondary
v_0: System velocity
$M_1 \sin^3 i$, $M_2 \sin^3 i$; M_1, M_2: Masses of the primary, secondary
$a_1 \sin i$, $a_2 \sin i$; a_1, a_2: Semi-major axes of the primary, secondary
$a \sin i$, a: Separation of the binary components ($a_1 \sin i + a_2 \sin i$ and $a_1 + a_2$)
i: Inclination of the binary system
R_1: Radius of the primary

Interpolating Harmanec's calibration (Harmanec 1988) for normal B1-type stars, Harmanec et al. (2002) found a mass of 10.78 $\mathrm{M}_{\odot}$ for the primary component of 59 Cyg (cf. Table 3.11).

The most interesting finding, however, is that the masses for the secondary star, M_2, calculated for the above mentioned velocity range and an eccentricity of e = 0.11 (Tab. 3.6) are significantly higher than those for normal sdO stars having masses less than 1 $\mathrm{M}_{\odot}$. If the most likely velocity amplitude K_1 = 24.77 $\mathrm{km/s}$ is adopted, the derived values for M_2 lie between 1.56 and 2.3 $\mathrm{M}_{\odot}$ and even are above the Chandrasekhar limit of 1.4 $\mathrm{M}_{\odot}$. This suggests that 59 Cyg represents an earlier stage of ϕ Per or possibly a precursory phase of a Be/X-ray binary.

The orbital and stellar parameters for both components of the binary system established in this study are listed in Tab. 3.11. For comparison, the results of Rivinius & Štefl (2000) and Harmanec et al. (2002) are also shown.

3.7 Emission variability phase-locked to the orbital period

Based on the period of 28.192 d found in the present study the short-term variability of 59 Cyg is analysed. In this context "short-term variability" denotes variations that are locked to the orbital period and reappear after each cycle at the same orbital phase. In Figures 3.24, 3.25, and 3.26 dynamical spectra are shown for several absorption and emission lines of different ions. They were computed for a velocity range of $\pm$1000 up to $\pm$2000 $\mathrm{km/s}$ around the central wavelength of the studied lines. The line profiles were sorted into 20 phase bins applying the same procedure as in section 3.4.

The dynamical spectra of the photospheric absorption lines show the orbital motion of the Be primary component clearly by a periodical shift of the line profiles throughout the orbital cycle (Fig. 3.24). However, the inner parts of the blue and red absorption wings, close to the line centres, do not always seem to behave homogeneously. During some orbital phases the inner blue wings move towards the blue wing of the spectral lines, while the inner red wings seem to move to the opposite direction i.e. redwards. The resulting "knotty" structure of the line centres (see section 3.7.1) is well visible in He I 4471 and Hδ (Fig. 3.24). It could be misinterpreted as an effect of incorrect phase-binning due to a wrong period. The observed profile cannot be explained without taking into account the emission contribution.

The ultraviolet carbon doublet line C IV 1548, partly originating from absorption in the stellar wind of the Be star, follows the orbital motion of the Be primary, too.

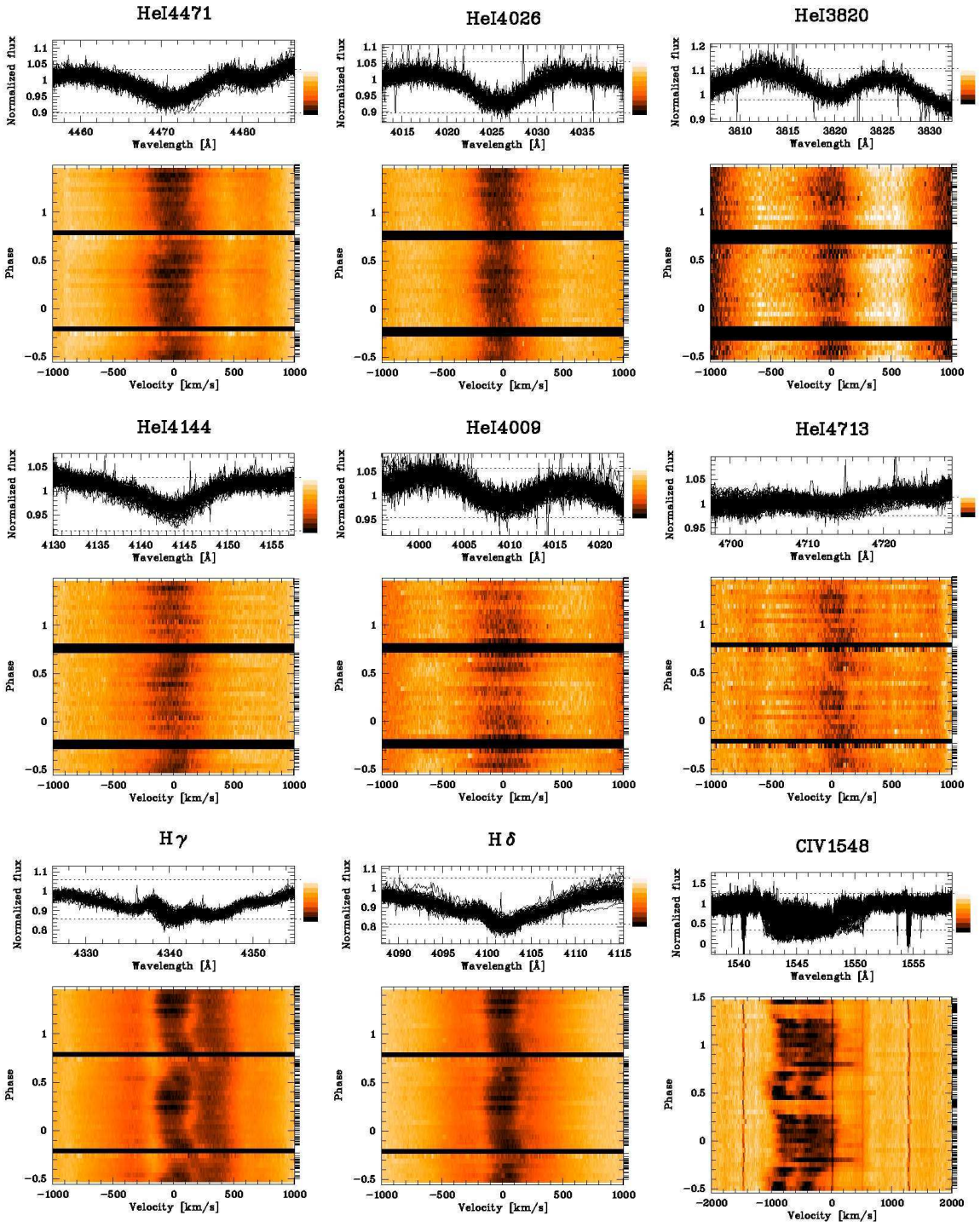

Figure 3.24: Line profiles and dynamical spectra of absorption lines of 59 Cyg. Additionally, the ultraviolet wind absorption line C IV 1548 is shown.

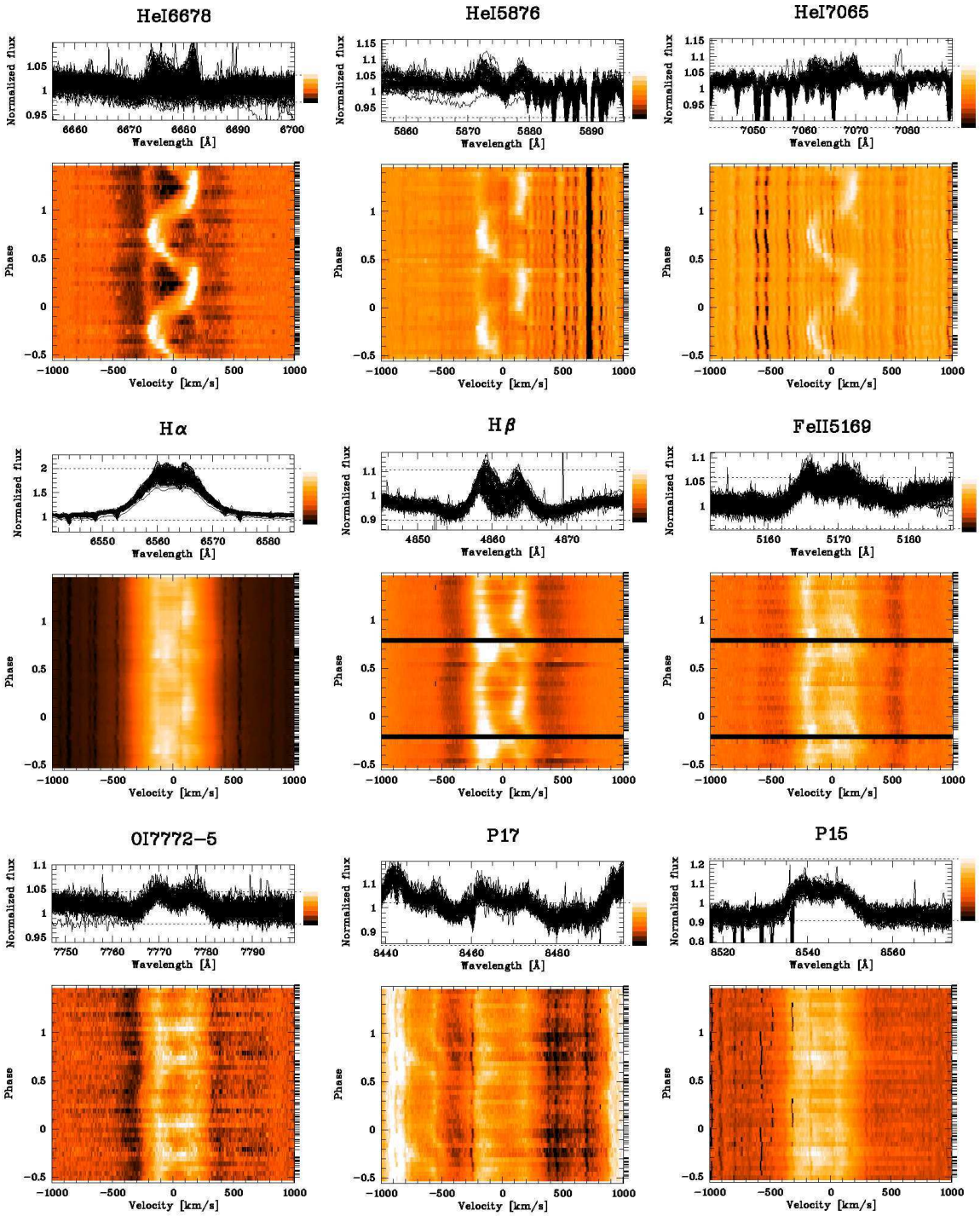

Figure 3.25: Line profiles and dynamical spectra of emission lines of 59 Cyg.

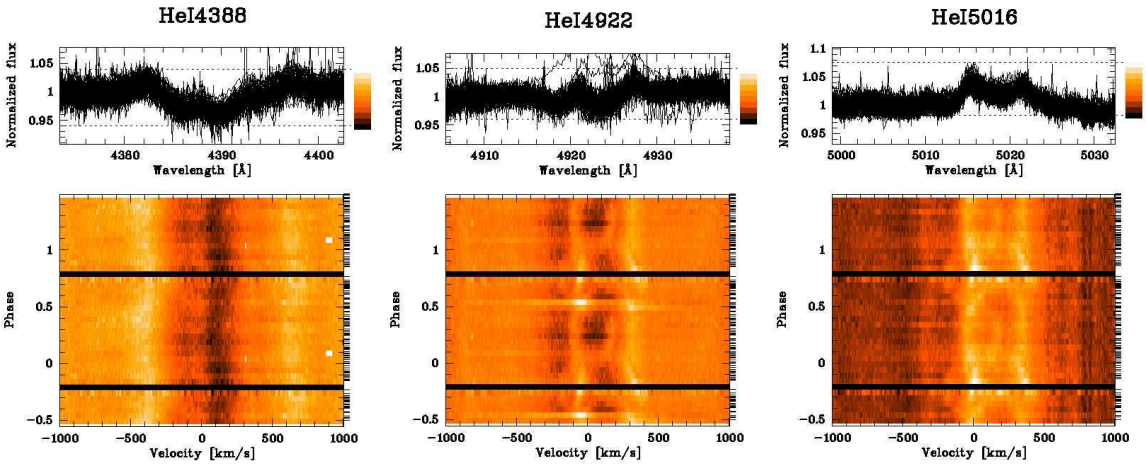

Figure 3.26: Line profiles and dynamical spectra of blended lines of 59 Cyg.

As mentioned above, an inspection of the dynamical spectra of the emission lines (Fig. 3.25) reveals the presence of two clearly distinguishable emission components. One is phase-locked to the orbital period and varies in emission strength over one orbital cycle (section 3.7.2). The other one consists of two parts, visible in the blue and red wings of the line profiles. They follow the motion of the underlying photospheric absorption profile and are located at velocities of roughly $+200\ \mathrm{km/s}$ and $-200\ \mathrm{km/s}$. They represent the blue and red components of the double-peaked disc emission which is also visible in single Be stars.

To distinguish the double-peaked disc emission from the phase-locked, variable emission component, it is named "invariant emission", as defined in section 3.5, page 43. This means that it is not variable in emission strength over one orbital cycle. But since it represents the stage of the entire circumstellar disc of the Be star, it varies, of course, on a larger timescale measured in years (Fig. 3.27). In general, the blue component of the invariant disc emission is visible more clearly than the red one.

The invariant disc emission is best visible in the blue wings of He I 6678 and He I 5876 between orbital phases 0.0 and 0.5 at roughly $-200\ \mathrm{km/s}$ (Fig. 3.25, see also Fig. 3.19, page 42). In lines with strong emission contribution, like Hα and Hβ, or in blended lines, like O I 7772–5 and Fe II 5169, (Fig. 3.25) it mixes more and more with the phase-locked emission. This is most obvious in the red part of the line profiles at phases between 0.05 and 0.4. It is, therefore, more difficult to find and distinguish the invariant from the phase-locked, variable emission component.

The phase-locked emission component is variable in strength over one orbital cycle and best visible in He I 6678, 5876, and 7065 (Fig. 3.25, cf. Fig. 3.19, sec-

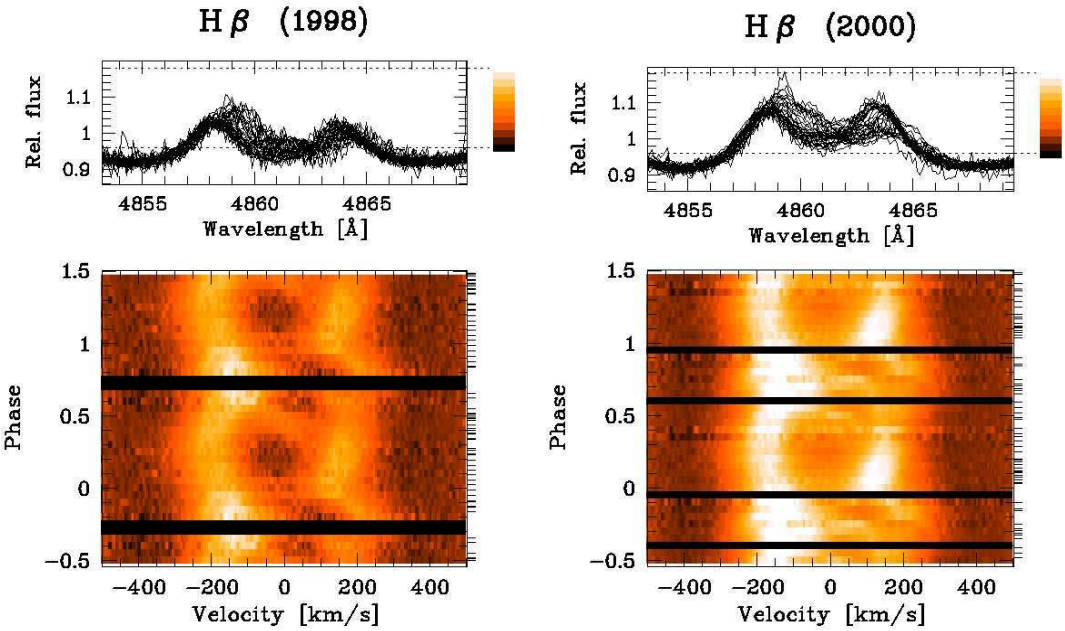

Figure 3.27: Long-term variability of the emission strength. Dynamical spectra of Hβ for 1998 (left) in comparison to 2000 (right). The invariant and the superimposing variable emission component are very well visible in the blue wing of the line profiles at roughly -200 km/s. The invariant emission is best visible between orbital phases 0.0 and 0.5. The phase-locked, variable emission has a higher intensity and is most obvious between phases 0.6 and 0.9.

tion 3.5). It moves in anti-phase to the Be primary and is confined to a velocity range of roughly ± 200 km/s. In this range the invariant disc emission also appears. This is a hint that the variable emission component is formed in the disc surrounding the Be star, too. It is strongest pronounced at roughly -200 km/s in the blue and roughly $+200$ km/s in the red line wing respectively. In He I 6678 the underlying absorption profile is also well visible, allowing for direct comparison of the components.

In Figure 3.27 dynamical spectra of Hβ are shown for the data obtained in 1998 and 2000 separately. Both emission components are clearly visible, especially in the blue line wing at roughly -200 km/s. They are much stronger in 2000 compared to 1998. The same is found for Hα and He I 6678, both showing emission components. In He I 7065, having nearly no invariant disc emission, the variable emission is enhanced in 2000, too. The fact, that the emission strengths of both components behave analogously, suggests that the variable emission forms in the same region as the constant emission, namely in the Be disc.

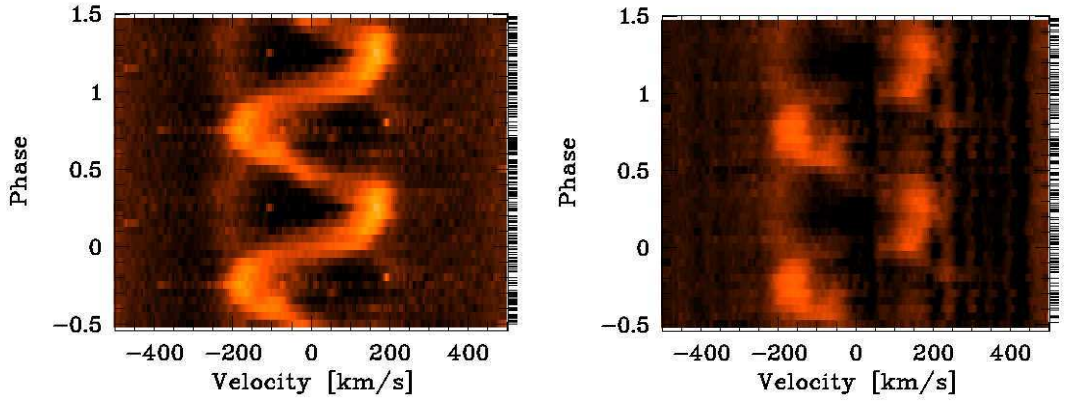

Figure 3.28: Central parts of the emission lines He I 6678 (left) and He I 5876 (right). The cut values for the line intensities are chosen in a way that the course of both emission components, the invariant and the phase-locked one, becomes clearly visible. The knotty absorption structure appears when the variable emission component is less pronounced like in He I 5876.

3.7.1 Knotty absorption structure

A "knotty" absorption structure like the one observed in the absorption lines (Fig. 3.24) is also visible well in the line centres of some emission lines, e.g. He I 5876, Hβ, and P17 (Fig. 3.25). A comparison of Hβ (Fig. 3.25), Hγ, and Hδ (Fig. 3.24) reveals the nature of this feature. All three lines show such a "knotty" structure of the underlying absorption profile, becoming more and more pronounced in Hγ and Hβ owing to increasing emission contribution. Hδ seems to be free of emission. In Hγ both emission components, the standard disc emission following the Be primary and the variable emission moving in anti-phase to the Be star, are already discernible. Especially in the blue wing both components are clearly distinguishable. Compared to Hδ, the knotty structure is more developed. Hβ basically looks like Hγbut shows much more emission. The knotty structure is more pronounced as well.

In emission lines with a less pronounced variable emission component within ± 100 km/s like He I 5876 and P17 the knotty structure is also visible quite well. But it is not visible in emission lines like He I 6678 or Hα with strong central emission. This is demonstrated in Figure 3.28, where the central parts of He I 6678 and 5876 are compared. Hence, it follows that the "knotty" structure is caused by superposition of the variable emission component and the absorption profile of a spectral line (Fig. 3.29, lower left panel). Vice versa, a spectral line must have a contribution of the variable emission component if its line centre shows such a knotty absorption structure.

3.7.2 Variable emission

As already mentioned in section 3.2, almost all spectral lines of 59 Cyg show some emission at least during certain orbital phases. This temporary emission, appearing as a single-peaked feature in the central parts of the line profiles, is the variable emission component. Even if the emission is too weak to produce a clear emission feature, it will cause a knotty structure in the underlying absorption profile. This is also true for the absorption lines used or the radial velocity measurements to derive the orbital elements. The knotty absorption is present in the dynamical spectra of He I 4471, 4144, and 4026 (Fig. 3.24). Therefore, it was not possible to determine the correct radial velocities for all orbital phases. This resulted in an overestimation of the eccentricity of the binary system (cf. section 3.5).

To confirm this finding He I 6678 is compared to He I 4471 and the blend of He I 4922 and Fe II 4924 (Fig. 3.29). In this figure, the radial velocities of the two emission components, the variable and the invariant disc emission, were measured by fitting a Gaussian to their position in the single line profiles of He I 6678. The results were plotted in a two-dimensional frame analogous to the dynamical spectra. The blue part of the invariant disc emission is represented by blue crosses, the red part by red crosses. The variable component moving in anti-phase to the Be primary is shown by black circles. For a better understanding how the emission, especially the variable one, alters the appearance of the absorption profiles, the radial velocities of the variable component were plotted over the dynamical spectra of the presented lines.

The presence of the variable emission component is the key to understand the quite complicated structure of spectral lines with strong emission like Hα or blends with emission contribution. This is demonstrated for the blend of He I 4922 and Fe II 4924 (Fig. 3.29, lower panel). Some of the structures which are found in the blended line are well identifyable as features caused by the variable emission component. The emission superposing the He I 4922 absorption line is marked with blue, the emission superposing the Fe II 4924 emission line with black circles.

In Figures 3.30 and 3.31 the short-term emission variability of 59 Cyg is shown for an entire orbital cycle with line profiles in an one-dimensional frame. The 20 phase-binned, averaged line profiles were extracted from the two-dimesional dynamical spectra. They were plotted with increasing phase upwards. Absorption and emission lines with different emission strengths are compared.

The variable emission component is visible best in He I 6678, since the invariant disc emission is only little pronounced there. Shortly after superior conjunction, when the secondary star is in front of the primary, an emission feature becomes visible in the red wing of the line profile at a velocity of roughly $+100$ km/s. With increasing strength this component moves further to the red part of the spec-

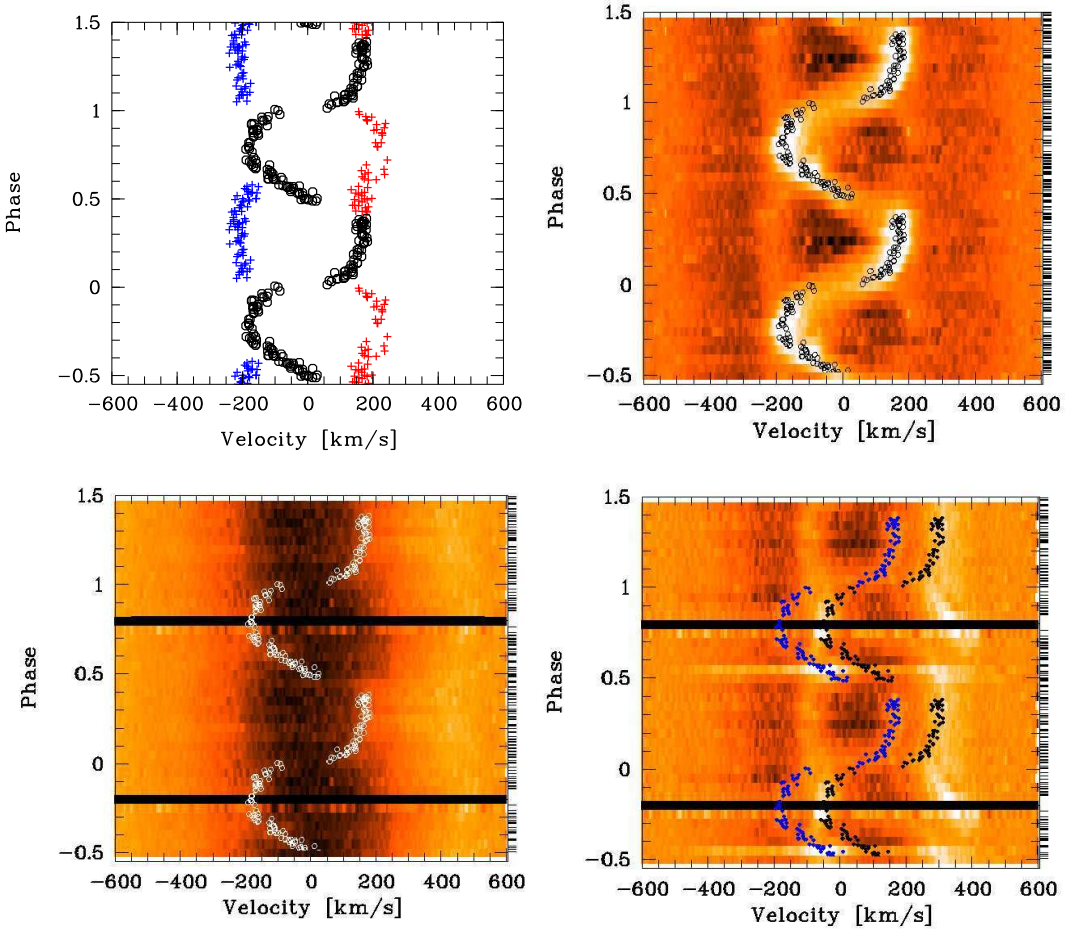

Figure 3.29: Identification of variable emission in different types of line profiles. Upper panel, left: Radial velocities of invariant (blue and red crosses) and variable emission component (black circles), measured for He I 6678; upper panel, right: He I 6678 emission; lower panel, left: He I 4471 absorption; lower panel, right: Blend of He I 4922 and Fe II 4924. The radial velocities of the variable emission are plotted over the dynamical spectra to show their influence on the profiles.

trum. At orbital phases between 0.2 and 0.3 a well definded, strongly pronounced emission peak is visible at roughly $+200\,\mathrm{km/s}$ where the red part of the invariant disc emission is located, too. The feature becomes weaker and broader around phase 0.35. It starts to move a little bit back to the blue part of the spectrum and disappears around phase 0.45. The weak emission feature visible around 0.5 at roughly $+200\,\mathrm{km/s}$ is attributed entirely to the invariant disc emission.

At orbital phase 0.4, just before the above described feature has totally disapeard, a second emission peak forms in the centre of the line profile. While it gets

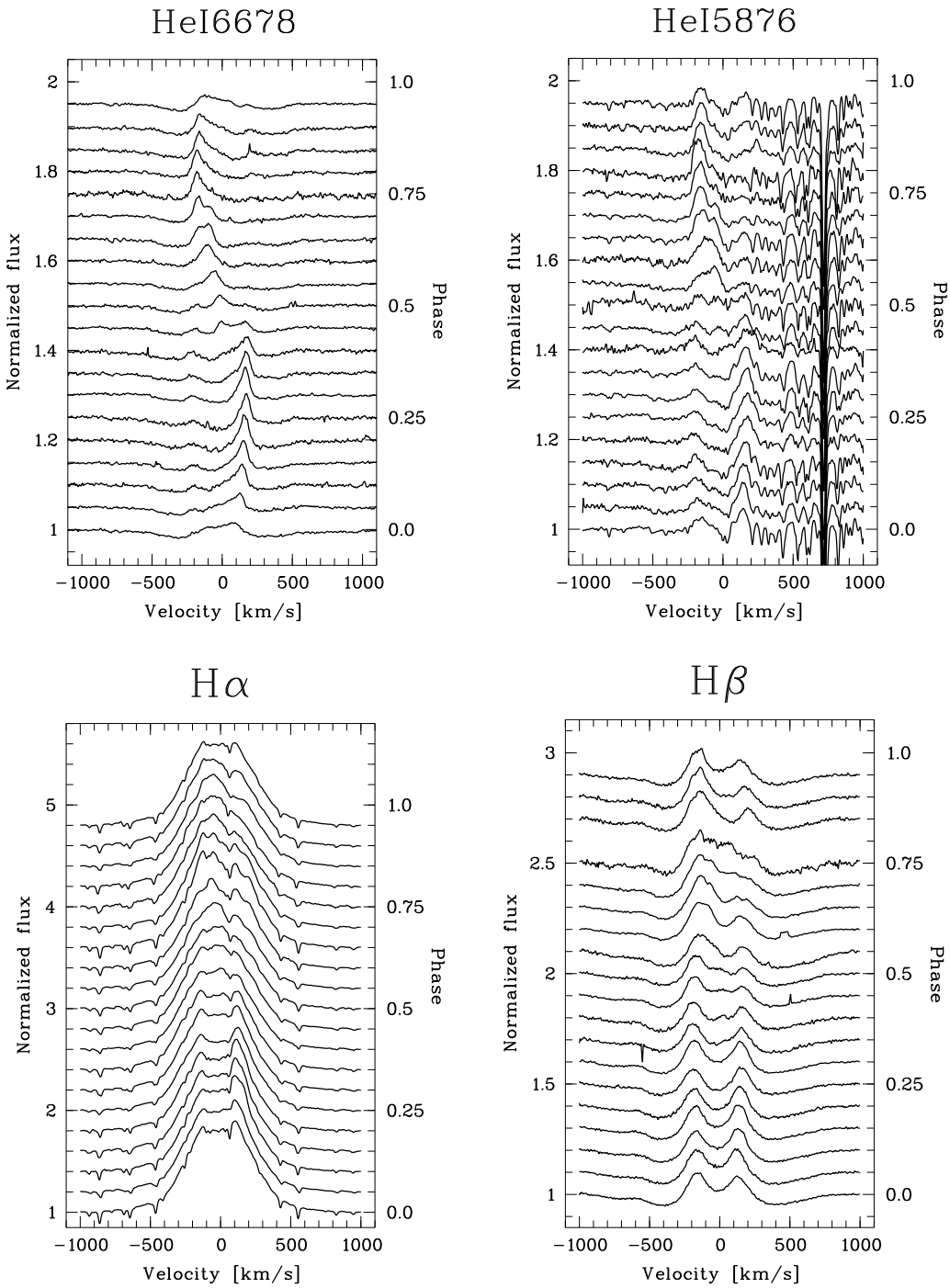

Figure 3.30: Phase-locked variability of the variable emission component throughout an entire orbital cycle for emission lines with different emission strengths. The spectra were sorted in 20 phase bins and averaged for each bin within a velocity range of $\pm 1000\ \mathrm{km/s}$. The averaged lines are plotted one over another with increasing orbital phase.

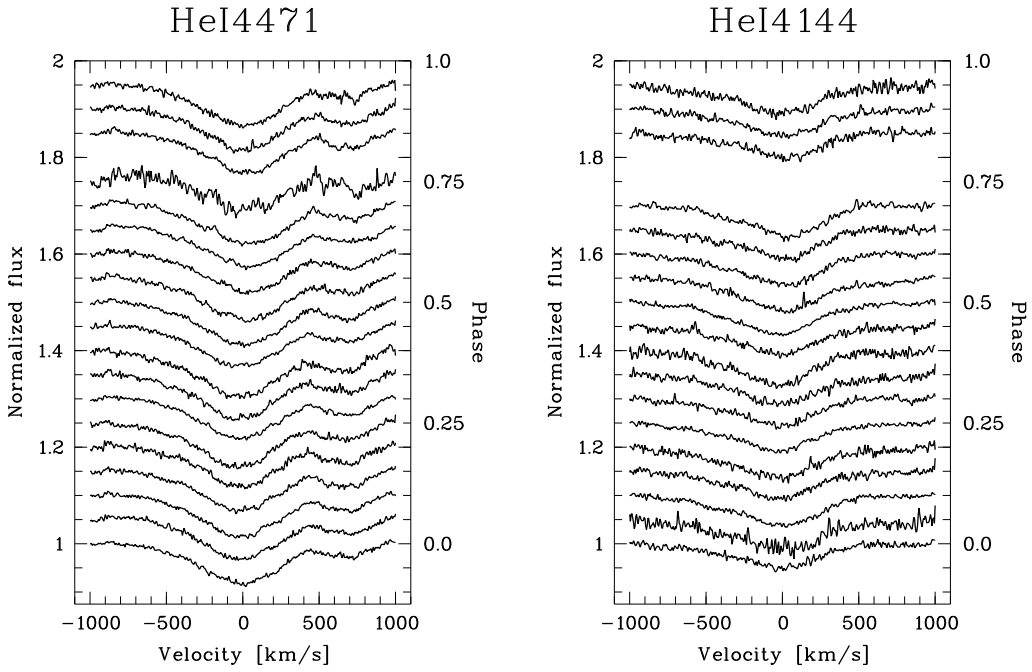

Figure 3.31: Short-term variability of absorption lines for an entire orbital cycle. The spectra were sorted into 20 phase bins and averaged for each bin. The averaged profiles are plotted one over the other with increasing orbital phase. A phase-locked variability due to the variable emission is not detectable.

stronger and broader it moves more and more to the blue part of the spectrum. Around phase 0.65 it is very broad and strongly pronounced, showing a characteristic double-peaked structure, the so-called satellite absorption (Fig. 3.32). This feature is visible in many known Be binaries. It is not explicable by a disc around a single Be star. Therefore, it is taken as a characteristic feature of Be binaries (cf. section 5). Around phase 0.7 the blue peak of this emission feature becomes more enhanced, while the red peak decreases. Between phases 0.75 and 0.85 a well defined, less pronounced, and narrow single emission peak is visible, located at roughly $-200\ \mathrm{km/s}$. It becomes weaker around phase 0.9 and starts to disappear around 0.95.

This kind of variability pattern is also found in the other lines with variable disc emission. In lines with stronger invariant emission like Hα and Hβ it is more difficult to discover and to interpret, but nevertheless present.

In the phase-binned and averaged profiles of He I 4471 and 4144 an emission component is hardly detectable. But some of the single spectra show weak emission peaks close to their line centre. Since both lines show a knotty absorption structure in the dynamical spectra at least a small component of variable disc

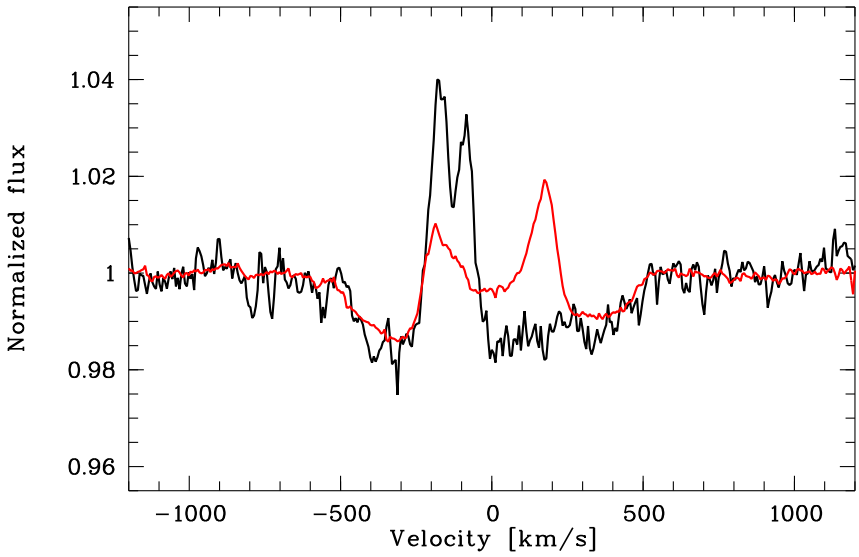

Figure 3.32: Satellite absorption visible in the blue wing of He I 6678 (black) and shift-corrected, averaged profile of He I 6678 (red). In the spectrum of 59 Cyg satellite absorptions occur at orbital phases around 0.68 which is shortly after the periastron passage (phase 0.57).

emission must be there. This is further strengthened by the finding that in 2000, compared to 1998, the knotty structure became more pronounced in He I 4471, and the line seems to be filled in a little bit in the central parts of the profile, where the variable emission is concentrated. This is interpreted as an increase of the variable disc emission analogous to the longterm behaviour of the emission lines. A constant contribution from the Be disc is not detectable.

3.7.3 Phase-locked variability of the equivalent width

Equivalent widths were measured for Hα, Hβ, and He I 6678. The equivalent widths and, therefore, the emission strength of the strong emission lines Hα and Hβ are clearly connected to the orbital cycle (Fig. 3.33). Since Hα and Hβ are dominated by emission, their equivalent widths are negative by definition. For convenience, they were multiplicated by a factor of -1 and shown for two orbital cycles. For He I 6678, a variability is not detectable unambiguously, since the emission is too weak to produce such a feature.

The shape of the curves given by the values of the equivalent widths of Hα and Hβ clearly follows the motion of the secondary component. This behaviour can

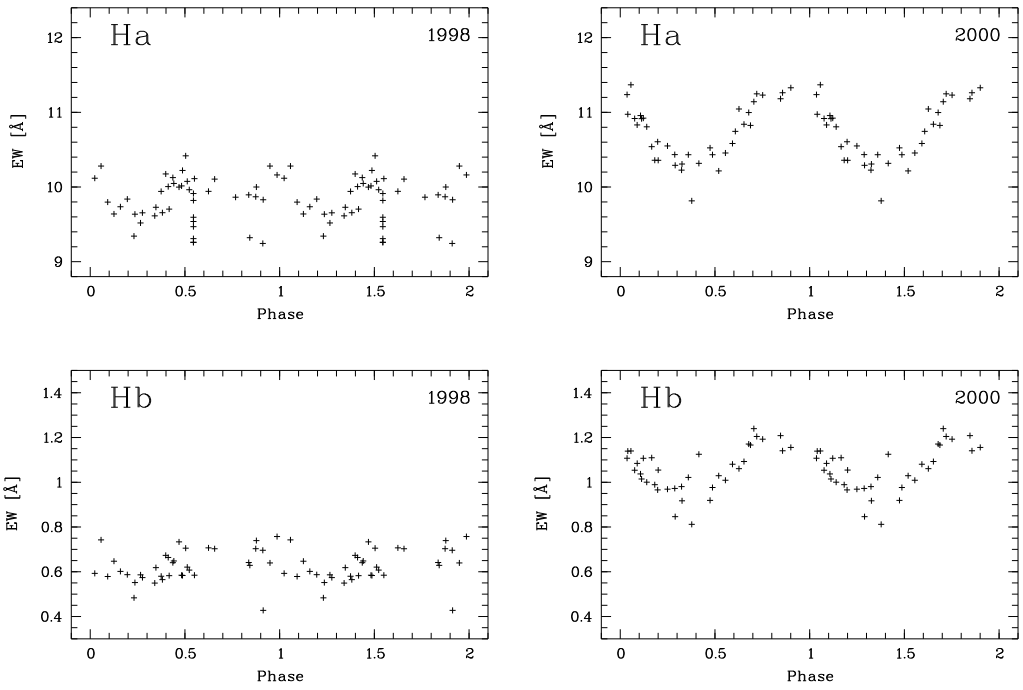

Figure 3.33: Variability of the equivalent widths of Hα and Hβ in 1998 and 2000. The values were multiplicated by a factor of -1 and plotted for two orbital cycles.

be explained qualitatively by the illuminated disc sector. At phases 0.0 and 0.5 the sector is directly in front or behind the Be star, respectively. Since the binary is visible at an inclination larger than 60 ^{o} and lower than 80 ^{o}, the plane and the edge of the Be disc are well visible. At phase 0.0 the projected area of the disc sector in direction to an observer, including plane and edge of the disc, is maximal. Therefore, a maximal amount of variable emission, originating in the illuminated sector, is visible. At phase 0.5 the projected area of the disc sector is minimal, since only the surface of the sector is visible, but not the edge. The amount of variable emission, detectable for an observer, is expected to be minimal.

As shown in Figure 3.33, this expectation is not matched by the observations. The equivalent widths start to increase again around phase 0.4, instead of showing a minimum at phase 0.5. This is explicable by the periastron passage which takes place at phase 0.57. When the secondary moves towards the Be star, it is closer to the disc and illuminates a larger sector. Additionally, it is expected that also deeper layers will be photoionized. This is expected to result in enhanced emission around periastron, which is exactly what is observed. Therefore, the properties of the periodic variability of the equivalent widths confirms an eccentric orbit for 59 Cyg (cf. (Harmanec et al. 2002)).

Long-term variations are also detectable in the behaviour of the equivalent widths (Fig. 3.33). In 1998, maximum values for the equivalent widths of Hα and Hβ occur and, hence, maximal emission strength is detectable at phases 0.0 and 1.0, respectively, and around 0.5. These phases correspond to superior and inferior conjunction, when the secondary is in front or behind the Be primary. The emission strength is minimal around phase 0.25, when the illuminated sector is maximally redshifted. Around phase 0.75, when the disc sector is maximally blueshifted, a second minimum is detectable. But it is less pronounced than the one occuring at phase 0.25.

In 2000, the emission was stronger in general (cf. Fig. 3.27). For Hα and Hβ, the emission strength was minimal at phase 0.4. In contrast to 1998, no further minimum occured. One maximum appeared around phase 0.8 for Hβ and around phase 0.9 for Hα. These maxima were much stronger pronounced than the two different maxima, visible for Hα and Hβ in 1998. Since the emission was stronger in 2000, the emission strength around periastron, as described above, is expected to be also enhanced. This should result in larger values derived for the corresponding equivalent widths. This is observed, since the maximum of emission strength around and after periastron is much stronger pronounced and much broader in 2000 than in 1998. This confirms the finding that the size of the illuminated disc sector varies with the orbital phase.

Chapter 4

Modelling the phase-locked emission variability

The short-term emission variability of 59 Cyg (cf. section 3.7.2) resembles that observed for ϕ Per. A He I 6678 emission, moving in anti-phase to the Be primary, was reported for ϕ Per by several authors (e.g. Gies et al. 1993; Božić et al. 1995; Štefl et al. 2000). According to Štefl et al. (2000), this variability is caused by an emission component that originates in a sector of the circumstellar disc the Be star which faces the secondary. This sector is partially photoionized by the radiation of the hot companion. Since this emission component arises only in a part of the disc of the Be star, it is single-peaked and linked to the motion of the secondary. Thus, it moves in anti-phase to the radial velocity curve of the Be primary.

Assuming this model, Hummel & Štefl (2001) successfully reproduced the variability of the He I 6678 and He I 5876 emission of ϕ Per. Contrary to earlier models, this model is the first quantitative model and requires the least number of physical components, i.e. the Be primary, the hot secondary, and the circumstellar disc of the Be star. In the following, this model is adapted to 59 Cyg.

4.1 Model-geometry of 59 Cyg

The assumed geometry of the primary component of 59 Cyg, viewed from above the orbital plane, is shown in Figure 4.1 for orbital phases 0.0, 0.25, 0.5, and 0.75. Phase 0.0 corresponds to superior conjunction of the primary, when the secondary and, hence, the photoionized disc sector are in front of the Be star. The primary is surrounded by a circumstellar disc, co-planar to the orbital plane of the binary system. The disc sector that faces the secondary component is illuminated by the radiation of the hot companion.

In Fig. 4.1 the He I 6678 emission observed at the given orbital phases is also

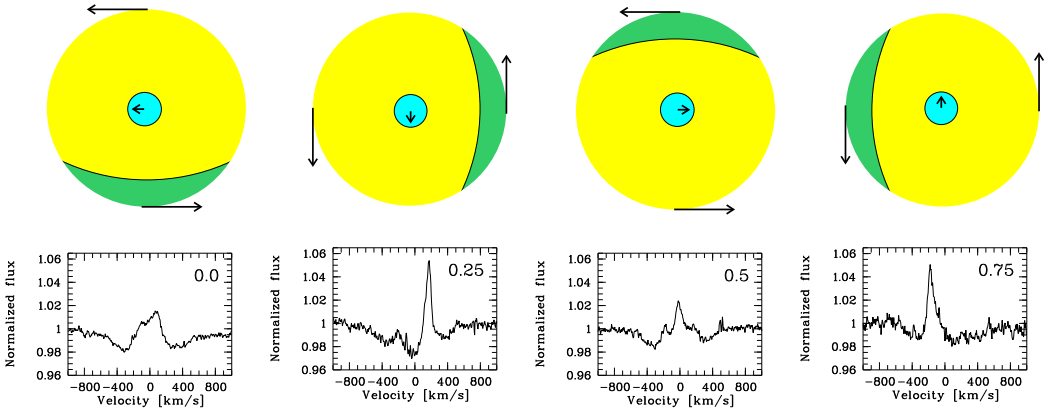

Figure 4.1: Model-geometry of 59 Cyg, viewed from above the orbital plane, and He I 6678 emission for orbital phases 0.0, 0.25, 0.5, and 0.75 (from left to right). Light-blue: Be primary; yellow: Circumstellar disc of the Be star; green: Disc sector facing the secondary, photoionized by the UV continuum radiation of the sdO star. The long arrows mark the sense of rotation of the disc. The short arrow marks the direction of movement of the Be star.

shown. The emission is dominated by the V/R variability. In the scope of the model, this is caused by the single-peaked emission, originating in the illuminated disc sector. The invariant double-peaked emission of the circumstellar disc of the Be star appears as a small emission peak in the inner part of the blue wing at roughly -200 km/s (phase 0.25) or the red wing at about $+200$ km/s (phase 0.75) of He I 6678. At orbital phase 0.5, the invariant emission is detectable in both line wings. At phase 0.0 the line profile is almost featureless, except for a weak emission peak. This is the single-peaked emission that just becomes visible in the red wing of the line profile. The model does not allow for non-zero eccentricities. However, it should be noted that, according to the orbital parameters derived in section 3.5, the periastron is situated at orbital phase 0.57.

4.2 Sector model

The parameters of the emission regions of individual lines can be determined with the sector model by Hummel & Štefl (2001). In this model the above described geometry is assumed. The emission which arises from a disc sector is modelled by fitting phase-resolved line profiles over an entire orbital cycle. It is assumed that the sector is photoionized by the UV continuum radiation of the hot companion and not by single fluorescence lines. Hence, the incoming exciting radiation is expected to be independent of wavelength. The phase-locked variability of the

emission lines is assumed to be caused by geometric effects. This variability is simulated, therefore, by modelling the time-dependent geometrical distribution of the emission.

In the model it is assumed that discs around Be stars in binary systems and around single Be stars have the same physical properties. The disc is assumed to be in the equatorial plane of the primary, which is also assumed to be the orbital plane of the binary. The disc is taken to be axisymmetric in density and isothermal. The temperature of the disc is approximated as 2/3 of the effective temperature of the Be primary. Due to the secondary star, which affects the gravitational potential and the kinematics of the disc of the Be star, the rotational velocity of the circumstellar gas is not Keplerian. These effects are considered as a disturbance to a Keplerian flow.

The disc sector is defined by two angles ϕ_1 and ϕ_2. The model allows to fix a phase shift $\Delta\phi$, which is the angle between the node-line, connecting the binary components, and the centre of the photoionized sector $(\phi_1 + \phi_2)/2$. This is required if symmetric emission profiles appear before or after phases 0.0 and 0.5. These orbital phases correspond to superior and inferior conjunction.

The model is restricted to circular orbits and orbital inclinations $\leq 84\,^{\circ}$. The Roche radius of the primary star limits the radial extension of the disc. Effects of self-absorption in the disc, shell absorption, and stellar obscuration are included in the model.

The input parameters for the model are the inner and outer radius of the line emitting region, $R_{\rm i}$ and $R_{\rm d}$, the emissivity of the sector, $S_{\rm l}$, the inclination i, the equatorial radius $R_\star$ and the effective temperature $T_{\rm eff}$ of the Be star, the Kepler rotation, i.e. the rotation velocity at the inner radius of the disc, $v_{\rm K}$, the occupation density n_0, the full opening angle of the sector, $\phi_2 - \phi_1$, a phase shift of the centre of emission, $\Delta\phi$, and the ionisation radius of the secondary, $R_{\rm sec}$. The parameters $R_{\rm i}$, $R_{\rm d}$, $v_{\rm K}$, i, n_0, $S_{\rm l}$, $\phi_2 - \phi_1$, $\Delta\phi$, and $R_{\rm sec}$ can be fitted. Up to six of these parameters can be modelled simultaneously. For the multi-parameter fit a simplex method is used.

4.3 Modelling and results

The above described sector model was applied to fit the He I 6678 emission of 59 Cyg. An effective temperature of $\log T_{\rm eff}$ = 4.413 (Harmanec et al. 2002) was adopted. Models were calculated for a range of likely inclinations and corresponding primary masses as determined in section 3.6. For an inclination of i = 65 $^{\circ}$ a primary mass of M_1 = 9.72 $\mathrm{M}_\odot$, for i = 70 $^{\circ}$ a mass of M_1 = 8.72 $\mathrm{M}_\odot$, and for i = 75 $^{\circ}$ a mass of M_1 = 8.03 $\mathrm{M}_\odot$ was adopted. In contrast to the inclination, which is an input parameter for the model, the stellar mass is not directly used. It is taken

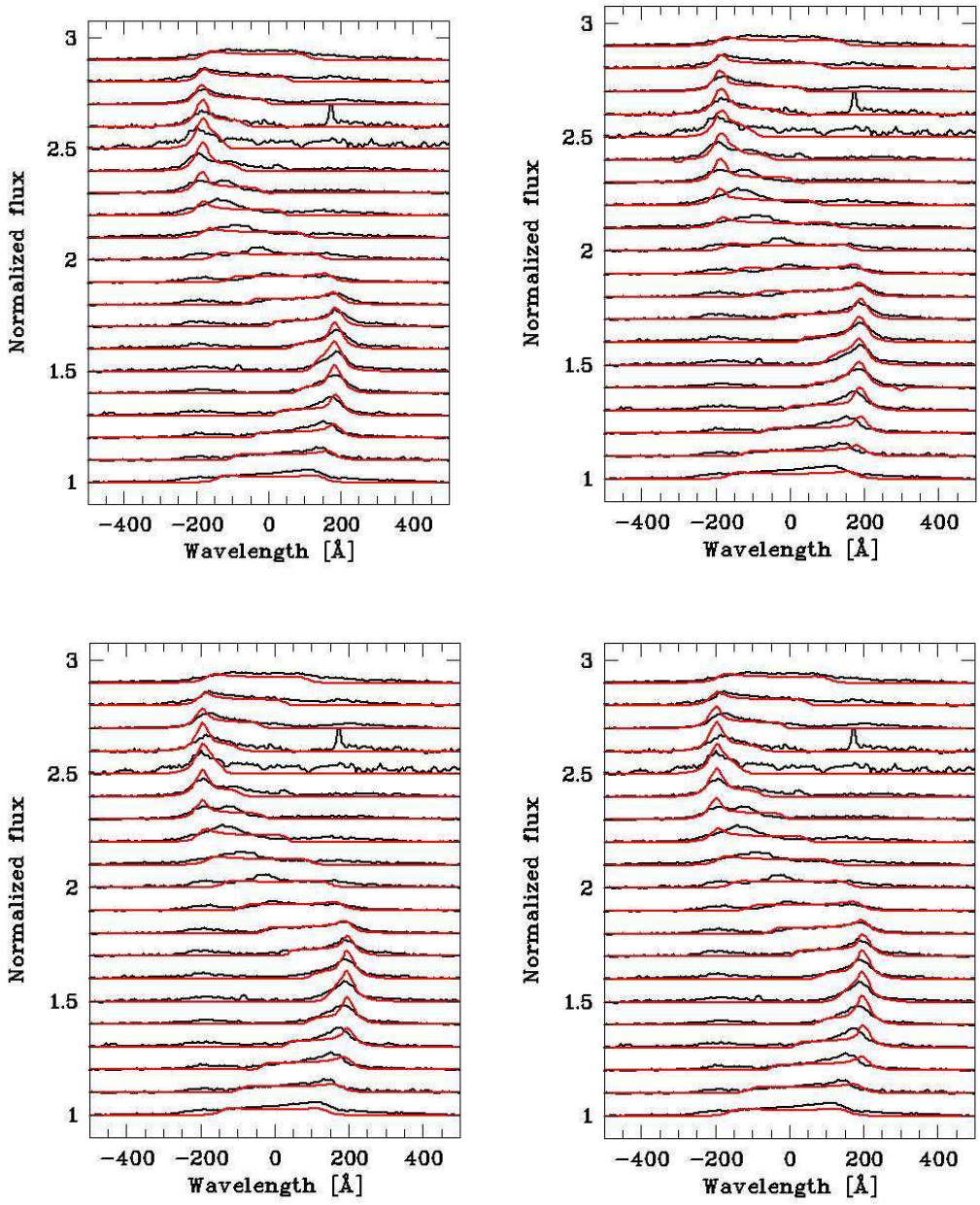

Figure 4.2: Modelling results (red) for the He I 6678 emission of 59 Cyg. The observed line profiles (black) are phase-binned and averaged for each bin. Upper left: Model 1; Upper right: Model 2; Lower left: Model 3; Lower right: Model 4. The input parameters for the models are listed in Tab. 4.1.

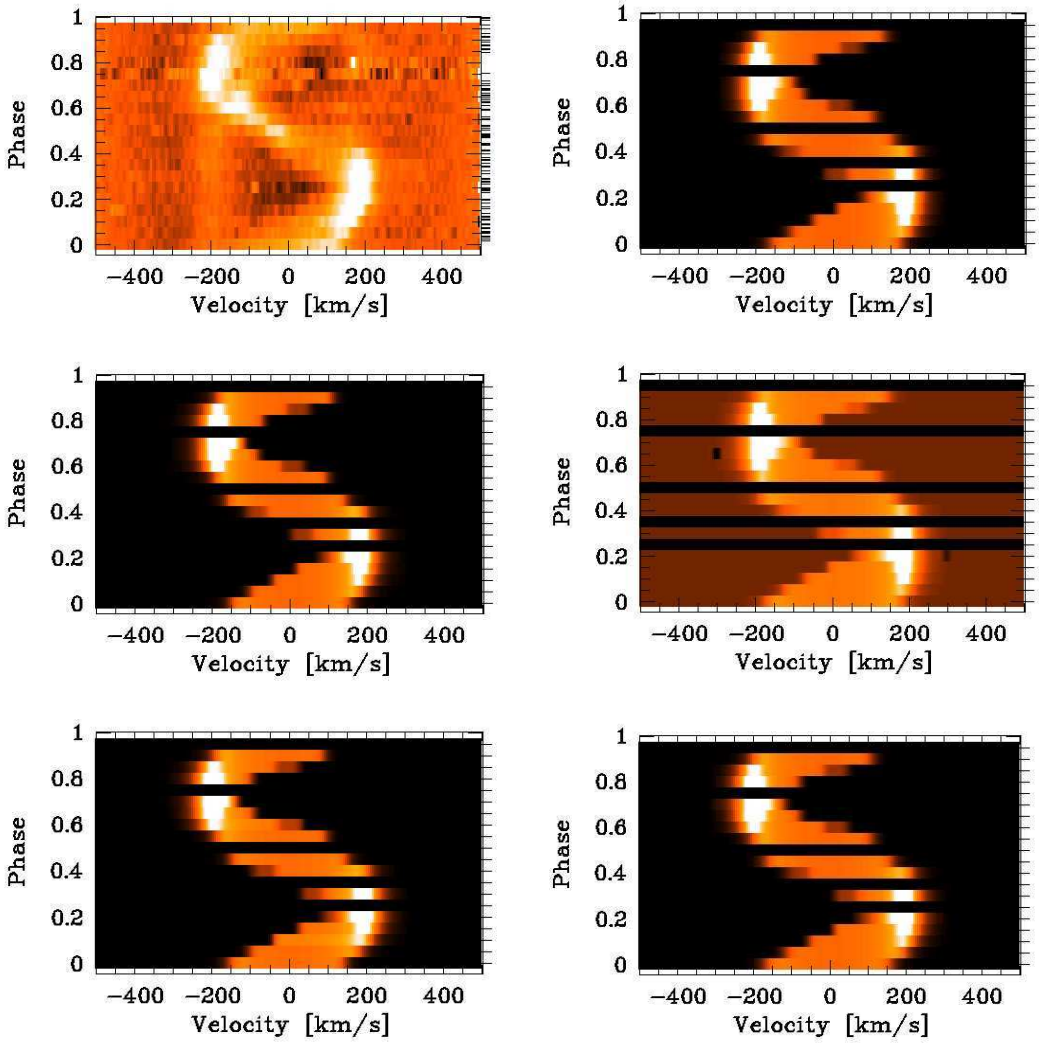

Figure 4.3: Modelling results for the He I 6678 emission of 59 Cyg. Dynamical spectra for the observed and modelled data. Upper left: Doppler-shift corrected observed line profiles of He I 6678; Upper right: Model 5; Middle left: Model 1; Middle right: Model 2; Lower left: Model 3; Lower right: Model 4. The input parameters for the models are listed in Tab. 4.1.

to calculate the Keplerian velocity for a given stellar radius.

With their evolutionary models, Claret & Giménez (1995) derived stellar radii and effective temperatures for initial masses between 7.5 and 11 $M_{\odot}$. Compared to radii derived from observational fundamental parameter calibrations (Harmanec 1988), these radii seem to be systematically smaller. Since Maintz et al. (2002), modelling the line profile variability of single Be stars, also derived quite small

Table 4.1: Input parameters for the models of He I 6678 shown in Figs. 4.2 and 4.3 (i: Inclination; $R_{\rm eq}$: Equatorial radius; $V_{\rm Kepler}$: Keppler velocity; $\phi_2 - \phi_1$: Opening angle of the illuminated disc sector).

Parameter	i	$R_{\rm eq}$	$V_{\rm Kepler}$	$\phi_2 - \phi_1$
Model 1	$65^{\rm o}$	$6.0\,{\rm R}_\odot$	$680\,{\rm km/s}$	$100^{\rm o}$
Model 2	$70^{\rm o}$	$6.0\,{\rm R}_\odot$	$644\,{\rm km/s}$	$120^{\rm o}$
Model 3	$70^{\rm o}$	$5.25\,{\rm R}_\odot$	$688\,{\rm km/s}$	$90^{\rm o}$
Model 4	$75^{\rm o}$	$5.25\,{\rm R}_\odot$	$661\,{\rm km/s}$	$100^{\rm o}$
Model 5	$75^{\rm o}$	$5.31\,{\rm R}_\odot$	$622\,{\rm km/s}$	$110^{\rm o}$

radii compared to observational calibrations, only radii of 3.0, 3.5, and 4.0 $\rm R_\odot$ were considered for the modelling. For each combination of inclination and stellar mass, simulations were carried out for these three radii.

In the literature stellar radii are given for non-rotating or slowly rotating stars only. Since Be stars rotate close to their critical limit (Owocki 2003), their equatorial radii are roughly 1.5 times larger than their polar ones (Harmanec 1988). Stellar radii as given in the literature for non-rotating stars correspond quite well to the polar radii of stars that rotate critically. Therefore, the above mentioned radii have to be multiplied by a factor of 1.5 to get an estimate for the equatorial radii. These are required as input parameter for the model and to derive Kepler velocities for given stellar masses.

To take the findings of Harmanec et al. (2002) into account, models were calculated for an equatorial radius of 5.31 $\rm R_\odot$, too. This radius was derived for 59 Cyg by Harmanec et al. using the HIPPARCOS parallax. Models were also computed for a stellar radius of 4.85 $\rm R_\odot$. According to Harmanec's calibration (1988), this is the radius of a star with an effective temperature of $\log T_{\rm eff}$ = 4.413 as derived for 59 Cyg by Harmanec et al. (2002). The corresponding stellar mass adopted was 10.78 $\rm M_\odot$.

Modelling results are shown in Figs. 4.2 and 4.3. In Table 4.1 the input parameters for these models are given. The models match the general appearance of the variability well. The parameters describing the Be disc are very similar for all models. Concerning inclination, Keplerian rotation to derive the primary mass, and equatorial radius, no marked set of best fitting parameters is found. The models, calculated for different combinations of these parameters, yield comparable results. Therefore, it is not possible to further constrain these parameters by the modelling.

In general, models computed with equatorial radii of 5.25 and 6.0 $\rm R_\odot$ (corre-

sponding to polar radii of 3.5 and 4.0 $R_{\odot}$) match the observed data better. This is true also for models with higher Kepler velocities and thus smaller radii. Models fitting well the variability in the blue wing do not match well the variability in the red wing and vice versa. In general, the observations are matched quite well if disc sectors with opening angles between 90 ^{o} and 120 ^{o} were assumed. The models reproduce the variability in the blue wing better, if sectors with larger opening angles are assumed, while the variability in the red wing is better matched with lower opening angles. Models adopting the stellar radius derived by Harmanec et al. (2002) match the data better if an inclination of 75 ^{o} is used instead of 65 ^{o} or 70 ^{o}.

The single-peaked emission is more strongly pronounced in the blue than in the red line wing. This may provide a clue why the variability in the blue or red line wing is matched by different sets of input parameters, in particular for orbital phases around 0.68. Also the values for the equivalent widths of Hα and Hβ are generally larger between orbital phases 0.5 and 1.0, especially after the periastron passage at phase 0.57, than between phases 0.0 and 0.5 (cf. section 3.7.3). This is interpreted assuming that a larger part of the disc of the Be star becomes photoionized when the secondary is closer to the outer edge of the disc. This supports that the single-peaked emission in the blue wing is generally better matched by a disc sector with larger opening angle. Since the sector model is only designed for circular binary orbits and hence for a constant opening angle, this finding cannot be checked by this model.

Due to the successful modelling of the phase-locked variability of the He I 6678 emission, the assumptions for the disc model are confirmed. A photoionized disc sector facing a hot companion can explain the characteristic features which are attributed to evolved Be binaries with hot, compact companions.

Chapter 5

Be binaries with evolved companions

Many Be stars show weak absorption cores in the blue or red peak of double-peaked emission lines (Fig. 5.1). Concerning Hα, these absorption cores are different from the telluric line near Hα which is present in the red component of the double-peaked emission. These so-called satellite absorptions occur at specific orbital phases and reappear periodically in the spectra of e.g. 59 Cyg, ϕ Per, and HR 2142. Such features cannot be explained by a disc around a single Be star. As satellite absorptions are visible in the spectra of many confirmed Be binaries, they are taken as indicator for binarity (Maintz et al. 2003). They were used as preselection criterion for candidate stars for evolved Be binaries with hot, compact companions.

The confirmed Be + sdO binaries ϕ Per and 59 Cyg, and the well-known Be binary HR 2142 show common spectral features that are explicable by the presence of a hot, compact companion. These features reappear periodically with the orbital period of the binary systems. They include phase-locked emission variability and short-lived shell phases and are taken as characteristic features for evolved Be binaries with hot companions. These spectral features are used for the identification of Be + sdO and Be + WD binaries within a sample of preselected candidate stars for evolved Be binaries. If these features are detected unambiguously in the spectrum of a candidate star, this star is confirmed to be an evolved Be binary with a sdO or WD companion.

The spectral variability of ϕ Per and HR 2142 is described in sections 5.1 and 5.2. A comparison of the periodic spectral features of 59 Cyg, ϕ Per, and HR 2142, which are assumed to characterize Be binaries with hot, compact companions, is presented in section 5.3. In section 5.4 these features are used to identify Be + sdO or Be + WD binaries within a sample of preselected candidates for evolved Be binary systems.

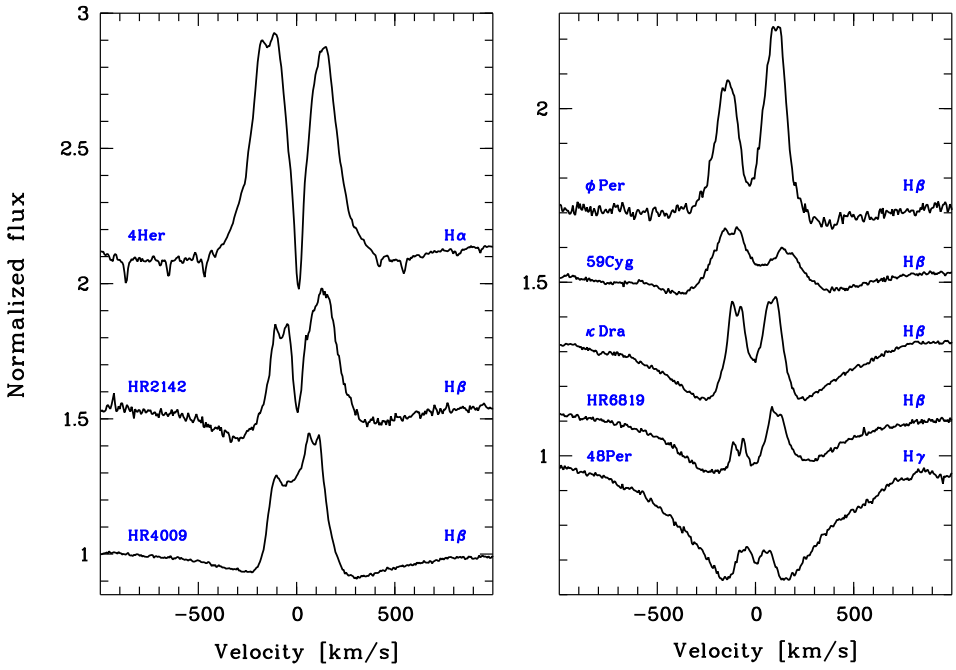

Figure 5.1: Satellite absorptions, visible in the blue or red peak of the double peaked emission profiles of Hα, Hβ, and Hγ of the confirmed Be binaries 4 Her, HR 2142, ϕ Per, 59 Cyg, and 48 Per and the suspected Be binaries HR 4009, κ Dra, and HR 6819.

5.1 ϕ Per

The first Be star proved to be a Be + sdO binary was ϕ Per (HD 10516, HR 496; B1.5Ve, Slettebak 1982; B0.5III–Ve+sdO6, Thaller et al. 1995, Gies et al. 1998). Since the beginning of the 20th century (Cannon 1910; Ludendorff 1910) it is known to be a spectroscopic binary with a period of $\mathcal{P} \simeq 127$ d. Its optical spectrum is characterized by broad photospheric absorption profiles, strong emission of hydrogen and metal lines, strong blends, like in 59 Cyg, and shell absorption features in the cores of Balmer and He I lines. These shell lines have maximal intensity around superior conjunction of the primary, i.e. when the secondary is in front of the Be star (cf. Poeckert 1981 and Štefl et al. 2000; Fig. 5.2). In some lines, shell features are visible only around the time of superior conjunction.

Using high resolution spectrograms, Poeckert (1979, 1981) found He II 4686 emission and derived a radial velocity curve. Since this had a large amplitude and was in anti-phase to the radial velocity curve of the Be primary, he suggested that ϕ Per consists of a rapidly rotating early B-type star and a hot peculiar companion. The companion would be the helium-rich remnant of a once more massive star that had transferred mass and angular momentum to the nowadays primary.

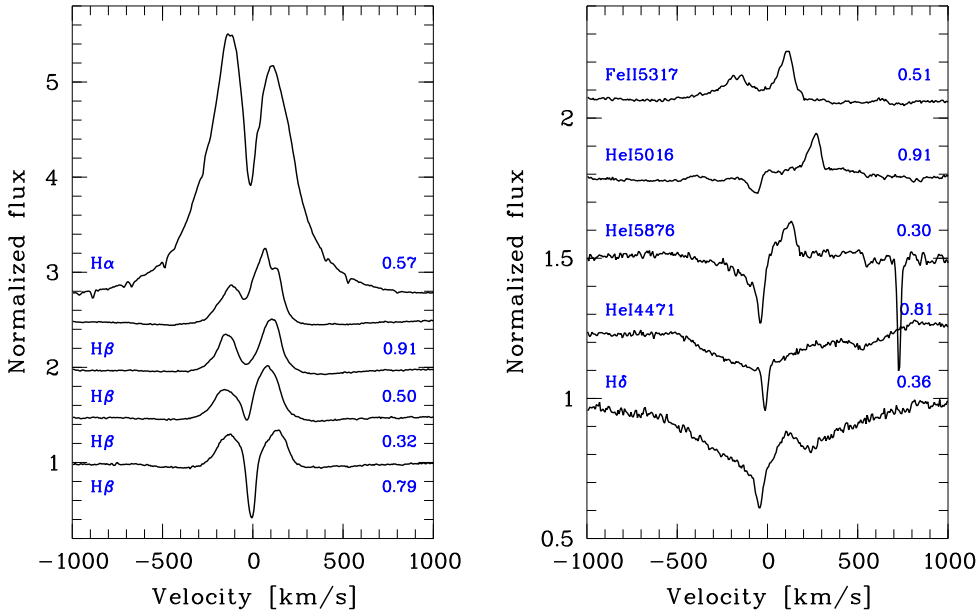

Figure 5.2: Examples of broad absorption, emission, and shell lines of ϕ Per. The numbers indicate the orbital phase. He I 5016 is blended by Fe II 5018. The sharp absorption close to He I 5876 is the interstellar Na I line at 5890 Å.

He assumed both components to have circumstellar discs. The He II emission should then arise in the disc of the secondary. An orbital solution for the binary system gave masses of 21 $M_\odot$ for the primary and 3.4 $M_\odot$ for the secondary star, respectively (Tab. 5.1).

Furthermore, Poeckert discovered shell lines of H I and He I, following the velocity curve of the primary, and weaker secondary shell lines of He I, following the radial velocity curve of the companion. He found a phase-locked strengthening of He I shell lines, which were assumed to form in the circumstellar disc of the Be star, close to primary superior conjunction. Because of this enhanced shell phase and a phase-locked V/R variability of the Balmer emission lines, Poeckert suggested that the part of the Be disc facing the secondary, is a region of enhanced density.

Gies et al. (1993) found that the He I 6678 emission resolves into two components at quadrature phases. Both components move in anti-phase to the motion of the primary. The velocity curve of the stronger component was found to be very similar to the one of the He II emission. Therefore, it was assumed to originate in the circumstellar gas close to the secondary. The weaker component with smaller semi-amplitude would, then, form in a gas stream between the binary components.

Table 5.1: Published stellar parameters and orbital elements of ϕ Per.

Published by	**Poeckert (1981)**	**Božić et al. (1995)**	**Gies et al. (1998)**
Primary:			
Spectral type	B0 to B2	B0.5IVe	B0.5III–Ve
$T_{\rm eff}$			29 300 K
$\log g$			3.7
$v \sin i$	450 km/s	500 km/s	450 km/s
Secondary:			
Spectral type	O-type		sdO
$T_{\rm eff}$	50 000 K		53 000 $\pm$3000 K
$\log g$			4.2 $\pm$0.1
Orbital elements:			
Period, $\mathcal{P}$	126.696 $\pm$1.987 d	126.6731 $\pm$0.0071 d	126.6731 $\pm$0.0071 d [1]
$T_{\rm SC}$ (MJD)		35046.23	50122.94
$T\,(p = 0.0)$ (MJD)	24473.0		
T_0 (MJD)	43554.8 $\pm$71.7		
p_{T_0}	0.62 $\pm$0.06		
Eccentricity, e	0.02 $\pm$0.04	0.0	0.0 [1]
Periastron length, Φ	145 $\pm$20.3 $^{\rm o}$		
K_1	16.8 $\pm$1.7 km/s	10.39 $\pm$0.68 km/s	9.97 km/s
K_2	105.3 $\pm$7.4 km/s	100.8 $\pm$6.2 km/s	81.3 $\pm$0.6 km/s
System velocity, v_0	$-$8.4 $\pm$1.4 km/s	$-$6.12 km/s	$-$1.98 km/s
Stell. parameters:			
$M_1 \sin^3 i$	21.1 $\pm$5.6 $\rm M_\odot$	16.35 $\rm M_\odot$	8.91 $\pm$0.26 $\rm M_\odot$
$M_2 \sin^3 i$	3.4 $\pm$0.8 $\rm M_\odot$	1.69 $\rm M_\odot$	1.09 $\pm$0.09 $\rm M_\odot$
$a_1 \sin i$	42.0 $\pm$4.3 $\rm R_\odot$		
$a_2 \sin i$	264.4 $\pm$18.7 $\rm R_\odot$		
$a \sin i$	306.3 $\pm$23.0 $\rm R_\odot$	278.2 $\rm R_\odot$	228.3 $\pm$2.5 $\rm R_\odot$
Inclination, i	80 $^{\rm o}$ – 88 $^{\rm o}$	65 $^{\rm o}$ < i < 90 $^{\rm o}$	80 $^{\rm o}$
Mass of prim., M_1		16.4 < M_1 < 21.8 $\rm M_\odot$	9.3 $\pm$0.3 $\rm M_\odot$
Mass of sec., M_2		1.7 < M_2 < 2.2 $\rm M_\odot$	1.14 $\pm$0.04 $\rm M_\odot$
Binary separation, a		278 < a < 307 $\rm R_\odot$	232 $\rm R_\odot$

[1]: Orbital element adopted from Božić et al. (1995)

$T_{\rm SC}$: Time of superior conjunction of the primary, orbital phase 0.0
$T\,(p = 0.0)$: Time of orbital phase 0.0, used by Poeckert (1981) instead of $T_{\rm SC}$
T_0: Time of periastron passage
p_{T_0}: Orbital phase of periastron passage
K_1, K_2: Velocity amplitude of primary, secondary
$M_1 \sin^3 i$, $M_2 \sin^3 i$: Mass of primary, secondary
$a_1 \sin i$, $a_2 \sin i$: Semi-major axis of primary, secondary

Additionally, the equivalent width of the He I 6678 emission as a whole was found to increase very much near superior conjunction of the primary.

Božić et al. (1995) determined orbital elements for both binary components on the basis of radial velocities measured for the emission wings of Balmer lines and the He I 6678 emission (Tab. 5.1). In contrast to Gies et al. (1993), they interpreted the He I 6678 emission as double-peaked emission, arising in the circumstellar disc of the secondary entirely, like the double-peaked He II 4686 emission. They found that the emission of the Balmer lines and of He I 6678 had weakened simultaneously in recent years. Since this emission was thought to arise in the circumstellar discs of primary and secondary component, respectively the simultaneous variability was interpreted as binary interaction.

A feature similar to the He I 6678 emission was discovered in He I 5876 by Hummel & Vrancken (1995). They argue, however, that all He I emission forms in the disc around the Be primary.

Direct evidence for a hot companion of ϕ Per was found by Thaller et al. (1995) and Gies et al. (1998). Using high resolution UV spectra observed with IUE and the Hubble Space Telescope, respectively, they reconstructed the individual spectra of both components with Doppler tomography. The resulting spectrum of the secondary is similar to the one of a sdO6 star (Thaller et al. 1995). Furthermore, Gies et al. (1998) measured radial velocities of lines in the reconstructed spectra and derived an orbital solution for the binary (Tab. 5.1).

Štefl et al. (2000) showed that the variable He I 6678 emission feature originates entirely in the outer part of the circumstellar disc of the Be primary. The variability is fully explained by photoionization of a disc sector by the UV continuum radiation of the secondary. This sector faces the secondary component. Emission features with phase-locked variations were found in three more He I lines. In contrast to Poeckert (1981), they found that the maximum shell absorption in He I 6678 appeared at orbital phase 0.8. (Phase 0.0 corresponds to superior conjunction of the primary.) Additionally, a long-term V/R variability of the emission lines has started in 1996. This variability and the shift of the shell phase maximum is explicable, if a global density pattern in terms of a one-armed disc oscillation (Okazaki 1991, 1997) is assumed, as it occurs also in single Be stars.

Assuming the above mentioned illuminated disc sector, Hummel & Štefl (2001) successfully modelled the phase-locked variability structure of He I 6678 and 5876. According to the modelling, both emission lines arise in a region within 10 $R_\star$ in the circumstellar disc of the primary. This agrees with an emission radius of 10 stellar radii found for Hα by interferometric observations (Quirrenbach et al. 1997).

Vanbeveren et al. (1998) computed evolutionary tracks for ϕ Per and classified it as an intermediate-mass post case B mass transfer system (for definition see footnote on page 3).

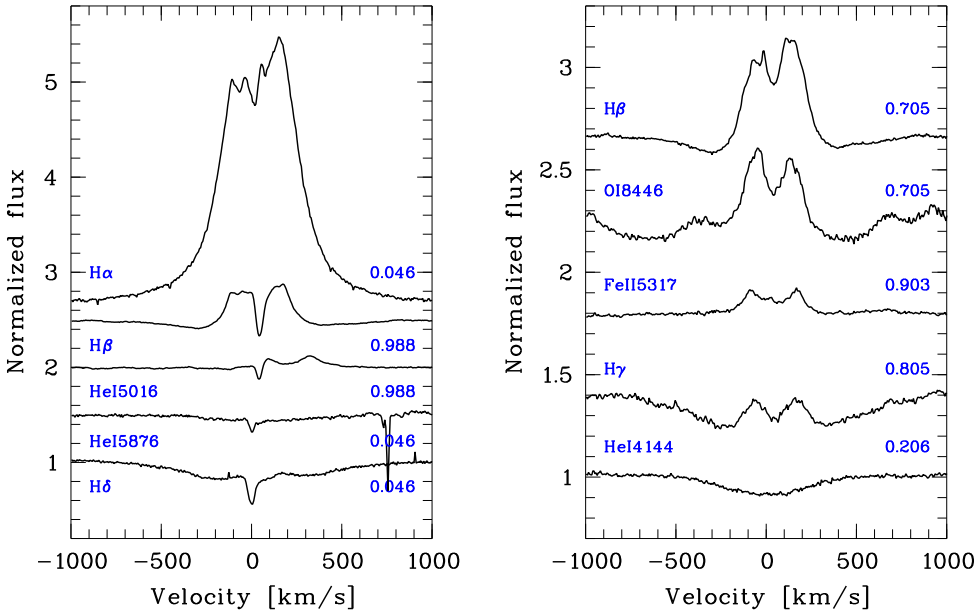

Figure 5.3: Examples of broad absorption, emission, and shell lines of HR 2142. The numbers indicate the orbital phase. He I 5016 is blended by Fe II 5018. The sharp absorption close to He I 5876 is the interstellar Na I line at 5890 Å. O I 8446 is blended by P18 in the blue wing.

5.2 HR 2142

HR 2142 (HD 41335; B2IVe, Slettebak 1982; B1.5IIIen, Chauville et al. 2001) is a well studied Be binary with an orbital period of 80.860 d (Peters 1983). The rapidly rotating Be primary has a $v \sin i$ of roughly 350−400 km/s (Peters 1972; Slettebak 1982). It shows phase-locked short-term variability of the same kind as observed in the spectra of ϕ Per and 59 Cyg.

The optical spectrum is characterized by broad absorption lines and strong line emission (Fig. 5.3). The Balmer lines are visible in absorption with a strong central double-peaked emission feature, decreasing in strength quickly towards higher lines. The Paschen lines show very strong emission. He I is in absorption, but some of the lines show a central emission like the Balmer lines. Fe II , O I 7772–5, and O I 8446 are visible in emission. C II 4267 is visible in absorption.

V/R variations of the emission components in Hβ, Hγ, and Hδ were reported since the early 20th century (Perrine 1923). Miczaika (1949) found central absorption components in the emission features of Hβ–Hϵ. Permanent weak central absorptions were found in Hβ, Hγ, and stronger Fe II lines by Peters (1971).

Table 5.2: Orbital elements for the Be binary HR 2142 from Peters (1983).

Orbital parameter	HR 2142
Orbital period, $\mathcal{P}$	80.860 $\pm$0.005 d
Superior conj., $T_{\rm SC}$ (MJD)	41990.0 $\pm$1.1
Eccentricity, e	0.0
Velocity amplitude, K_1	9.4 $\pm$0.9 km/s
System velocity, v_0	24.1 $\pm$0.6 km/s
Mass function, $f(M)$	0.007 $\pm$0.002 $M_\odot$
Binary separation, $a \sin i$	14.9 $\pm$1.4 $R_\odot$

The most conspicuous feature of HR 2142 is a "two-component shell phase" (Peters 1972, 1983), occuring strictly periodically around superior conjunction of the primary. It consists of a pimary and a secondary shell phase with roughly the same intensity of the Balmer cores. The pimary shell phase lasts roughly 6 d. It is characterized by redshifted shell lines. The duration of the secondary shell phase is only 1.5 d. The secondary shell lines are blueshifted. Between primary and secondary shell phase there is a gap of about five days. Shell features appear in the Balmer cores, He I 3889, 3964, and 5016.

Shell features appear in Hβ already at orbital phase 0.895. In the higher Balmer lines they become visible at phase 0.925. The sharp Balmer cores and the shell features in the helium lines reach maximal strength at phase 0.965. Finally, the intensity decreases rapidly as the star approaches superior conjunction (phase 0.0). The shell lines disappear at phase 0.980. They reappear again during the secondary shell phase, lasting from phase 0.027 – 0.044, with about the same strength.

Peters interpreted the occurance of the two shell phases in terms of binary interaction. HR 2142 is, therefore, assumed to be a mass-transfer binary system. The companion is supposed to be a cool giant, filling its Roche-lobe, and transfering material to the Be primary. In this scenario the pimary shell phase occurs, when the Be primary is visible through a main gas stream from the secondary. The secondary shell phase is explicable, if the Be star is visible through "counter streaming" material.

On the basis of radial velocities, measured for the absorption wings of the broad Balmer and He I lines, Peters derived an orbital solution for the binary system (Tab. 5.2). The orbital period is so accurate that it was possible to predict a shell phase for 2002 February 26 till March 10. The primary shell phase was monitored with the echelle spectrograph FEROS at the ESO 1.52 m telescope at La Silla, Chile. Unfortunately, observing time was available only till March 6. Therefore,

the secondary shell phase could not be observed.

The nature of the companion star has not been identified yet. Peters (1983) argued in favour of a cool, Roche-lobe filling giant. Since Waters et al. (1991), however, could not find a signature of a cool giant star in the infrared spectral energy distribution of the binary, they suggested that the companion is a hot helium star.

5.3 Characteristic features due to a hot companion

The analysis of 59 Cyg revealed spectral features which are explicable within the scope of the sector model described by Štefl et al. (2000); Hummel & Štefl (2001). This model is based on the assumption that a Be star is an evolved Be binary with a hot, low-mass secondary component. The companion is either a helium star or a hot white dwarf. The above mentioned spectral features are generally predicted by this model and, therefore, characteristic for this kind of double stars.

These features arise due to emission that originates in a sector of the Be disc which is photoionized by the hot secondary. This emission is detectable in three ways: Firstly, as single-peaked emission that moves in anti-phase to the velocity curve of the pimary, secondly, as phase-locked V/R variability, and thirdly, as knotty absorption structure visible in the central parts of absorption lines or emission lines with only litte variable emission. If on of these features is found in the spectrum of a Be star, then, it is a promising candidate for a Be + sdO or Be + WD binary. If all of these features are unambiguously confirmed, then the Be star is a Be + sdO or Be + WD binary. Therefore, these features can be used for the search for candidates as well as for the proof of evolved Be binaries with hot, compact companions.

The illuminated disc sector is locked to the position of the secondary. Its surface area, visible for an observer, hence varies with orbital phase. This holds in particular for binaries with larger inclination angles, when also the edge of the sector becomes visible. This results in a cyclic variability of the line strength and, therefore, the equivalent widths of optically thick emission lines which form in that sector. Such a variability is clearly detectable only for Be stars only which show no regular shell events. Therefore, such variations are not taken as a general signature of evolved Be binaries with hot companions.

A hot, compact companion in an evolved Be binary is assumed to be the stripped-down helium core of an once more massive star. Such an object has a very high effective temperature. As it is an O-type star, its spectrum is characterized by photospheric He II absorption. A double-peaked He II emission can arise in a circumstellar disc around that star (Poeckert 1981). The presence of a He II absorption or emission in the spectrum of a Be star is, therefore, the direct proof of

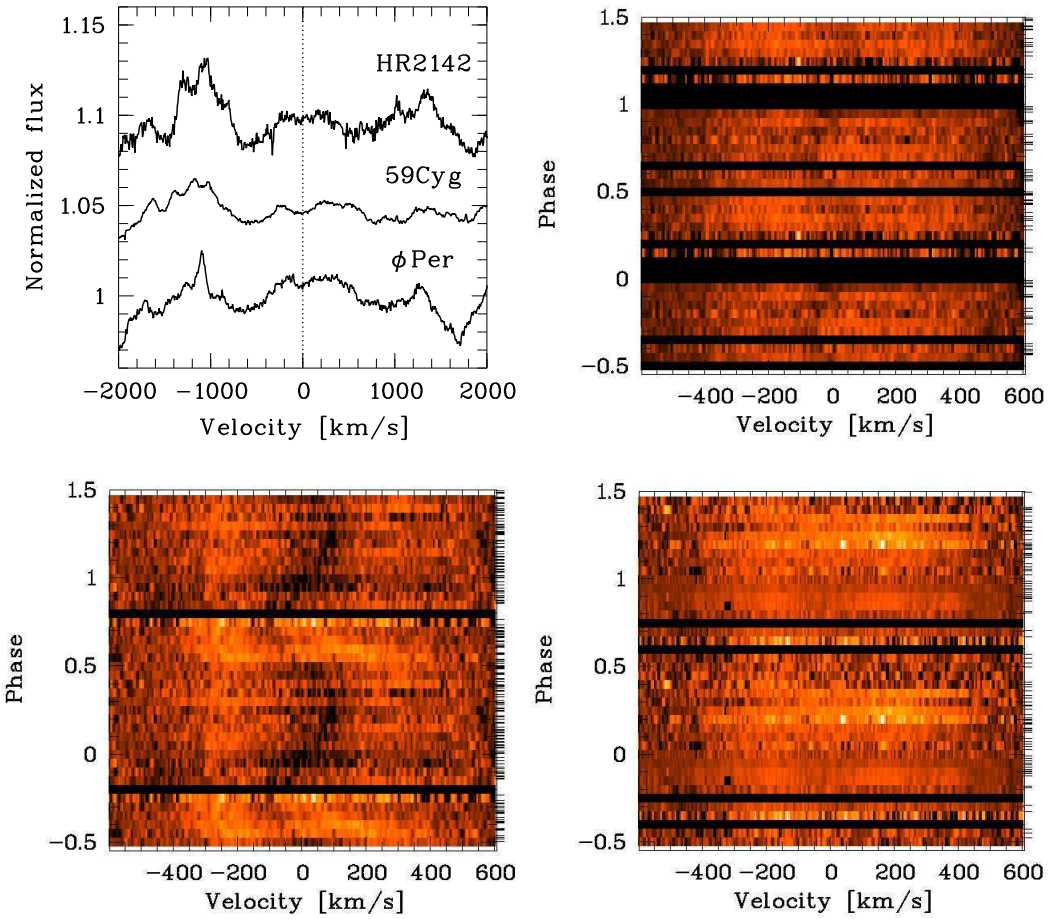

Figure 5.4: He II 4686: Averaged line profiles (upper left) and dynamical spectra of 59 Cyg (upper right), ϕ Per (lower left), and HR 2142 (lower right).

an evolved Be binary with a hot, compact companion.

If absorption cores appear in the hydrogen or helium lines of a Be star, then the star passes through a shell episode. According to the sector model, short-lived shell phases in the hydrogen and helium lines are expected to occur periodically around superior conjunction if a evolved Be binary is visible at high inclinations. Shell lines form when the illuminated disc sector passes the line of sight towards an observer. More light can be absorbed due to the enhanced excitation of the circumstellar matter in this part of the Be disc. Periodically appearing shell events are, therefore, a further characteristic feature that reveals a Be + sdO or Be + WD binary, but only if the disc of the Be star is observed edge-on.

In the following sections it will be demonstrated that the spectral features, char-

acteristic for Be + sdO or Be + WD binaries, occur not only in the spectra of 59 Cyg and ϕ Per, but also in the spectrum of HR 2142, for which a Be + sdO nature has yet to be confirmed.

5.3.1 He II 4686

In Fig. 5.4 averaged line profiles and dynamical spectra of 59 Cyg, ϕ Per, and HR 2142 are shown. They cover the region of He II 4686. The averaged line profiles of all three stars look very similar. Only for ϕ Per a reliable emission feature is visible. Due to the strong emission of neighbouring lines in this spectral region and the large rotational broadening of the line profiles, a reliable He II 4686 emission is not detectable in the averaged line profiles of 59 Cyg and HR 2142. The He II 4686 absorption found in the spectrum of 59 Cyg is clearly visible only if the line profiles are shift-corrected and averaged.

A weak absorption feature is clearly detectable in the dynamical spectra of 59 Cyg and ϕ Per. The double-peaked He II 4686 emission of ϕ Per is only litte pronounced in the dynamical spectrum. HR 2142 shows no reliable absorption or emission feature.

5.3.2 Short-term emission variability

The short-term emission variability is very well visible in the spectrum of 59 Cyg, in particular in He I 6678 (Fig. 5.5, upper left). It appears as single-peaked disc emission that moves in anti-phase to the primary component and as phase-locked V/R variability. Such a single-peaked emission is less pronounced in ϕ Per, but still very well visible in He I 6678 (Fig. 5.5, upper right), in particular between phases 0.65 and 0.95 at a velocity of roughly -150 km/s in the blue absorption wing. In the red absorption wing it is most pronounced between phases 0.15 and 0.35 at a velocity of roughly $+100$ km/s. Concerning the He I 6678 emission, the similarity between 59 Cyg and ϕ Per is striking.

In HR 2142 such variable disc emission is clearly detectable only in Hα (Fig. 5.5, lower panel). The course of the weak single-peaked feature, moving out of phase to the double-peaked invariant disc emission, is marked in Fig. 5.5 (lower right panel). Compared to the invariant emission, the phase of the variable emission is shifted by roughly 0.25. It is not clear why this phase shift occurs. Possibly this could be due to a superposition of a long-term variability like a one-armed global oscillation as in ϕ Per. There, the phase of the maximum strength of the shell lines is shifted from superior conjunction at phase 0.0 (Poeckert 1981) to about phase 0.8 after 1996 (Štefl et al. 2000). However, the detection of a single-peaked emission variability in Hα shows that a variable emission component is also present in the spectrum of HR 2142.

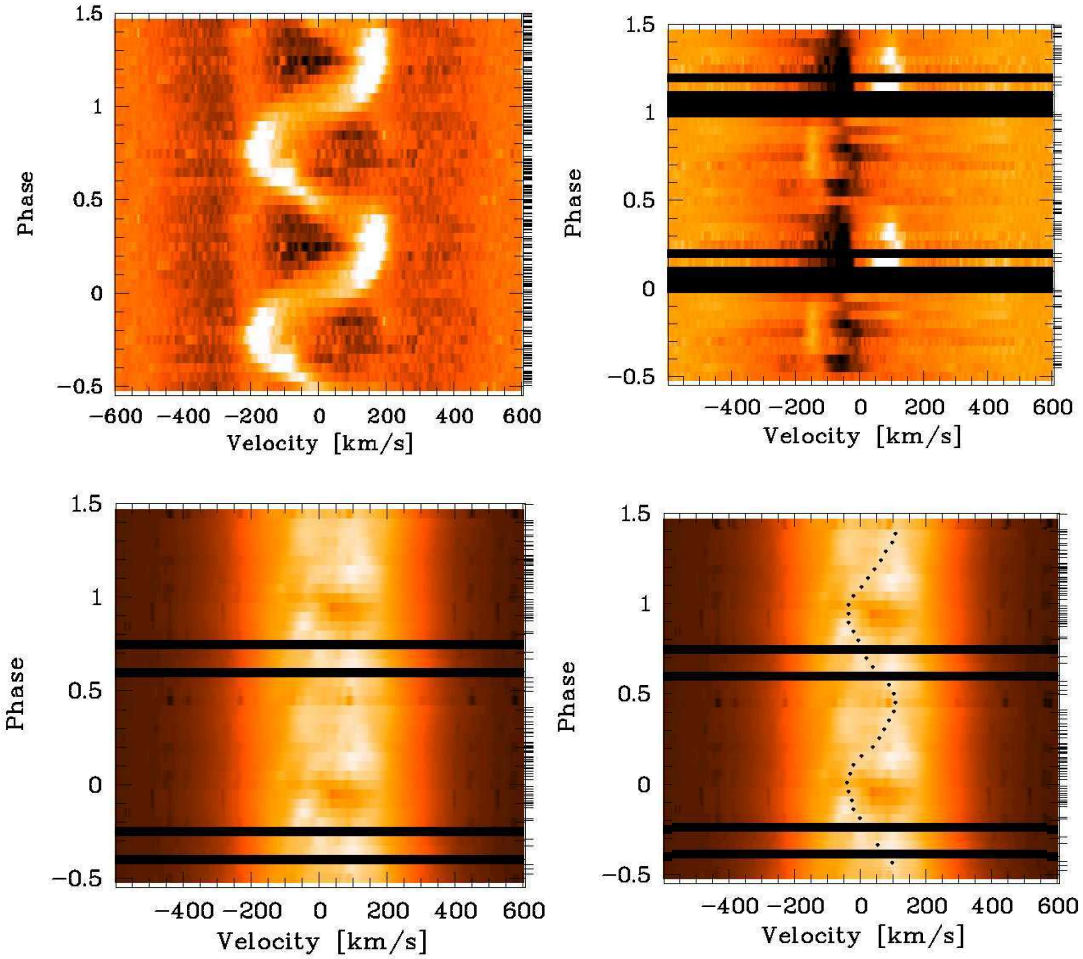

Figure 5.5: Short-term emission variability in dynamical spectra of 59 Cyg (upper panel left), ϕ Per (upper panel right), and HR 2142 (lower panel). For 59 Cyg and ϕ Per He I 6678 is shown, while for HR 2142 Hα is shown. Since the single-peaked emission is only less pronounced in Hα, additionally, the course of the feature is demonstrated by black dots in the lower right panel.

In Figure 5.6 phase-binned spectra are shown to demonstrate the appearance of the phase-locked emission variability in single line profiles. The profiles are plotted one over the other with inceasing phase. The single-peaked emission visible in He I 6678 is shown for 59 Cyg (upper panel left) and ϕ Per (upper panel right). In the lower panel the line profile variability of Hα is shown for 59 Cyg (left) and HR 2142 (right). Due to the strong underlying invariant emission, the variable component is difficult to detect in the phase-binned profiles of HR 2142. A weak red emission peak is clearly visible between phases 0.0 to 0.3 at velocities of roughly $+150$ km/s. The emission peak is best visible, however, in the blue

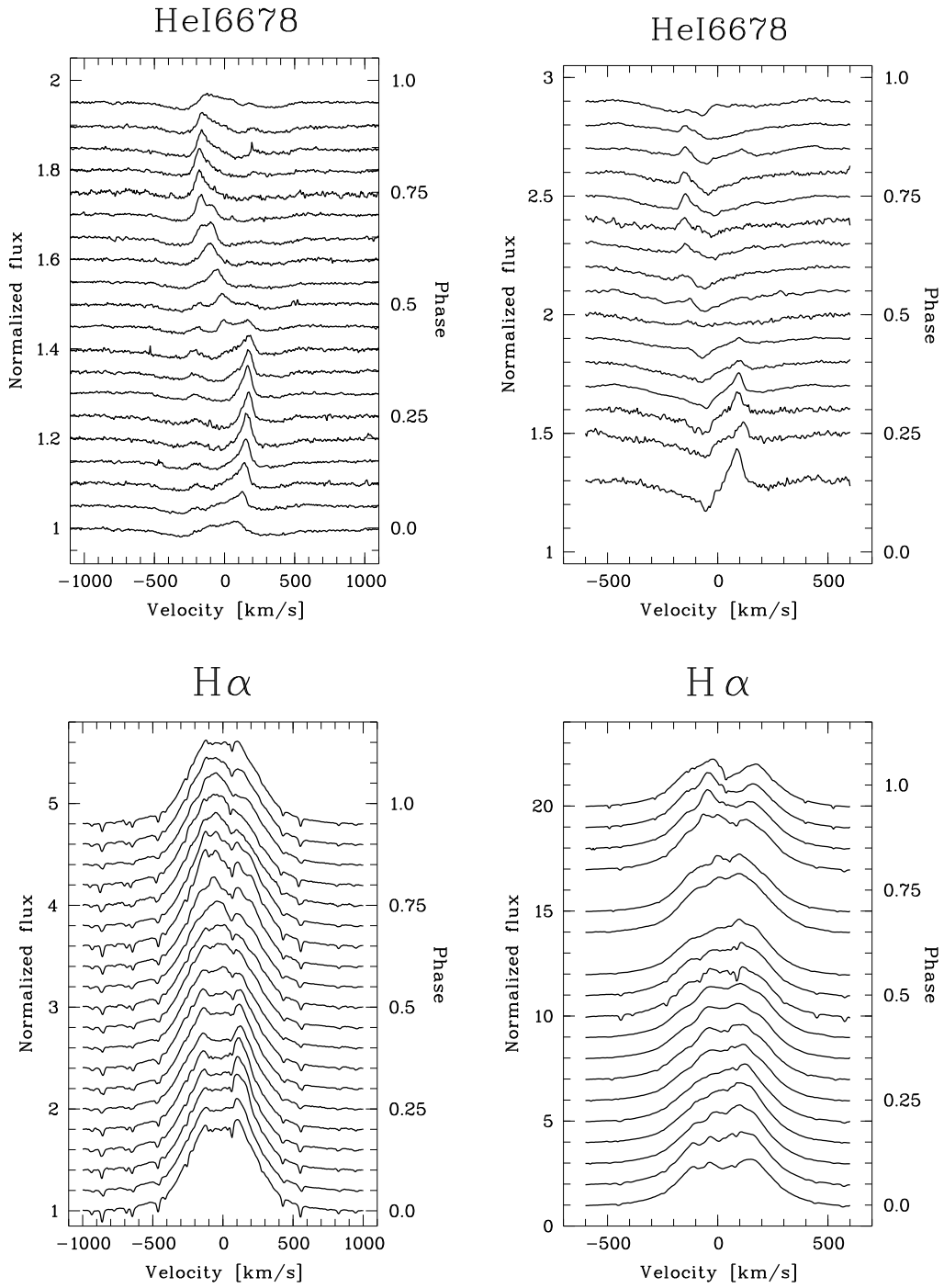

Figure 5.6: Short-term emission variability of 59 Cyg (upper left and lower left), ϕ Per (upper right), and HR 2142 (lower right). The line profiles are phase-binned and plotted one over the other with orbital phase increasing upwards.

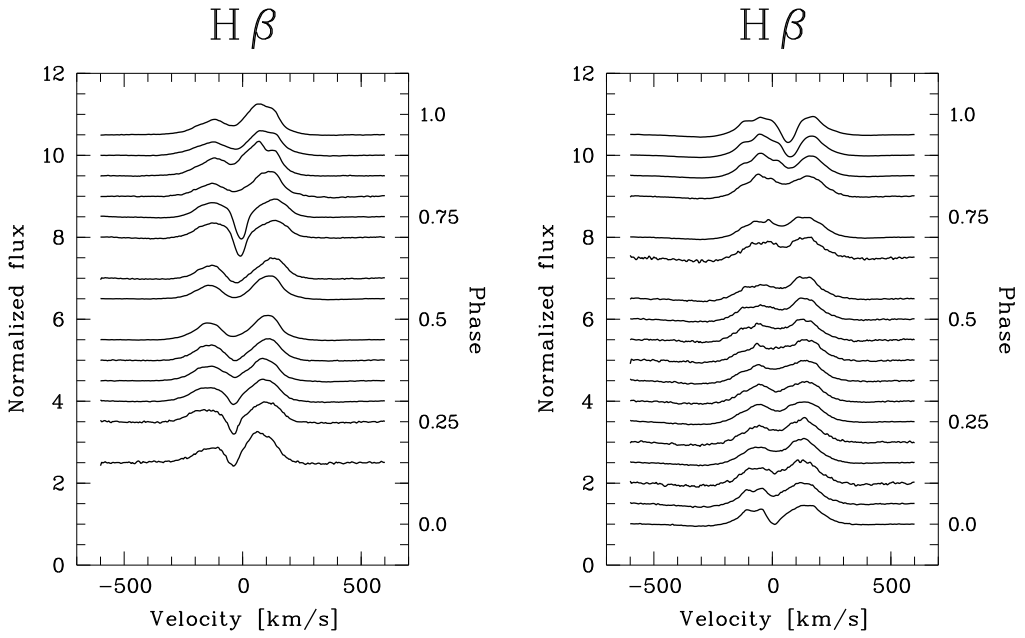

Figure 5.7: Short-term emission variability of Hβ, shown for ϕ Per (left) and HR 2142 (right). The line profiles are phase-binned and plotted one over the other, according to their orbital phase.

wing between phases 0.8 to 0.85 at velocities of roughly -50 km/s.

The short-term emission variability of Hβ is shown in Fig. 5.7 for ϕ Per (left) and HR 2142 (right). Despite of the difference in phase when the shell features appear, the similarity of the line profiles is evident. For instance the red emission peak of the double-peaked line profile visible in ϕ Per at phase 0.15 is strongly pronounced and broad, like in the profile of HR 2142 at phase 0.0. A V/R variability of the blue and red emission peaks is present in both stars.

5.3.3 Knotty absorption structure

Figure 5.8 shows spectral lines in which a knotty structure of the absorption profile is evident. Such a structure is very well visible in 59 Cyg in He I 4471 (upper panel left) and Hβ (upper panel right). In ϕ Per it is well pronounced in He I 6678 (middle panel left) and He I 4471 (middle panel right). In HR 2142 a knotty structure is only little pronounced, but clearly detectable in He I 6678 (lower panel left) and Hδ (lower panel right).

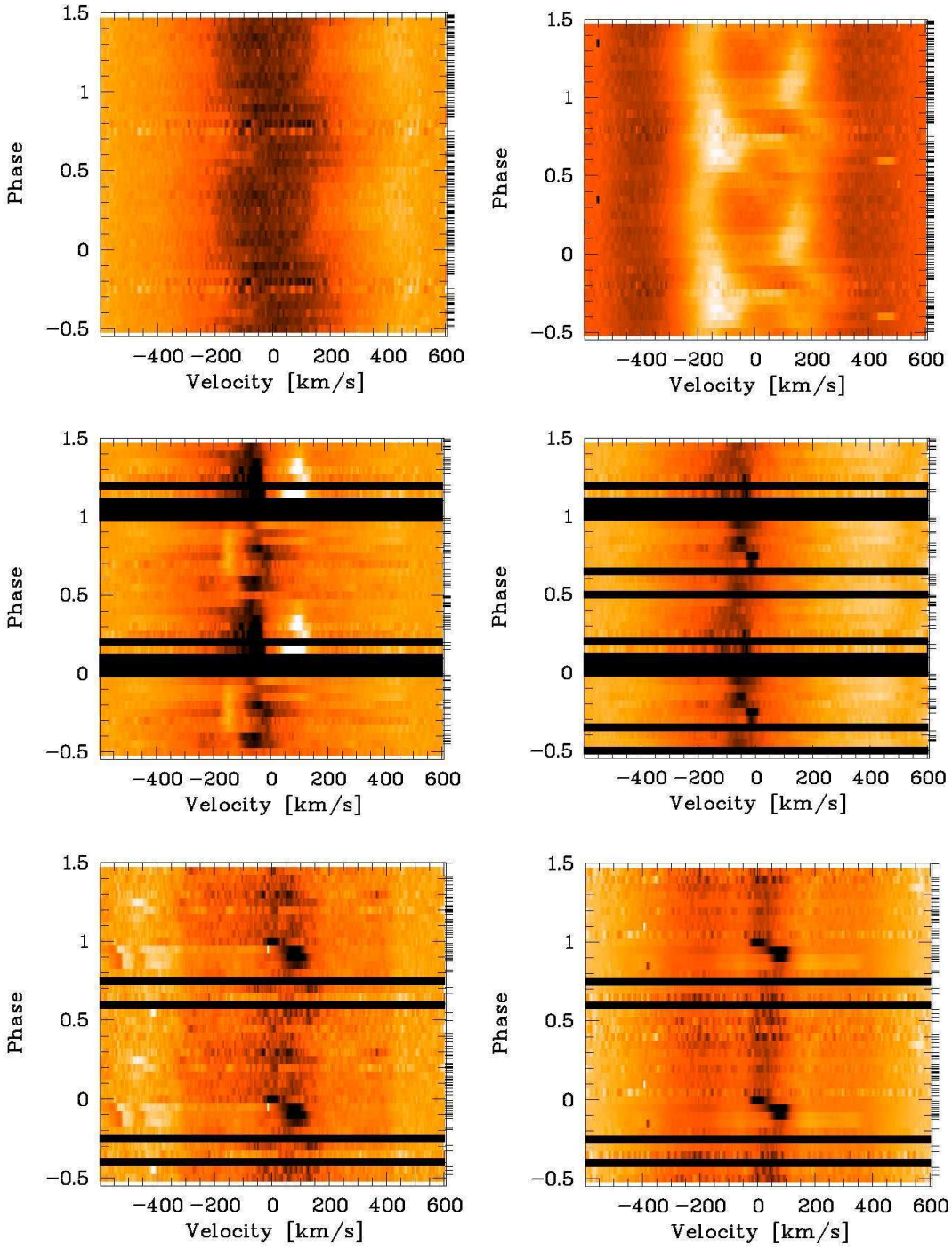

Figure 5.8: Knotty absorption structure in the line profiles of 59 Cyg, He I 4471 (upper panel left) and Hβ (upper panel right), ϕ Per, He I 6678 (middle panel left) and Hδ (middle panel right), and HR 2142, He I 6678 (lower panel left) and Hδ (lower panel right).

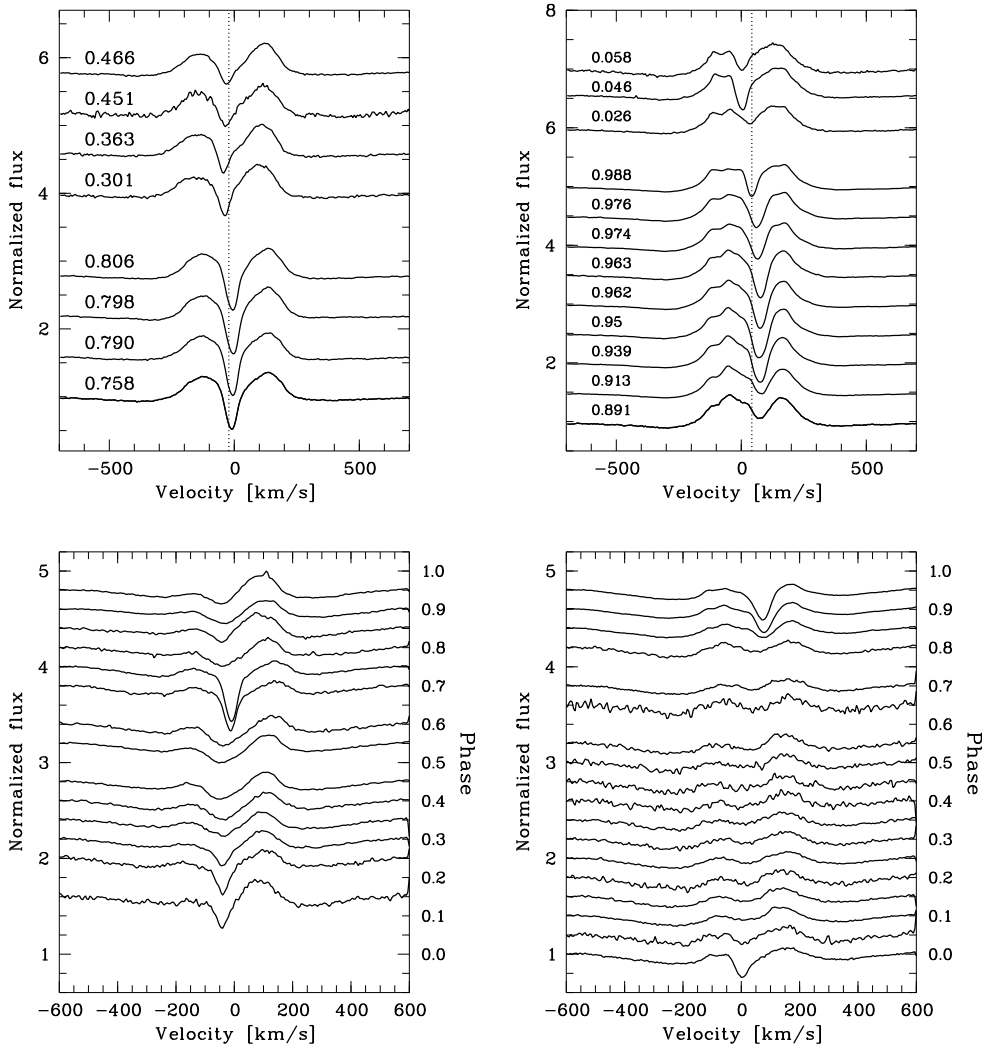

Figure 5.9: Shell lines of ϕ Per and HR 2142. Upper panel: Individual line profiles of Hβ for ϕ Per (left) and HR 2142 (right). The numbers on the left side of the plots mark the orbital phase at which the spectra were taken; Lower panel: Phase-binned, averaged line profiles of Hγ, covering an orbital cycle, for ϕ Per (left) and HR 2142 (right).

5.3.4 Short-lived shell phases

Another common feature of ϕ Per and HR 2142 is the occurance of an enhanced shell phase. Shell lines appear in hydrogen and helium lines before and after superior conjunction. In Figure 5.9, upper panel, individual profiles of shell lines of Hβ are shown for both stars. The orbital phases during which the spectra were taken are given on the left side of the plots. For both stars the shell lines

appearing before superior conjunction are blueshifted. After conjunction, they are redshifted.

In Figure 5.9, lower panel, phase-binned, averaged line profiles are shown to demonstrate the course of the shell phases. Other than in HR 2142, the occurance of the most pronounced shell lines of ϕ Per before superior conjunction is shifted to earlier phases between 0.7 and 0.8. This is attributed to a global density pattern in the inner part of the circumstellar disc of the primary component of ϕ Per (Štefl et al. 2000). Besides this, the shell phases of both stars take a similar course.

For 59 Cyg, only one shell episode is reported for the early 1970s (Barker 1982). Except of this, no futher shell event was observed. The inclination of 59 Cyg is lower than 80°. Therefore, regular shell phases are not expected to occur. Instead Hummel (1998) explained that particular shell events by adopting a temporarily tilted disk.

5.3.5 Conclusions

In the last sections it was demonstrated that the spectral features, characteristic for Be + sdO or Be + WD binaries, are also detectable in the spectrum of HR 2142. The variable emission, forming in a Be binary due to the presence of a hot companion, is clearly visible as phase-locked V/R variability in Hα and Hβ. In Hα, the variable emission is also traceable as single-peaked emission component, moving in anti-phase to the double-peaked invariant emission. A knotty absorption structure is very well visible in Hδ. HR 2142 shows an enhanced shell phase that is similar to the shell phase of ϕ Per. As HR 2142 is not known to be an X-ray source (which would be indicative for an accreting white dwarf), it is assumed to be a Be + sdO binary such as ϕ Per and 59 Cyg.

The formation and appearance of the above desribed features can be entirely explained by a single physical component, namely the disc of the Be star. They occur in the spectra of all confirmed Be + sdO binaries. Therefore, such features can be taken as reliable indicators for Be binaries with evolved companions.

5.4 Candidates for evolved Be binaries

In the following sections the spectra of promising candidates for evolved binary systems are studied. Spectral features characteristic for Be + sdO or Be + WD binaries are identified in the spectra of the candidate stars.

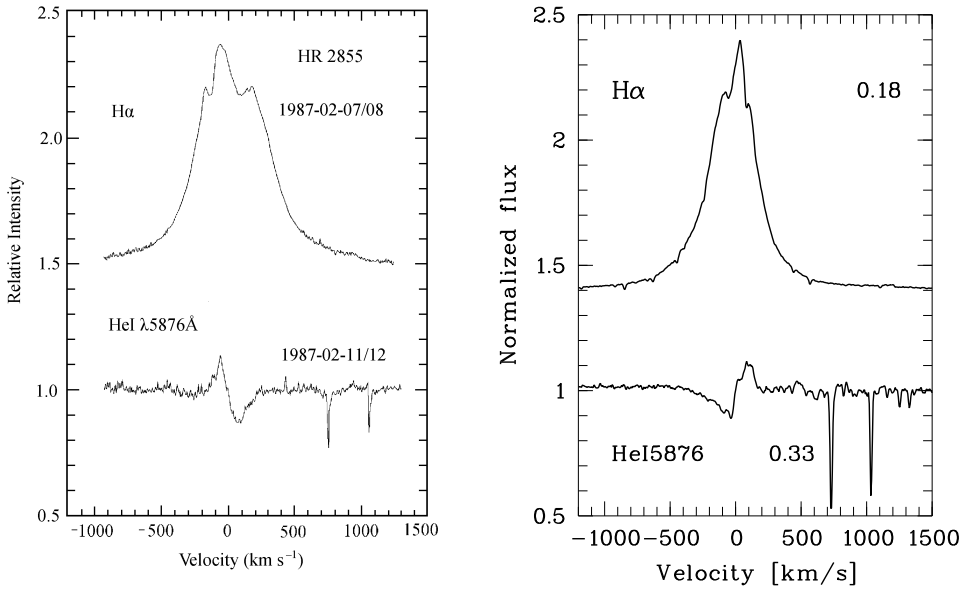

Figure 5.10: Comparison of Hα and He I 5876 line profiles of FY CMa (left, taken from Cao 2001) and ϕ Per (right). The numbers in the right figure indicate the orbital phases.

5.4.1 FY CMa

FY CMa (HD 58978, HR 2855) is known as single B0.5IVe star (Slettebak 1982) showing emission in the Balmer and He I lines in the optical and mass loss via a wind in the UV (Peters 1988). During 1987 April till May striking activity was observed by Peters (1988) in the circumstellar envelope. The V peak of the former invariant Hα emission feature had increased in strength by 30% on May 2. A double-peaked emission appeared in the blue absorption wing of He I 6678. This feature was interpreted as a structured, inverse P Cygni-type profile by Peters. These line profiles stayed until the end of the observing run on May 6 and were visible again in spectra taken on 1987 August 25 and 26. IUE observations taken during the event in early May showed redshifted shell lines of intermediately ionized species like S III and narrow blueshifted components in N V. Such features were not observed two months before. A line profile of He I 5876 from 1987 February 11/12 (Fig. 5.10, left) also reminded of an inverse P Cygni profile (Dachs et al. 1992; Cao 2001).

All these spectral changes were explained by simultaneously infalling and outflowing matter in front of the star (Peters 1988; Cao 2001). Due to large-scale magnetic loops material originating close to the pole would fall back on the star, causing sudden accretion events. IUE data are compatible with the occurance of several such events since 1979 (Peters 1988).

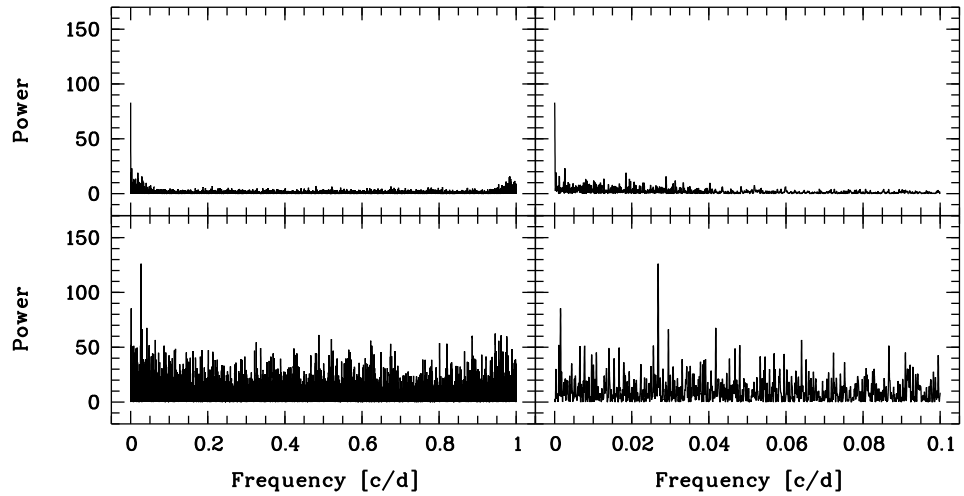

Figure 5.11: Results of the frequency analysis with the AOV method for FY CMa. Window function (upper panel) and power spectrum (lower panel) are shown for the entire studied frequency space (left), and in the range of the orbital period (right).

However, transient shell phases are also known for FY CMa. Chauville et al. (2001) for instance observed very sharp and deep shell lines in Hγ and He I 4471.

In Figure 5.10 the He I 5876 line profile of FY CMa, which was interpreted as inverse P Cygni profile by Cao, and an "unusual" Hα profile are compared to line profiles of ϕ Per. The profiles of FY CMa are taken from Cao (2001). They almost look like mirror images of the line profiles of ϕ Per. Due to this similarity and the observed shell lines in Hγ and He I 4471 (Chauville et al. 2001), it is concluded that these features are caused by a shell phase and that FY CMa represents a further evolved Be binary with a hot, compact companion.

As no optical data of FY CMa were available, a period analysis was carried out using 96 high resolution IUE spectra taken in the short wavelength range. They were downloaded from the IUE Final Archive. Radial velocities were measured with cross-correlation (see section 3.1) for the N V doublet line at 1238 and 1242 Å. A frequency analysis, carried out with AOV (see section 3.2), yielded a single stable period around 37.2 d (Fig. 5.11). Orbital elements were derived with the program VELOC (see section 3.4), allowing also the period as free parameter to converge. The results are listed in Table 5.3. The orbital period was found to be 37.26 d.

In Figure 5.13 dynamical spectra of the N V doublet lines at 1238 and 1242 Å, the C IV doublet lines at 1548 and 1550 Å, Si II 1265, and He II 1640 are shown. They are well sorted by the 37.26 d period. The structure of the absorption profiles

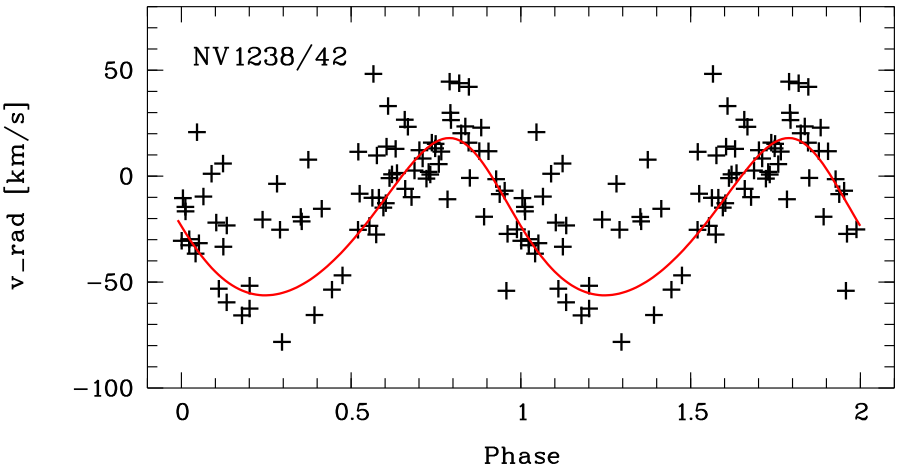

Figure 5.12: Measured radial velocities for the N V doublet line at 1238 and 1242 Å of FY CMa and orbital solution, calculated with the program VELOC.

of Si II 1265 and He II 1640 remind of the knotty absorption structure found in many lines of 59 Cyg.

Sterken et al. (1996) found periodic variability in photometric data of FY CMa with a period of 92.7 d. This period is not compatible with the period determined in this study. Testing the phases of all published spectra, i.e. the occurance of shell phases, inverse P Cygni-type profiles etc., also points to a period of 37 days. Peters (1988) reports that the "unusual features" observed in Hα and He I 6678 profiles on 1987 May 6 were identical to those observed in 1987 August 25/26. If a period of 37.26 d is assumed, these features reappeared exactly after three cycles. Therefore, it is concluded that FY CMa is a spectroscopic binary with an

Table 5.3: Orbital elements of FY CMa computed with the program VELOC.

Orbital parameter	FY CMa
Orbital period, $\mathcal{P}$	37.26 d
Superior conj., $T_{\rm SC}$ (MJD)	51033.21
Periastron, T_0 (MJD)	51027.6
Eccentricity, e	0.14
Periastron length, Φ	28°
Velocity amplitude, K_1	37.11 km/s
System velocity, v_0	-23.63 km/s

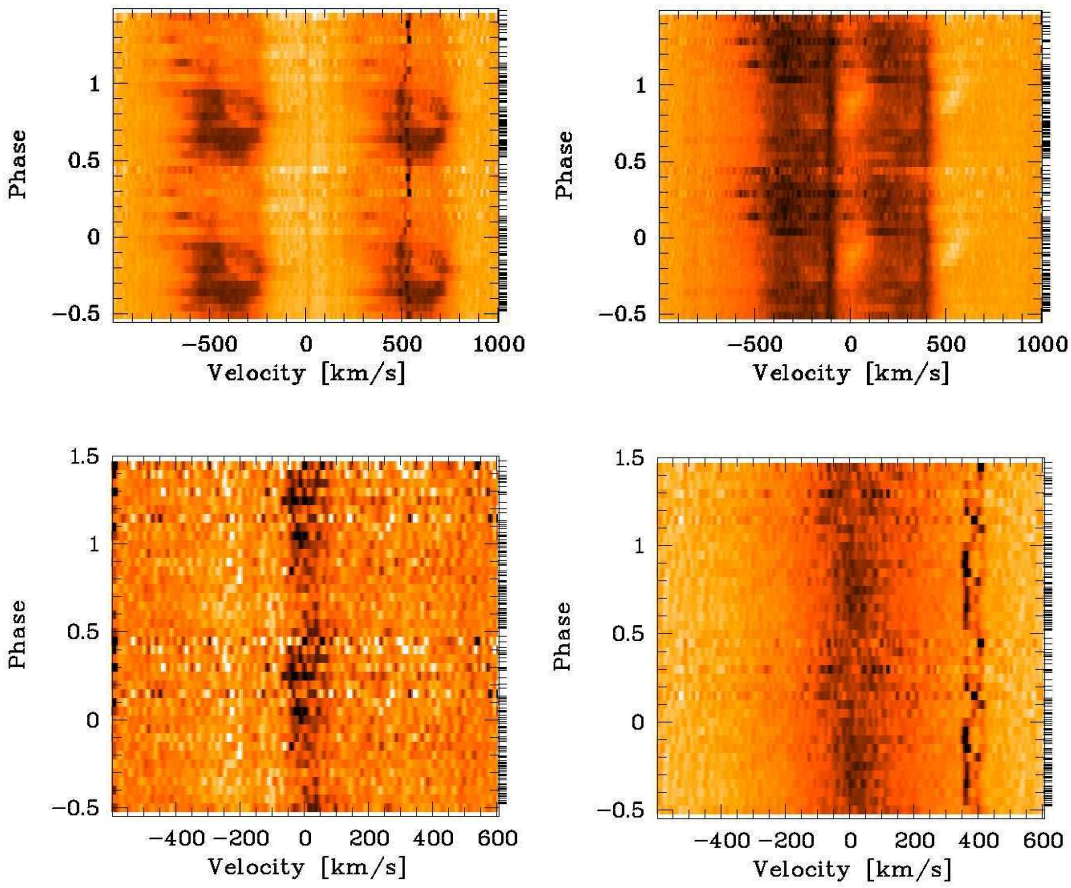

Figure 5.13: Dynamical spectra for the N V doublet lines at 1238 and 1242 Å (upper left), the C IV doublet lines at 1548 and 1550 Å (upper right), Si II 1265 (lower left), and He II 1640 (lower right) of FY CMa.

orbital period of 37.26 d. Due to the occurance of shell features (Chauville et al. 2001) and the analogy to ϕ Per (Fig. 5.10) it suggested that FY CMa is also an evolved Be binary with a hot companion. These findings should be checked by the analysis of optical data.

5.4.2 κ Dra

κ Dra (HD 109 387, HR 4787; B5IIIe Slettebak 1982; B5-6IVpe Chauville et al. 2001) is a suspected X-ray source with an X-ray luminosity of a few 10^{31} erg/s (Peters 1982). It is, hence, a candidate for a Be + WD binary. Juza et al. (1991) derived an orbital period of 61.55 d and a radial velocity amplitude of K_1 = 6 to 7 km/s. They determined a circular orbit.

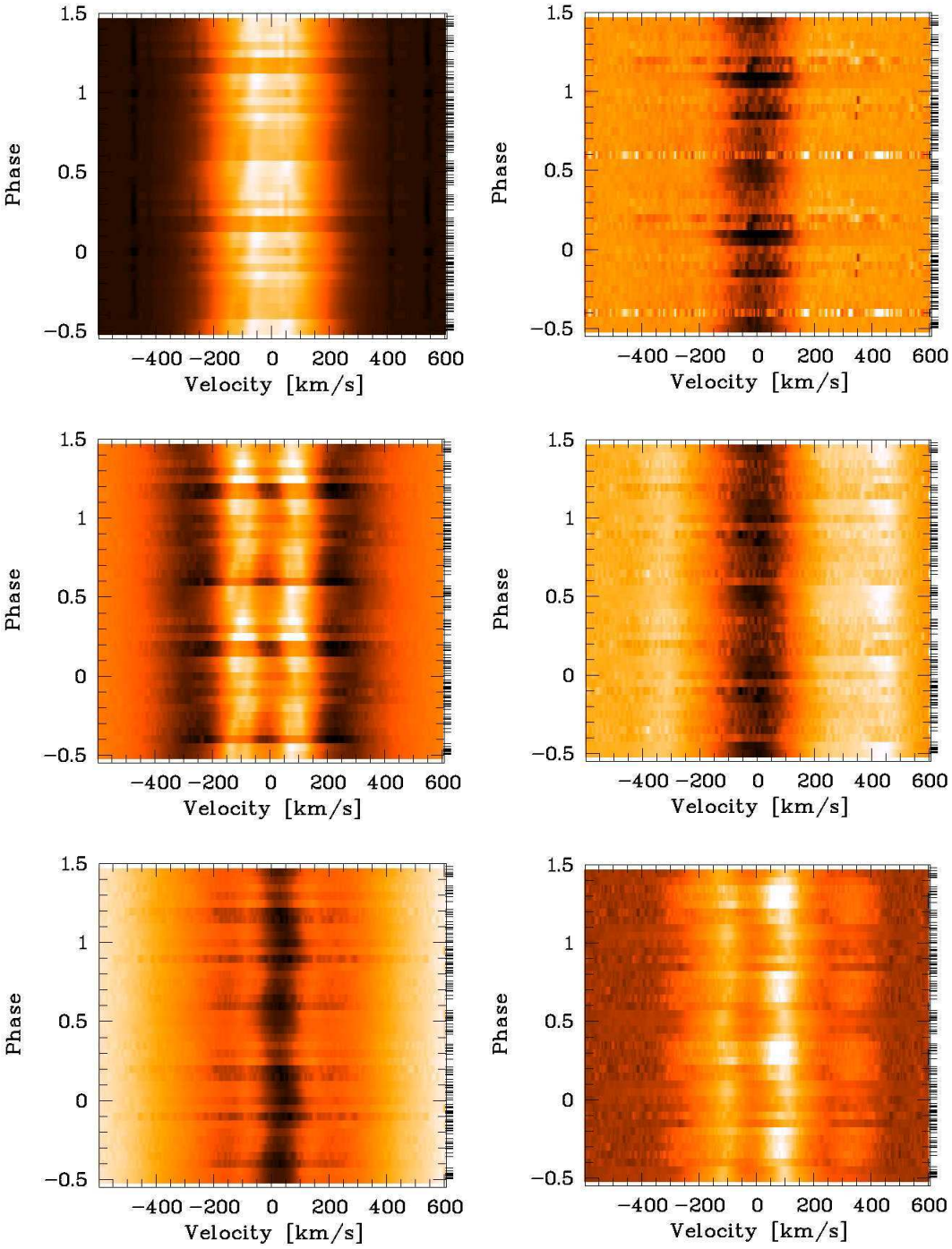

Figure 5.14: Dynamical spectra of emission and absorption lines of κ Dra. Upper left: Hα; Upper right: He I 6678; Middle left: Hβ; Middle right: He I 4471; Lower left: Hγ; Lower right: Fe II 5169.

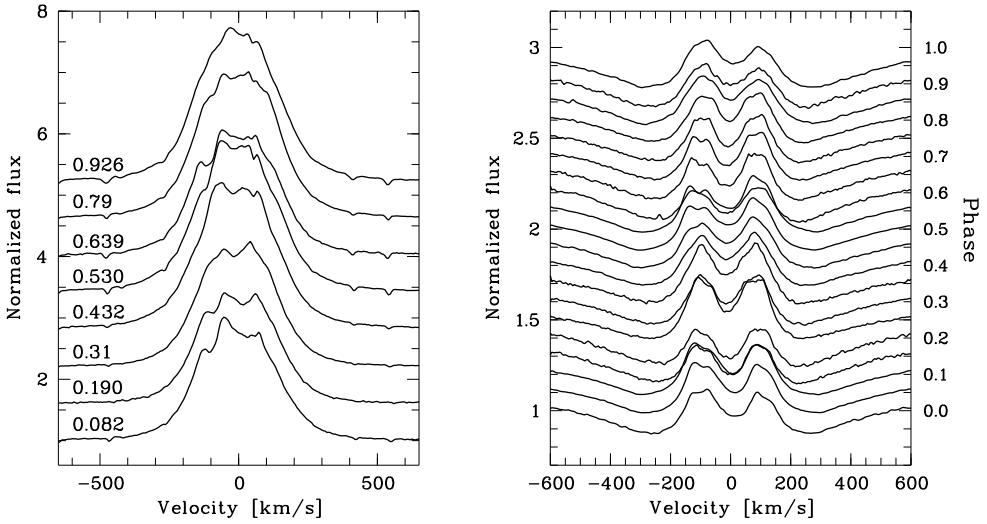

Figure 5.15: Line profile variability of κ Dra. Left: Individual line profiles of Hα taken at different orbital phases. The phases are denoted in the plot. Right: Phase-binned, averaged line profiles of Hβ, covering one orbital cycle. The lines are plotted one over the other with increasing orbital phase.

Adopting this orbital period, the spectral variability of κ Dra was analyzed using the available HEROS data. A He II 4686 emission or absorption was not discovered. Shell lines are also not visible. In Figure 5.14 dynamical spectra of the Balmer lines Hα to Hγ, He I 6678, 4471, and Fe II 5169 are plotted. Hα is dominated by emission. The central parts, where the variable emission should be visible, looks very complicated. A single-peaked emission is hardly traceable, strongly reminding of HR 2142. The blue and red emission peaks of Hβ also show a complicated a substructure. It is not possible to detect a single-peaked emission feature, although the central parts of Hβ look like there would be some knotty absorption structure. Also Hβ strongly remind to HR 2142.

A knotty absorption structure is, however, pronounced in Hγ. He I 6678, 4471, and the central part of the Fe II 5169 emission also show a knotty absorption structure. Fe II 5169 reminds of the corresponding line of ϕ Per. The emission moves smoothly according to the primaries motion and seems not to be disturbed by any additional component.

Individual line profiles of Hα and phase-binned line profiles of Hβ are shown in Fig. 5.15. Hα shows a strong variability of the line shape. A phase-locked V/R variability is difficult to detect since the Hα profiles show no clear blue and red emission peaks. The blue and red emission peaks of Hβ vary both in shape and strength. This variability is very similar to the one observed for ϕ Per, but without

shell lines. Also, a weakly pronounced phase-locked V/R variability is detectable in Hβ. This is even better visible in individual line profiles. Also this line strongly reminds to Hβ of ϕ Per.

Only the knotty absorption structure, typical for a Be + sdO or Be + WD nature, is clearly detectable for κ Dra. However, the general level of similarity is quite high. Therefore, taking into account the X-ray luminosity, it is suggested that κ Dra is a Be + WD binary.

5.4.3 4 Her

4 Her (HD 142 926, HR 5938; B7IVe Slettebak 1982) is a Be binary with an orbital period of 46.192 d (Koubský et al. 1997). Adopting this period, dynamical spectra were calculated for the Balmer lines up to Hδ and for He I 6678 and Fe II 5169 (Fig. 5.16). The variability observed in Hα resembles that observed in HR 2142 and κ Dra. Since 4 Her is a shell star, all lines show clearly defined absorption cores, but no particular enhancements around superior conjunction. The absorption may be "knotty". A single-peaked emission, moving in anti-phase to the absorption profile, is not clearly detectable. A Be + sdO or Be + WD nature cannot be ruled out, but also no further evidence supporting such a nature was found.

5.4.4 HR 6819

For the southern Be star HR 6819 (HD 167 128; B3IIIe Slettebak 1982; B3IIIep Chauville et al. 2001) twelve spectra were obtained with FEROS in 1999 from July 17 till August 4 (Fig. 5.17). It is not known to be a binary, but the observed radial velocity variations (Fig. 5.17) leave little room for other interpretations. It is evident from the line profiles that only about half an orbital cycle was observed. The orbital period of that system is hence in a range of about 30 to 60 days depending on eccentricity.

The periodic line profile variability reveals two stellar components, a very broad one with a high $v \sin i$ and a "normal" one. The broad component is well visible in HeI4471 (Fig. 5.17, left, fourth line profile from the bottom). At roughly -100 $\mathrm{km/s}$ a weak additional absorption component becomes apparent in the blue wing of the profile. While the main absorption moves towards the red part of the spectrum, this component seems to roughly stay in place.

In Fig. 5.18 dynamical spectra are shown, computed for Hβ for orbital periods of 30 d, 35 d, and 40 d. These spectra confirm the presence of at least two stellar components. An absorption profile seems to be superimposed by an emission moving in anti-phase to the absorption. Since both components are visible in the spectra, HR 6819 probably represents a Be + B binary. The narrower absorption

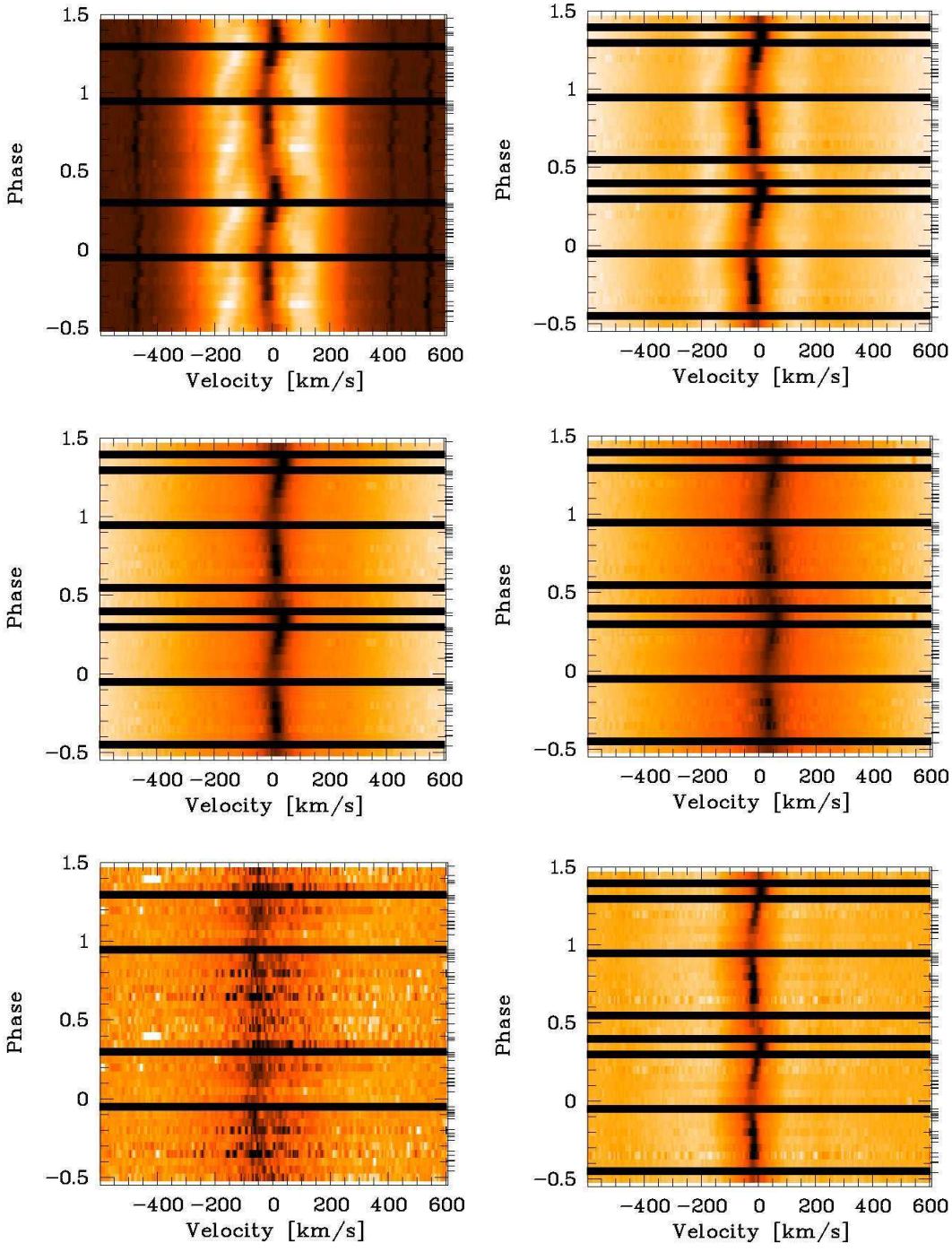

Figure 5.16: Dynamical spectra for 4 Her: Upper left: Hα; Upper right: Hβ; Middle left: Hγ; Middle right: Hδ; Lower left: He I 6678; Lower right: Fe II 5169.

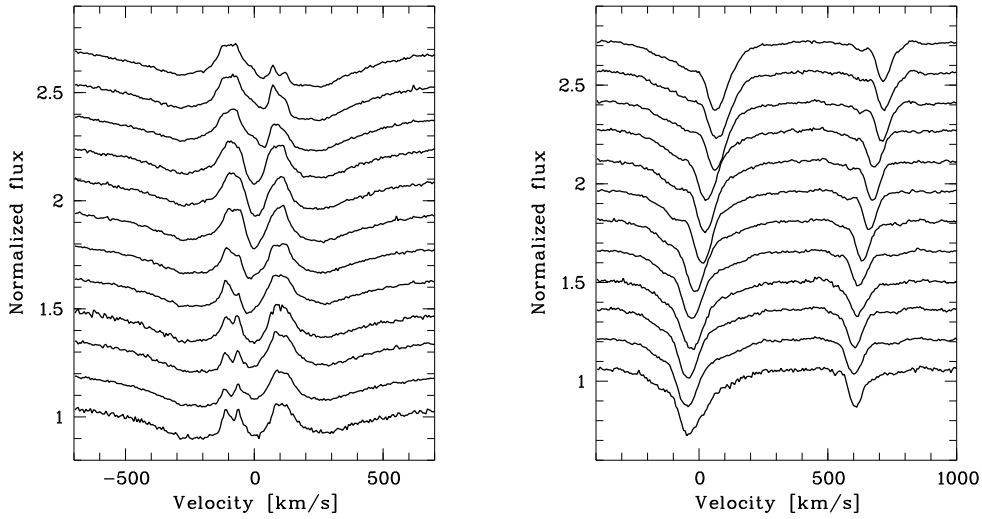

Figure 5.17: Individual line profiles of HR 6819, taken from 1999 July 17 to August 4. Left: Hβ; right: He I 4471.

component would, then, be a normal B-type star, while the broader absorption component as well as the emission belong to the Be star.

5.4.5 Further candidates

For the programme stars 48 Per, 88 Her, 17 Tau, η Tau, and ζ Tau only a little number of spectra was available for the present study (cf. section 2.3, Tab. 2.6). Hence, it was not possible to make assumptions about a Be + sdO or Be + WD nature.

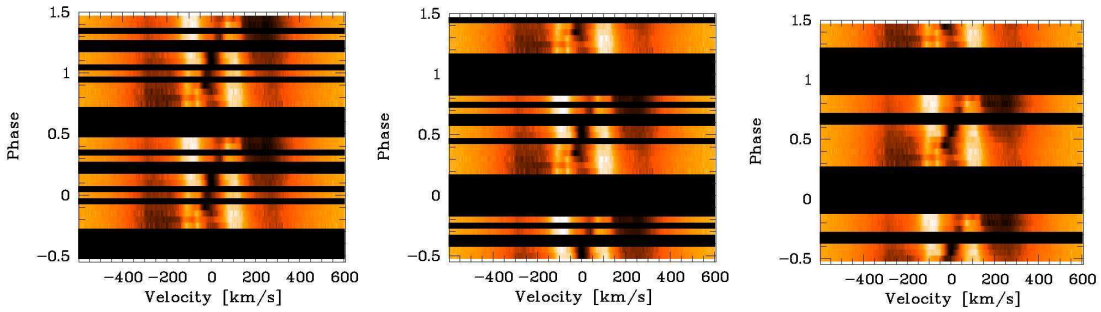

Figure 5.18: Dynamical spectra of HR 6819 for Hβ, phased with an orbital period of 30 d (left), 35 d (middle), and 40 d (right).

Chapter 6

Discussion

6.1 Direct detection of the companion spectrum

The large number of spectra enabled the detection of a weak He II 4686 absorption in the phase-binned dynamical spectrum of that particular spectral region (section 3.4). This feature moves in anti-phase to the velocity curve of the Be primary. Since He II 4686 does not occur in B-type stars, it must represent a photospheric absorption line of the secondary component of the binary. This constitutes a direct proof for the companion and confirms the Be + sdO nature of 59 Cyg. Apart from ϕ Per, it is the only confirmed Be binary with a helium-star companion. There are strong indications that a third star, HR 2142, is also a Be + sdObinary. Instead of a direct proof, all three essential features for an indirect confirmation were found. A He II 4686 emission as reported by Rivinius & Štefl (2000) could not be confirmed for 59 Cyg.

A radial velocity curve was determined for He II 4686 by measuring the trajectory of the absorption feature interactively in the dynamical spectrum. The resulting velocities were used to derive an orbital solution for the secondary (section 3.5) and to shift-correct the phase-binned line profiles which were extracted from the dynamical spectrum. The averaged spectrum of these shift-corrected lines shows a narrow absorption profile with an equivalent width of 14 $\mathrm{m\AA}$.

6.2 Orbital period

The orbital period of the binary system (derived by means of the radial velocities of He I 4471) is 28.192 $\pm$0.004 d (section 3.3). For this line 99 spectra were available, covering a time interval of 13 years. This period confirms the finding of Tarasov & Tuominen (1987) who, in the late 1980s, suggested that 59 Cyg is a spectroscopic binary with a 29-d period. The period of 28.1971 $\pm$0.0038 d, de-

rived by Harmanec et al. (2002) on the basis of photometric observations spanning 43 years, is in good agreement with the period estblished in this study.

Rivinius & Štefl (2000) determined an orbital period of 28.1702 $\pm$0.0014 d. The difference to the 28.19-d period, found by Harmanec et al. and in this work, may have resulted from their additional use of IUE spectra of C IV 1548 to find the correct period in their analysis of the He I 4471 absorption profiles taken with the HEROS spectrograph between 1990 and 1998. Since C IV 1548 is a line that is in part formed in the stellar wind, it may not represent the true orbital motion of the Be star.

6.3 Orbital elements

In the present study, the orbital elements were determined for the primary and secondary component of 59 Cyg, using the radial velocities measured for He I 4471 and He II 4686 (section 3.5). The amplitude of the radial velocity curve of the primary is K_1 = 24.77 $\mathrm{km/s}$. For the secondary it is K_2 = 120.13 $\mathrm{km/s}$. The values derived for the epoch (time of the periastron passage, T_0), periastron length, Φ, and systemic velocity, v_0, for both components agree well. Only the values for the eccentricity differ significantly. For the primary an eccentricity of e = 0.27 and for the secondary of e = 0.11 was found. The reason for that difference is the appearance of emission during specific orbital phases in the line profiles of He I 4471.

In contrast to Rivinius & Štefl (2000) and this work, Harmanec et al. (2002) argue that only the outer wings of the emission lines should reflect the orbital motion of the Be star correctly (cf. Božić et al. 1995). This emission arises from the inner parts of the disc around the Be star. There, the circumstellar matter should be distributed more axially symmetric and not be affected by possible asymmetries in the outer parts of the disc. They measured radial velocities for the outer wings of the Hα and He I 6678 emission and for the absorption wings of He I 6678. Assuming a circular orbit, they derived a velocity amplitude of 13.0 $\pm$1.0 $\mathrm{km/s}$ for Hα, of 31.3 $\pm$1.6 $\mathrm{km/s}$ for the He I 6678 emission, and of 25.4 $\pm$3.0 $\mathrm{km/s}$ for the He I 6678 absorption wings. They favour the result for Hα and assume it to be the true velocity amplitude of the primary component of the binary.

Rivinius & Štefl (2000), who also used the He I 4471 absorption for their study of the orbital elements of 59 Cyg, found a velocity amplitude of 27.2 $\pm$8.5 $\mathrm{km/s}$ for the Be star. Concerning this finding, Harmanec et al. (2002) argue that a variable emission contribution, observed as phase-locked V/R variation in lines like He I 6678 and 5876, could disturb the photospheric profiles by filling in the line wings asymmetrically. As a consequence, the position of the absorption wings are shifted and the measured radial velocities of the line profiles are too high.

Since this kind of emission is also visible in He I 4471, the velocities derived are expected to be too large, leading to a wrong velocity amplitude for the primary.

In principle, this is exactly what is expected to happen during the orbital phases when the single-peaked emission becomes very strong in the red or blue part of the line profile. However, as demonstrated in section 3.7, this variable emission component affects only the central parts of the line profiles significantly and is confined to a velocity range of roughly ± 200 km/s. The outer parts of the line wings are less influenced. That is true even for lines with strong emission like He I 6678 and Hβ. In lines with less emission the line centres are also less affected. In an almost pure absorption line, such as He I 4471, the wings are not expected to show this effect. Furthermore, only a limited number of lines close to the above mentioned special orbital phases are expected to be influenced, resulting in measured radial velocities which are slightly too high. Therefore, the main effect would be an overestimation of the eccentricity of the binary orbit due to a shift of the velocity maximum to higher or lower orbital phases, respectively. But the velocity amplitude itself will be little affected.

As shown in section 3.5, the radial velocities of the invariant disc emission are approximated well by an orbital solution for the Be primary, calculated with the eccentricity of e = 0.11 as found for the secondary. This emission corresponds to the double-peaked emission of single Be stars. For several emission lines the velocity amplitude of the invariant emission was examined. The amplitudes derived lie between 20 and 30 km/s. Since the invariant emission follows the orbital motion of the Be star, its velocity amplitude is a reliable measure for the velocity amplitude of the primary component of the binary. Therefore, a velocity amplitude of roughly 25 km/s is the most likely one, and the value of 24.77 km/s, derived with the He I 4471 absorption profiles, is considered to be the true velocity amplitude of the Be primary.

It is noteworthy that the velocity amplitude measured by Harmanec et al. (2002) for the absorption wings of He I 6678 is nearly the same as the one found for He I 4471 in this study. If the periodic emission component had a strong influence on the velocity measurements in general, one would expect the effect to be much stronger if a line shows a strong phase-linked V/R variability. This should result in a higher velocity amplitude for a line with more variable emission contribution. In this case, the velocity amplitude derived for the absorption wings of He I 6678 should be much larger than the one determined for He I 4471.

An overestimation of the eccentricity of the binary orbit may be avoidable if only the outer wings of those absorption lines showing variable emission in their line centres are considered.

6.4 Stellar parameters of the binary components

The detection of the secondary does not only enable a correction of the orbital elements derived for the Be primary but also a determination of the masses and semi-major axes of the binary components. These quantities were computed for binary inclinations between 40 and 90 ° (section 3.6). Due to the high $v \sin i$ of at least 450 $\mathrm{km/s}$ (Hutchings & Stoeckley 1977; Harmanec et al. 2002; cf. Fig. 3.23, page 46), low inclinations are unlikely. Since neither eclipses nor regular shell events are observed, very high inclinations are also ruled out. According to an effective temperature of $\log T_{\mathrm{eff}}$ = 4.413 (Harmanec et al. 2002), 59 Cyg is a B-type star of spectral class between 1 and 1.5 (Harmanec 1988). The mass of a B1 star of 11.03 $\mathrm{M}_{\odot}$ (Harmanec 1988) is used as a lower limit for the inclination. This leads to a an inclination for the binary system likely to be larger than 60 ° and lower than 80 °. Therefore, the mass of the primary lies in the range of 7.57 to 11.14 $\mathrm{M}_{\odot}$ and of the secondary between 1.56 and 2.3 $\mathrm{M}_{\odot}$. The semi-major axis of the primary orbit is in the range of 13.92 to 15.83 $\mathrm{R}_{\odot}$ and of the secondary orbit between 67.53 and 76.79 $\mathrm{R}_{\odot}$.

Harmanec et al. (2002) derived masses for the secondary and binary separations for the two extremes of possible inclinations of i = 45 ° and 90 °, respectively. They assumed the velocity amplitude of 13 $\mathrm{km/s}$, derived for the Hα emission, a circular orbit, and a primary mass of 10.78 $\mathrm{M}_{\odot}$. According to Harmanec's calibration (1988), this mass corresponds to a star with an effective temperature of $\log T_{\mathrm{eff}}$ = 4.413 as determined for 59 Cyg. They found a mass for the secondary which is between 1 and 2 $\mathrm{M}_{\odot}$ and a separation of roughly 90 $\mathrm{R}_{\odot}$.

In contrast to Harmanec et al. (2002), the masses and separations derived in the present study are based on radial velocity curves of both binary components. Therefore, only these values are taken into account in further discussions.

6.5 Variable and invariant disc emission

Rivinius & Štefl (2000) found that one component of the He I 6678 emission of 59 Cyg varies in anti-phase to the orbital motion of the Be star. A similar result was found by Gies et al. (1993) for ϕ Per. In contrast, Harmanec et al. (2002) showed that the radial velocity curve of the wings of the double-peaked He I 6678 emission follows the motion of the Be star, analogous to the outer wings of the Hα emission. They conclude that the He I 6678 emission follows fully the Be primary and that the He I 6678 emission originates, like the outer wings of the Hα emission, in the inner region of the circumstellar disc of the Be star.

Since Harmanec et al. (2002) derived the radial velocities of the He I 6678 emission by measuring the positions of the double-peaked emission wings, their find-

ing is not contradictory to the finding of Rivinius & Štefl (2000). As demonstrated in section 3.7.2, the He I 6678 emission indeed consists of two components which are superimposed and which can be distinguished in the dynamical spectrum of that line. The first component is the invariant disc emission. This arises in the entire disc and is visible as a double-peaked emission feature also in the spectrum of single Be stars. This was the component which was measured by Harmanec et al. (2002). The second component is the variable emission. This only forms in a sector of the Be disc, which is phase-locked to the companion (Štefl et al. 2000; Hummel & Štefl 2001).

As mentioned before, the variable emission is traceable in most emission and absorption lines (section 3.7). It occurs as phase-locked, single-peaked emission feature and V/R variability in the emission lines, respectively. It is confined to the central parts of the line profiles within the velocity range that is enclosed by the blue and red peaks of the invariant disc emission. It is very well visible in emission lines like He I 6678, 5876, 7065, Hα, and Hβ. Furthermore, it causes the knotty structure of the profiles of absorption lines like He I 4471 (section 3.7.1, cf. section 3.5). The radial velocity curve of the variable emission component is only measurable if the position of the single-peaked emission component in the line profile is derived.

6.6 Sector model

The variable disc emission, observable in the spectra of the Be + sdO binaries 59 Cyg and ϕ Per, has been explained in different ways by different authors. Gies et al. (1993) interpreted the variable He I 6678 emission of ϕ Per in terms of two different emission components. Both components were found to move in anti-phase to the velocity curve of the primary. The stronger component with a larger semi-amplitude is expected to originate in the circumstellar gas near the companion. The weaker one, with smaller semi-amplitude, should form in a gas flow between the binary components.

Božić et al. (1995) argued that the He I 6678 emission of ϕ Per is a double-peaked emission, arising in the circumstellar disc around the secondary like the double-peaked He II 4686 emission (cf. Poeckert 1981. Furthermore, they found that the strength of the Balmer emission and of the He I 6678 emission decreased simultaneously. Since they attributed the origins of these emission lines to discs around the primary and the secondary, they interpreted this simultaneous decrease as a kind of interaction between the binary components.

Harmanec et al. (2002) measured the V/R variability of the Hα and He I 6678 emission of 59 Cyg. They found that the V/R variability is roughly in phase with the radial velocity curve of the Hα emission. This is explained by an enhancement

of circumstellar matter and emission power in the part of the Be disc that faces the seondary.

Štefl et al. (2000) demonstrated for ϕ Per that this emission arises in a sector of the Be disc which faces the secondary component and is photoionized by its ultraviolet continuous radiation. This sector is locked to the orbital motion of the companion. Hence, the emission that forms in this sector is single-peaked and follows the motion of the secondary in anti-phase to the radial velocity curve of the primary. The single-peaked emission appears as phase-locked V/R variability. As shown in this study, it causes a knotty structure that is visible in most absorption lines. Such a structure is also visible in the centres of emission line with a smaller amount of variable emission. It is confined to the velocity range enclosed by the red and blue part of the double-peaked disc emission. The phase-locked variability of the variable emission component is described in section 3.7.2.

The sector model naturally explains the origin and appearance of the variable emission and the above mentioned findings. Two separate physical components (Gies et al. 1993) are no longer needed. The simultaneous decrease of the Balmer and He I 6678 emission (Božić et al. 1995) is easily explicaple if the corresponding lines origin in the same environment, namely the disc surrounding the Be star (cf. section 3.7). The V/R variability is well explained by enhanced ionisation in the illuminated disc sector (cf. Harmanec et al. 2002).

6.7 Modelling the variable disc emission

Assuming the sector model, Hummel & Štefl (2001) simulated the emission of the He I 6678 and 5876 lines of ϕ Per successfully. They were able to reproduce the variability of the single-peaked emission, which appears as phase-locked V/R variability or vice versa, and shell lines that are visible in He I 5876 at specific orbital phases. In this study, the emission of He I 6678 of 59 Cyg was successfully reproduced with the same model (chapter 4).

Several models were calculated for different values of inclination, equatorial radius, and Kepler velocity at the stellar surface which allows for an indirect examination of the primary. The primary masses, calculated for the most likely range of inclinations (section 3.6), were used to derive reliable estimates for the Kepler velocities for the corresponding range of inclinations. Since most of these models yielded comparable results, it was not possible to find a set of best fitting values for the above mentioned input parameters. Disc sectors with opening angles between 90 and 120 fitted the data quite well. The parameters found for the physical conditions of the Be disc are comparable for all reliable models.

In general, the models matched the observed data better if Kepler velocities were assumed for given primary masses that were derived with small equatorial

radii. Models computed with stellar radii smaller as the ones found in calibrations (cf. Harmanec 1988), but comparable to those found with evolutionary models (Claret & Giménez 1995) fitted the spectra also a bit better. This may be a hint that polar radii of rapidly rotating stars are generally smaller than those of stars with lower rotation velocities (Maintz et al. 2002). Due to rotational mixing or mass transfer a Be star can be less massive, but appear as a B-type star due to a higher effective temperature. Then the star is undermassive or overluminous, respectively. This was proposed for ϕ Per by Gies et al. (1998).

The single-peaked emission observed in the blue and in the red part of the line wings is reproduced better by different sets of input parameters. For the same input parameters, sometimes the emission variability in the blue was matched better if sectors with larger opening angles were used. Vice versa, the emission variability in the red wing was better fitted assuming smaller opening angles. This can be explained only if the orbit of 59 Cyg is eccentric. Then, the size of the photoionized sector changes during an orbital cycle with the total separation, when the secondary moves towards or away from the Be disc. This is confirmed by the finding that the equivalent widths of Hα and Hβ, which vary periodically, are especially strong between orbital phase 0.5 and 1.0 and, therefore, around and after the periastron passage (phase 0.57). Since the sector model is designed for a constant size of the illuminated disc sector, this finding cannot be proved by modelling.

The successful modelling of the emission observed in ϕ Per and 59 Cyg confirms the sector model and, therefore, the assumption that the above discussed spectral features form due to a disc sector which is photoionized by a hot companion.

6.8 Candidates for Be + sdO and Be + WD binaries

A comparison of the confirmed Be + sdO binaries 59 Cyg and ϕ Per and the assumed Be + sdO binary HR 2142 allowed for determination of characteristic spectral features (section 5). These are a double-peaked emission or absorption line of He II 4686, which is very prominent in sdO stars (Jaschek & Jaschek 1987), the above discussed features caused by the single-peaked sector emission, and the occurance of shell lines. The latter are formed due to enhanced absorption if the illuminated disc sector is visible in front of the primary. Shell lines are, therefore, another feature that is directly connected to the sector model. These features were taken as indicators for identifying evolved Be binaries with hot, compact companions within a sample of preselected candidates. The presence of low luminosity X-rays (10^{29}–10^{33} $\mathrm{erg/s}$ Waters et al. 1989) enables to distinguish a Be + WD binary from a Be + sdO binary.

One of the preselection criteria is the occurance of satellite absorptions in the blue or red peak of emission lines (Maintz et al. 2003). The formation of these weak absorption cores is observed in many known Be binaries. Since it is not explicable with a disc around a single Be star, it is taken as indicator for binarity.

HR 2142 is a well known binary with an orbital period of 80.86 d Peters (1983). Peters (1972) mentioned a spectral similarity to ϕ Per. Shell lines occur only in hydrogen and helium lines, but not in metal lines. Those are visible in Be binaries with late-type companions. Despite these findings, Peters (1983) proposed a cool, Roche lobe filling giant companion to explain the strictly periodic two-component shell phase of HR 2142 by binary interaction. Shell lines, occuring shortly before and after superior conjunction, were assumed to be caused by gas streams between the binary components. In contrast to this explanation, Poeckert (1981) pointed out that gas streams should only be visible before or after conjunction, but not at both times. Waters et al. (1991) searched for a cool giant companion in the spectral energy distribution of HR 2142. Since they could not find a spectral signature of a giant star, they suggested a Be + sdO nature for the companion.

HR 2142 could not be directly confirmed to be a Be + sdO binary in the present study, since HR 2142 shows neiter a He II 4686 emission nor absorption (section 5.2). As mentioned before, HR 2142 shows an enhanced shell phase analogous to ϕ Per. Shell lines are very well visible in Hβ to Hδ, and He I 5016. The variable emission component is visible as phase-locked V/R variability in Hα and Hβ. The V/R variability in Hβ is also reported by Peters (1972). In Hα, the motion of the single-peaked emission is traceable. The knotty structure is more difficult to identify, but well visible in Hδ.

In this study, all spectral features are confirmed for HR 2142, which are expected to occur according to the sector model. Since HR 2142 is not known as an X-ray source, it is assumed to be another Be + sdO binary, like ϕ Per and 59 Cyg.

A further candidate for an evolved Be binary with a hot, compact companion is FY CMa. Peters (1988) and Dachs et al. (1992) observed line profiles that are comparable to spectral lines observed for ϕ Per (section 5.4.1). Chauville et al. (2001) observed deep shell lines in Hγ and He I 4471. On the basis of IUE data, a period analysis was carried out in this work and an orbital period of 37.26 d was derived. Sterken et al. (1996) published an orbital period of roughly 92 d. Since the most likely period, derived from published spectroscopic data, is also around 37.2 d, the 92-days period is ruled out. Furthermore, Peters (1988) reported that one of the above mentioned spectral features, first observed on May 6, reappeared on August 25/26. This correspond almost exactly to a period of time of 3×37.26 days. Therefore, it is suggested that FY CMa is a Be binary with a hot, compact companion. Unfortunately, no own data were available for this study. To confirm a Be + sdO nature, optical spectra should be investigated.

For κ Dra an orbital period of 61.55 d was derived by Juza et al. (1991). The

dynamical spectra binned with this period are similar to those of HR 2142. The phase-locked variability is similar to ϕ Per. He II was not found in the spectrum. Since κ Dra is an X-ray source (Peters 1982) and due to the similarity to ϕ Per and HR 2142, a Be + WD nature is suggested.

6.9 Evolutionary state

The detection of both binary components of 59 Cyg allowed for derivation of the stellar masses. The mass of the primary is between 7.57 and 11.14 $\mathrm{M}_{\odot}$ and the mass of the secondary lies in a of 1.56 to 2.3 $\mathrm{M}_{\odot}$. Therefore, it is possible to speculate about the evolutionary stage of 59 Cyg and a possible further evolution.

For ϕ Per, Gies et al. (1998) published a primary mass of 9.3 $\mathrm{M}_{\odot}$ and a secondary mass of 1.14 $\mathrm{M}_{\odot}$, assuming an inclination of 80 °. Božić et al. (1995) give stellar masses for ϕ Per for a range of possible inclination larger than 65 ° and lower than 90 °. The mass of the pimary is in a range between 16.4 and 21.8 $\mathrm{M}_{\odot}$ and the secondary between 1.7 and 2.2 $\mathrm{M}_{\odot}$.

According to Vanbeveren et al. (1998), ϕ Per is an intermediate mass post case B mass-transfer binary. The subdwarf has to be a core helium burning remnant of a once more massive star after a Roche lobe overflow. The B-type star is a former mass gainer that has spun-up by mass transfer and has developed into a Be star. Vanbeveren et al. (1998) calculated evolutionary models for ϕ Per, using the component masses which are given by Gies et al. (1998) and Božić et al. (1995).

To end up with stellar masses in the range given by Božić et al. (1995), the initial masses must have been 10 $\mathrm{M}_{\odot}$ for the primary and 9 $\mathrm{M}_{\odot}$ for the secondary. Two models were calculated for initial orbital periods of 4.4 d and 10 d. After a case B mass transfer the mass of the former pimary decreased to 2.5 $\mathrm{M}_{\odot}$ and the mass of the former secondary increased to 16.5 $\mathrm{M}_{\odot}$. The initial periods extended to 46 d and 105 d, respectively. In the first scenario with shorter initial period a case BB mass transfer follows. In the other case, the former primary loses mass by a Wolf-Rayet like stellar wind. Then, the binary has reached the observed evolutionary state of a Be + sdO binary with a masses of 1.7 $\mathrm{M}_{\odot}$ for the sdO and 17.3 $\mathrm{M}_{\odot}$ for the Be star and an orbital period of 126 d. Since the mass of the sdO lies above the Chandrasekhar limit of 1.4 $\mathrm{M}_{\odot}$, it will explode as a supernova. Finally, the system will develop into a Be/X-ray binary or the system is disrupted, producing a single Be star.

Stellar masses as given by Gies et al. (1998) are produced if masses of 6 $\mathrm{M}_{\odot}$ for the initial primary, of 5 $\mathrm{M}_{\odot}$ for the initial secondary, and an initial orbital period of 13.5 d are assumed. After a case B mass transfer the initial primary developed into a sdO star with a mass of 1.5 $\mathrm{M}_{\odot}$. The former secondary developed into a Be star with a mass of 9.5 $\mathrm{M}_{\odot}$. In the following, the sdO star loses mass by a stellar

wind. The observed evolutionary state is reached, when the mass of the sdO has decreased to 1.2 $M_\odot$. The sdO will continue to lose mass by a stellar wind and will develop into a WD. Finally, the binary will develop into a Be + WD system and become a low X-Ray luminosity Be X-ray source like μ^2 Cru or HR 4804.

These evolutionary scenarios do not match the observed component masses of 59 Cyg perfectly, but also none of the models is ruled out. According to Božić et al. (1995), the range of likely masses for the sdO components of 59 Cyg and ϕ Per agree. But the possible masses for the Be component of 59 Cyg are much too low compared to the likely mass range for the Be component of ϕ Per. Compared to the masses for ϕ Per as given by Gies et al. (1998), the masses for the Be components of both Be + sdO binaries match, but the sdO component of 59 Cyg is too massive. Since these models are typical of the formation of Be-type binaries (Vanbeveren et al. 1998), 59 Cyg should evolve in a similar way.

Most likely, it represents an earlier stage than ϕ Per after the case B mass transfer and before a case BB mass transfer or a stellar wind occurs. This would fit the observed mass of the sdO companion and the orbital period of 59 Cyg which is much shorter compared to ϕ Per. Since the mass of 1.56 $M_\odot$ for the sdO companion of 59 Cyg is only a lower limit given by an unlikely inclination of 80 °, all described scenarios for a further evolution are equally possible. 59 Cyg can develop to a Be + WD binary, a Be/X-ray binary or a single Be star if the system is disrupted by a supernova explotion. If the lifetime of the Be star is shorter than the one of the sdO star (Pols et al. 1991), 59 Cyg will stay a Be + sdO binary, until the Be star will leave the main sequence.

6.10 Implications for Be star formation

For 59 Cyg, the binary nature was confirmed only recently (Rivinius & Štefl 2000; Harmanec et al. 2002). HR 2142 (Peters 1972, 1983) and κ Dra (Juza et al. 1991) were known Be binaries, but the companions were not identified. For FY CM, binarity was suggested (Gies 2000). In the present study, 59 Cyg and HR 2142 were confirmed as Be + sdO binaries. FY CMa is suggested to be a Be + sdO binary. κ Dra is suggested to be a Be + WD binary. This demonstrates that even well studied Be stars can hide a Be + sdO or Be + WD nature.

Models of close binary evolution show that Be stars can form in a binary system due to mass and angular momentum transfer (Pols et al. 1991; Van Bever & Vanbeveren 1997; Vanbeveren et al. 1998; Raguzova 2001). Gies (2000) lists 16 Be binary systems with cool, Roche lobe filling companions, 11 Be binaries with faint or undetected companions including Be + sdO Be + WD, and Be/X-ray binaries, and 13 possible Be binaries. He shows that examples can be found which seem to match most of the predicted stages of close binary evolution. Furthermore, 64

Be/X-ray binaries are known in the Milky Way (Coe 2000). Such systems can be detected easily in a large volume due to their X-ray luminosity. But according to model predictions, they should only represent a small fraction of all evolved Be binaries. This confirms that at least a fraction of Be stars can form due to close binary evolution.

This study demonstrates that it is very likely that many of the missing spectroscopic Be binaries (Jaschek & Jaschek 1987) are undetected evolved Be binaries with sdO or WD companions. Those binaries are characterized by spectral features caused by extra emission which arises in a sector of the Be disc that is illuminated by the continuum radiation of the hot secondary. The search for such features in the spectra of candidate stars allows for easier identification of further evolved Be binaries. Time-consuming monitoring campaigns can thus be concentrated to promising candidats.

The fraction of Be stars which are formed due to close binary evolution and, therefore, the fraction of Be + sdO and Be + WD binaries remains unknown. Estimates on the basis of the known Be/X-ray binaries are strongly dependent on the assumed evolutionary model. E.g. Van Bever & Vanbeveren (1997) assert that $5-20\%$ of all Be stars are formed due to close binary evolution. In contrast, Pols et al. (1991); Portegies Zwart (1995) contend a fraction of $50-100\%$. Improved methods for an easier identification of evolved Be binaries with hot, compact companions are expected to lead to the detection of many such binaries in the near future. Hence, the use of characteristic features, as discussed in this study, will allow an assessment of these issues on the basis of observations.

Chapter 7

Conclusion

59 Cyg is confirmed as Be + sdO binary. The companion was directly confirmed by a He II 4686 absorption. The lowest possible mass for the secondary lies above the Chandrasekhar limit. According to evolutionary models for Be binaries, 59 Cyg represents a ϕ Per like system in an earlier stage. It can be the progenitor of a Be + WD or Be/X-ray binary. In the latter case the helium star would represent a progenitor of a supernova.

The appearance of specific spectral features, characteristic for the confirmed Be + sdO binaries 59 Cyg and ϕ Per and for HR 2142, is fully explained by extra emission that originates in a sector of the Be disc. This sector is photoionized by the UV continuum radiation of the hot secondary. These characteristic features are a single-peaked emission component, moving in anti-phase to the primary, a phase-locked V/R variability, a knotty structure of absorption profiles, and shell lines.

These features were taken as indicators to identify further Be binaries with hot, compact companions. HR 2142 was confirmed as Be + sdO binary. It is suggested that FY CMa is a Be + sdO binary, too. κ Dra is suggested to be a Be + WD binary. It is confirmed that a fraction of the Be stars formed due to close binary evolution.

Bibliography

Baade, D. 1992, in Evolutionary Processes in Interacting Binary Stars, ed. Y. Kondo, R. F. Sistero, & R. S. Polidan, IAU Symp. No. 151 (Dordrecht: Kluwer), 147

Balona, L. A., Henrichs, H. F., & Le Contel, J. M., eds. 1994, Pulsation, Rotation, and Mass Loss in Early-type Stars, IAU Symp. No. 162 (Dordrecht: Kluwer)

Barker, P. K. 1982, ApJS, 49, 89

—. 1983, A. J., 88, 72

Berger, D. H. & Gies, D. R. 2001, ApJ, 555, 364

Božić, H., Harmanec, P., Horn, J., Koubský, P., Scholz, G., McDavid, D., Hubert, A.-M., & Hubert, H. 1995, A&A, 304, 235

Cannon, J. B. 1910, J. R. Astron. Soc. Can., 4, 195

Cao, H.-L. 2001, ChJAA, 1, 514

Carrier, F., Burki, G., & Burnet, M. 2002, A&A, 385, 488

Chauville, J., Zorec, J., Ballereau, D., Morrell, N., Cidale, L., & Garcia, A. 2001, A&A, 378, 861

Claret, A. & Giménez, A. 1995, A&AS, 114, 549

Coe, M. J. 2000, in The Be Phenomenon in Early-Type Stars, ed. M. A. Smith, H. F. Henrichs, & J. Fabregat, ASP Conf. Ser. No. 214, 656

Dachs, J., Hummel, W., & Hanuschik, R. W. 1992, A&AS, 95, 437

Doazan, V., Grady, C. A., Snow, T. P., Peters, G. J., Marlborough, J. M., Barker, P. K., Bolton, C. T., Bourdonneau, B., Kuhi, L. V., Lyons, R. W., Polidan, P. S., Stalio, R., & Thomas, R. N. 1985, A&A, 152, 182

ESO-MIDAS. 1995, User Guide, Vol. B: Data Reduction, ESO, Garching, p. 12-1

Floquet, M., Hubert, A. M., Chauville, J., Chatzichristou, H., & Maillard, J.-P. 1989, A&A, 214, 295

Gies, D. R. 2000, in The Be Phenomenon in Early-Type Stars, ed. M. A. Smith, H. F. Henrichs, & J. Fabregat, ASP Conf. Ser. No. 214, 668

Gies, D. R., Bagnuolo, Jr., W. G., Ferrara, E. C., Kaye, A. B., & Thaller, M. L. 1998, ApJ, 493, 440

Gies, D. R., Willis, C. Y., Penny, L. R., & McDavid, D. 1993, PASP, 105, 281

Hadrava, P. 1990, Contrib. Astron. Obs. Skalnaté Pleso, 20, 23

—. 1995, A&AS, 114, 393

—. 1997, A&AS, 122, 581

Hanuschik, R. W., Hummel, W., Sutorius, E., Dietle, O., & Thimm, G. 1996, A&AS, 116, 309

Harmanec, P. 1984, Hvar Observatory Bulletin, 7, 55

—. 1988, BAICz, 39, 329

Harmanec, P., Božić, H., Percy, J. R., Yang, S., Ruždjak, D., Sudar, D., Wolf, M., Iliev, L., Huang, L., Buil, C., & Eenens, P. 2002, A&A, 387, 580

Heger, A. & Langer, N. 2000, ApJ, 544, 1016

Hill, G. 1993, in New Frontiers in Binary Stars Research, ed. K.-C. Leung & I.-C. Nhu, ASP Conf. Ser. No. 38, 127

Hummel, W. & Štefl, S. 2001, A&A, 368, 471

Hummel, W. & Vrancken, M. 1995, A&A, 302, 571

Hutchings, J. B. & Stoeckley, T. R. 1977, PASP, 89, 19

Jaschek, C. & Jaschek, M. 1987, The Classification of Stars (Cambridge University Press)

Jaschek, M. & Groth, H.-G., eds. 1982, Be stars, IAU Coll. No. 98 (Dordrecht: D. Reidel)

Jaschek, M., Slettebak, A., & Jaschek, C. 1981, BeSN, 4, 9

Juza, K., Harmanec, P., Hill, G. M., Tarasov, A. E., Matthews, J. M., Tuominen, I., & Yang, S. 1991, BAICz, 42, 39

Kaufer, A. 1996, PhD thesis, Ruperto-Carola University of Heidelberg, Germany

Kaufer, A. 1998, in Reviews of Modern Astronomy Vol. 11, ed. R. E. Schielicke (Astronomische Gesellschaft), 177

Kaufer, A., Stahl, O., Tubbesing, S., Nørregaard, P., Avila, G., Francois, P., Pasquini, L., & Pizzella, A. 1999, The ESO Messenger, 95, 8

Kaufer, A., Stahl, O., Wolf, B., et al. 1996, A&A, 305, 887

Kaufer, A., Wolf, B., Andersen, J., & Pasquini, L. 1997, The ESO Messenger, 89, 1

Koubský, P., Harmanec, P., Kubát, J., Hubert, A. M., Božić, H., Floquet, M., Hadrava, P., Hill, G., & Percy, J. R. 1997, A&A, 328, 551

Kříž, S. & Harmanec, P. 1975, Bull. A. I. Czechoslovakia, 26, 65

Langer, N. & Heger, A. 1998, in Properties of Hot, Luminous Stars, ed. I. D. Howarth, ASP Conf. Ser. No. 131, 76

Ludendorff, H. 1910, A. N., 186, 17

Maeder, A. 1999, A&A, 347, 185

Maeder, A. & Eenens, P., eds. 2003, Stellar Rotation, IAU Symp. No. 215, proceedings in press

Maeder, A., Grebel, E. K., & Mermilliod, J.-C. 1999, A&A, 346, 459

Maeder, A. & Meynet, G. 2000, ARA&A, 38, 143

Maintz, M., Rivinius, T., Baade, D., & Štefl, S. 2002, in Radial and Nonradial Pulsations as Probes of Stellar Physics, ed. C. Aerts, T. R. Bedding, & J. Christensen-Dalsgaard, ASP Conf. Ser. No. 259, 222

Maintz, M., Rivinius, T., Štefl, S., & Stahl, O. 2003, in Stellar Rotation, ed. A. Maeder & P. Eenens, IAU Symp. No. 215, proceedings in press

Mandel, H. 1988, PhD thesis, Ruperto-Carola University of Heidelberg, Germany

Mandel, H. 1994, in The Impact of Long-Term Monitoring on Variable Star Research, ed. C. Sterken & M. de Groot, NATO ASI Series C 436, NATO ARW (Ghent: Kluwer), 303

Miczaika, G. R. 1949, A. N., 277, 167

Okazaki, A. T. 1991, PASJ, 42, 75

—. 1997, A&A, 318, 548

Owocki, S. 2003, in Stellar Rotation, ed. A. Maeder & P. Eenens, IAU Symp. No. 215, proceedings in press

Perrine, C. D. 1923, Pub. A. A. S., 4, 38

Peters, G. J. 1971, ApJ, 163, L107

—. 1972, PASP, 84, 334

Peters, G. J. 1982, in Be stars, ed. M. Jaschek & H. G. Groth, IAU Symp. No. 98 (Dordrecht: D. Reidel), 353

—. 1983, PASP, 95, 311

—. 1988, ApJL, 331, L33

Pickering, E. C. 1905, ApJ, 22, 87

Plavec, M. 1976, in Be and shell stars, ed. A. Slettebak, IAU Symp. No. 70 (Dordrecht: D. Reidel)

Poeckert, R. 1979, ApJ, 233, L73

—. 1981, PASP, 93, 297

Pols, O. R., Coté, J., Waters, L. B. F. M., & Heise, J. 1991, A&A, 241, 419

Popper, D. M. 1980, ARA&A, 18, 115

Portegies Zwart, S. 1995, A&A, 296, 691

Porter, J. & Rivinius, T. 2003, PASP, in press

Quirrenbach, A., Bjorkman, K., Bjorkman, J., et al. 1997, ApJ, 479, 477

Raguzova, N. V. 2001, A&A, 367, 848

Rappaport, S. A. & van den Heuvel, E. P. J. 1982, in Be stars, ed. M. Jaschek & H. G. Groth, IAU Symp. No. 98 (Dordrecht: D. Reidel), 327

Rinehart, S. A. 2000, MNRAS, 312, 429

Rivinius, T. & Štefl, S. 2000, in The Be Phenomenon in Early-Type Stars, ed. M. A. Smith, H. F. Henrichs, & J. Fabregat, ASP Conf. Ser. No. 214, 581

Scargle, J. D. 1982, ApJ, 263, 835

Schäfer, D. R. 2000, PhD thesis, Ruperto-Carola University of Heidelberg, Germany

Schmutz, W., Schweickhardt, J., Stahl, O., et al. 1997, A&A, 328, 219

Schwarzenberg-Czerny, A. 1989, MNRAS, 241, 153

Schwarzenberg-Czerny, A. 1993, in 5th ESO/ST-ECF Data Analysis Workshop, ed. P. J. Grosbøl & R. C. E. de Ruijsscher, ESO Conf. and Workshop Proc. No. 47 (Garching: ESO), 149

Secchi, A. 1867, A. N., 68, 63

Simkin, S. M. 1973, A&A, 31, 129

Slettebak, A., ed. 1976, Be and shell stars, IAU Symp. No. 70 (Dordrecht: D. Reidel)

Slettebak, A. 1982, ApJS, 50, 55

Slettebak, A. & Snow, T. P., eds. 1987, Physics of Be stars, IAU Coll. No. 92 (Cambridge: Cambridge Univ. Press)

Smith, M. A., Henrichs, H. F., & Fabregat, J., eds. 2000, The Be Phenomenon in Early-Type Stars, IAU Coll. no. 175 (ASP Conf. Ser., vol. 214)

Stahl, O., Kaufer, A., Wolf, B., Gäng, T., Gummersbach, C. A., Kovács, J., Mandel, H., Rivinius, T., Szeifert, T., & Zhao, F. 1995, The Journal of Astronomical Data, 1, 3, (on CD-ROM)

Štefl, S., Hummel, W., & Rivinius, T. 2000, A&A, 358, 208

Stellingwerf, R. F. 1978, ApJ, 224, 953

Sterken, C., Vogt, N., & Mennickent, R. E. 1996, A&A, 311, 579

Tarasov, A. E. & Tuominen, I. 1987, in Proc. Reg. Eur. IAU Meet., ed. P. Harmanec, Publ. Astron. Inst. Czechosl. Acad. Sci. 5, 70, 127

Thaller, M. L., Bagnuolo, Jr., W. G., Gies, D. R., & Penny, L. R. 1995, ApJ, 448, 878

Van Bever, J. & Vanbeveren, D. 1997, A&A, 322, 116

van den Heuvel, E. P. J. & Rappaport, S. A. 1987, in Physics of Be stars, ed. A. Slettebak & T. P. Snow, IAU Coll. No. 92 (Cambridge: Cambridge Univ. Press), 291

Vanbeveren, D., van Rensbergen, W., & de Loore, C. 1998, The brightest Binaries (Kluwer Academic Publishers)

Verschueren, W. & David, M. 1999, A&AS, 136, 591

Waters, L. B. F. M., Coté, J., & Pols, O. R. 1991, A&A, 250, 437

Waters, L. B. F. M., Pols, O. R., Hogeveen, S. J., Coté, J., & van den Heuvel, E. P. J. 1989, A&A, 220, L1

Abbreviations

A&A	Astronomy and Astrophysics
A&AS	Astronomy and Astrophysics Supplement Series
ARA&A	Annual Review of Astronomy and Astrophysics
AJ	Astronomical Journal
A. N.	Astronomische Nachrichten
ApJ	Astrophysical Journal
ApJL	Astrophysical Journal Letters
ApJS	Astrophysical Journal Supplement Series
ASP Conf. Ser.	Astronomical Society of the Pacific Conference Series
BAICz	Bulletin of the Astronomical Institute of Czechoslovakia
BeSN	Be Star Newsletter
ChJAA	Chinese Journal of Astronomy and Astrophysics
MNRAS	Monthly Notices of the Royal Astronomical Society
PASJ	Publications of the Astronomical Society of Japan
PASP	Publications of the Astronomical Society of the Pacific
Pub. A. A. S.	Publication of the American Astronomical Society

Acknowledgements

Sincere thanks are given to all who contributed to the success of this work. Especially I would like to thank:

Prof. Immo Appenzeller for the possibility to carry out this work at the Landessternwarte Heidelberg and the financial support to attend the IAU Symposium No. 195 on "Stellar Rotation"

Prof. Wolfgang Duschl for furnishing the second opinion for the thesis

Otmar Stahl and Thomas Rivinius for supervising the subject, support, fruitful discussions, and careful proof-reading

Stan Štefl for fruitful discussions, the support during my stays in Ondřejov, and careful proof-reading

All observers who assisted to build up the data archive of the Landessternwarte

Petr Hadrava and Wolfgang Hummel for placing their codes at my disposal and for their support

The staff of the Stellar Department in Ondřejov for their support of the HEROS observations, the kind assistance during my observing stays, the warm atmosphere and interesting discussions, the lessons in Czech, tea, biscuits, and apples during long observing nights

Fernando Ruzicka for the technical support of the HEROS observations at the Universitätssternwarte München at Wendelstein and in Ondřejov and the good cooperation during my first stay in Ondřejov

Ulla Anslinger and Martina Böse for their support concerning all kind of administration

The staff of the Landessternwarte Heidelberg for the very nice and warm atmosphere at the institute, for support and encouragement

Hans Martin Schmid, Olivier Schnurr, Claus Möllenhoff, and Dietrich Baade for fruitful discussions and motivation

"Grammar woman" Annette Sowa and Bernd Pistorius for careful proof-reading and language editing

Karl-Heinz Eischer, Markus Scheckeler, and André Fachat for configuring my laptop, telephone support, and any kind of help concerning soft- and hardware problems

Yulia Goranova, Arjan Bik, Martin Stuhlinger, and Thomas Rivinius for a very nice time during the NEON Summer School in 2001

My housemates and friends, and Siggi, Marie, and Charley for any kind of support, discussions, motivation, and encouragement – and that they are still my friends

My parents for supporting my study of physics and my dissertation

I am grateful to the Deutsche Forschungsgemeinschaft, the Academy of Sciences of the Czech Republic, the Deutsches Zentrum für Luft- und Raumfahrt, the International Astronomical Union, and the European Union for financial support and to the European Southern Observatory for allocation of observing time

Special thanks go to Mrs. Gerda Lempp and Dr. Jochen Götze